SINGLE-MOLECULE STUDY OF THE FORCE-INDUCED ACTIN POLYMERIZATION MEDIATED BY FORMIN

YUAN XIN

NATIONAL UNIVERSITY OF SINGAPORE

2015

SINGLE-MOLECULE STUDY OF THE FORCE-INDUCED

ACTIN POLYMERIZATION MEDIATED BY FORMIN

YUAN XIN

(*B. Sci.*, NKU)

A THESIS SUBMITTED

FOR THE DEGREE OF DOCTOR OF PHILOSOPHY

MECHANOBIOLOGY INSTITUTE
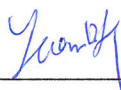
NATIONAL UNIVERSITY OF SINGAPORE

2015

DECLARATION

I hereby declare that this thesis is my original work and it has been written by me in its entirety.

I have duly acknowledged all the sources of information which have been used in the thesis.

This thesis has also not been submitted for any degree in any university previously.

_____

Yuan Xin

30 July 2015

Acknowledgement

24, July, 2015

Table of Contents

Abstract

Actin cytoskeleton is an essential cytoskeletal component that plays important roles in various cell functions including mechanotransduction. Many actin regulatory proteins are involved in the regulation of actin organization and dynamics. Among them, formin is a large family of actin nucleation and polymerization factors marked by conserved formin homolog 2 (FH2) domain. In general, formins are able to track elongating barbed ends via FH2 domains and responsible for the nucleation and generation of unbranched actin fibers. Many in-vivo experiments and theoretical studies have also suggested that formin may mediate the mechanical regulation of actin polymerization. In particular, tensile force on barbed-end FH2 dimer is supposed to reduce critical concentration and increase polymerization rate, as a novel mechanism of mechanosensing. However, probably due to the lack of accurate and reliable manipulation tool, it is still an open question how formin mediated polymerization can be accelerated by tension and whether critical concentration is mechanosensitive.

During the past decade, fast development of single molecule manipulation technologies makes it possible to explore force dependent dynamics of individual molecules. However, few attempts have succeeded in stretching single polymerizing filaments and revealing the effects of forces at single molecule level, except two recent studies based on microfluidics, which identified the acceleration of profilin-actin polymerization under flow drag forces. However, the inclusion of profilin and low accuracy of measurement to some extent obfuscates the understanding of the mechanism of acceleration.

Therefore, my PhD study aims to develop effective single-molecule methods that can be used to monitor the responses of actin polymerization to tension. The first attempt was made based on hydrodynamic flow, which provided the advantages of simple instrumentation and highest throughput. Although this method was capable of stretching single filaments and showed some evidence of promotion in the absence of profilin, there were still some challenges in applying accurate forces and detecting weak effects. Then, optical tweezers was employed to overcome the uncertainty of force application. However, the likelihood of multiple tethers limited the fidelity of quantification.

Finally, in order to take the advantages of above technologies and achieve high accuracy and reliability, a method combining magnetic tweezers, microfluidics and TIRF microscopy was developed. Here, the force is applied by external magnetic field instead of laminar flow, by which it can be maintained stable and constant without significant mechanical perturbation. After optimizing surface treatment and experimental procedures, the magnetic tweezers based approach was able to apply constant forces to single polymerizing filaments, with high signal-to-noise detection of polymeirzation speed. Using this method, I found that up to the highest force (~0.4 pN) that the magnetic tweezers could apply by the time, polymerization speed was nearly a constant. Such a force insensitivity in this range can be understood based on thermal fluctuation.

In summary, through developing and testing different approaches to stretch single polymerizing actin filaments mediated by formin, a robust platform based on a combination of magnetic tweezers, microfluidics and fluorescence imaging was finally developed. Compared to the flow-stretch approach, the magnetic tweezers

based appoach has various advantages such as the length detection of high spatial and temporal resolution and the capability of appling stable constant forces. Although the range of forces that the system can apply is currently less than 0.4 pN, it will be straightforward to increase the force range by using larger paramagnetic beads and stronger magnetic fields. As such, the new technical platform paves the way for future students in the lab to continue on elucidaitng how formin and other actin polymerizing proteins regulate actin polymerization through direct sense of mechanical forces.

List of Figures

List of Abbreviations

ADP	Adenosine diphosphate
APTES	(3-Aminopropyl) triethoxysilane
Arp2/3	Actin related protein 2/3
ATP	Adenosine triphosphate
BSA	Bovine serum albumin
Cryo-EM	Cryo-electron microscopy
C-terminus	Carboxyl-terminus
DAD	Diaphanous autoregulatory domain
DID	Diaphanous inhibitory domain
DRF	Diaphanous related formin
DTT	Dithiothreitol
ECM	Extracellular matrix
EDC hydrochloride	N-(3-Dimethylaminopropyl)-N'-ethylcarbodiimide
F-actin	Filamentous actin
FH1	Formin homolog 1 domain
FH2	Formin homolog 2 domain
fps	Frames per second
G-actin	Globular actin
GFP	Green fluorescence protein
GST	Glutathione S-transferase
GTPase	Guanosine triphosphate hydrolase
MES	2-(N-morpholino) ethanesulfonic acid
MW	Molecular weight
NHS	N-Hydroxysuccinimide
N-terminus	Amino-terminus

PBS	Phosphate buffered saline
PEG	Polyethylene glycol
RT	Room temperature
SC	Succinimidyl carbonate
SVA	Succinimidyl valerate
TIRF	Total internal reflection fluorescence microscope
WLC	Worm like chain

CHAPTER 1 Introduction

1.1 Actin dynamics and regulation

1.1.1 Actin cytoskeleton and functions

Actin is one of the most abundant proteins found in almost all eukaryotic cells. It is highly conserved even after the evolution of one billion years, with about 95% similarity from yeast to human.

Actin was first discovered in muscle cells in 1942 and denominated according to its functions in muscle contraction[1]. In sarcomere actin proteins exist in the form of actin bundles and serve as the track for myosin movement and muscle contractility. Later in 1966, non-muscle actin was isolated and characterized in plasmodium[2]. It is now clear that there are mainly 3 classes of actin isoforms: α isoform mainly exists in muscle, while β and γ are dominant in non-muscle cells. Despite some minor differences in kinetics, their major features and dynamics are fundamentally similar.

In non-muscle cells, actin is one of the three major components of cytoskeleton, in addition to microtubule and intermediate filaments. Actin cytoskeleton plays critical roles in many important cell functions, including cell migration, morphogenesis, cell division, endocytosis, membrane traffic, mechanical signaling and tissue organization.

1.1.2 Actin structure

Monomeric actin is a 42kD globular protein. It is highly abundant in normal cells, ranging from 10 to 100 μM. In certain conditions, actin monomers may polymerize into a form of long actin filaments. Therefore, a pool of actin may simultaneously

contain two populations: monomeric form (also called globular actin or G-actin) and filamentous form (also called filamentous actin or F-actin)[3].

Actin filament is of polarized structure, as revealed by the "arrowhead" appearance upon myosin coating in electron microscopy images. The end of barbed appearance was named barbed end (or plus end) while the other is named pointed end (or minus end)[4]. In many types of cells, actin cytoskeleton is arranged with strong directionality, with their barbed ends towards cell periphery, like those in lamellipodia, filopodia, focal adhesion and microvilli [5].

The structures of actin in both monomeric and filamentous forms have been resolved using X-ray crystallography and electron microscopy[6,7]. As shown in Figure 1.1.1, there are four subdomains, of which SD2 is oriented towards pointed end while SD3 is towards barbed end. Near the center of the molecule, there is an ATP binding cleft as well as a calcium-binding site. Either ATP hydrolysis or ion binding can influence actin conformation and dynamics[8, 9].
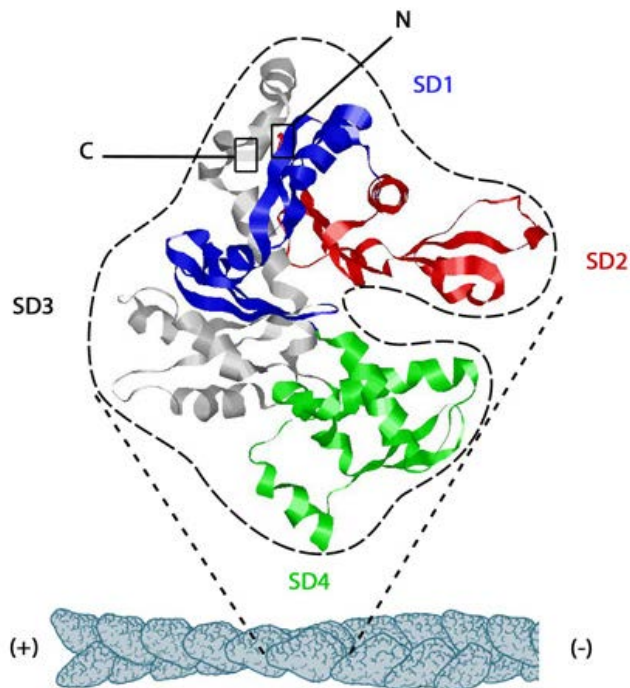
Figure 1.1.1 The structure of G-actin and its arrangement in F-actin.

The figure is reprinted from http://www.mechanobio.info/modules/go-0030041.

Atomic models of F-actin organization have been proposed based on EM images and X-ray diagram, and recently been further optimized using cryo-EM[10]. Although the appearance of actin filament in EM image is a right-handed helix made of two long chains twisting around each other, based on molecular interactions, it can be regarded as a single strand of subunits arranged in left-handed manner[10]. Each subunit gives an extension of 2.76nm with an axial rotation of -166.6°. The turn of 166.6° is very close to 180° so that the filament has a look of right-handed double helical structure with a periodic repeat of 13 subunits that extends 35.9nm. It is worth noting that there are some conformational changes of the assembled subunits in comparison with actin monomers, which may contribute to the changes of biochemical properties after polymerization[11].

1.1.3 Actin dynamics: nucleation, polymerization and treadmilling

In general, which form do actin proteins favor is mainly determined by environmental conditions. Polymerization conditions favor the conversion from monomers to filaments. From the initiation of assembly to the state of equilibrium, there are mainly three stages: nucleation, polymerization and treadmilling.

1.1.3.1 Actin nucleation

"Nucleation" is the process that new filaments are initiated from actin monomers. The precursor aggregate of two or three subunits is called nucleus, which can serve as the basis for continuous polymerization. Spontaneous nucleation is a limiting step for the production of new filaments simply because the initial nucleus is thermodynamically unstable[12].

Usually in cells, actin nucleation is regulated by nucleation proteins, which facilitate the formation of nucleus by recruiting actin monomers. These factors are important to cytoskeleton dynamics as they may regulate the spatial and temporal distribution of new actin fibers and networks[13].

1.1.3.2 Actin polymerization

Polymerization can start from actin nucleus to form a more stable filament. However, only when the monomer concentration exceeds a threshold that is called critical concentration (Cc), can the elongation be continued.

In general, the addition of new monomers is limited by diffusion as the rate of association R_+ is linearly dependent on G-actin concentration (C): $R_+ = K_{on} * C$, where K_{on} is the association constant at polymerizing end. Meanwhile, terminal subunits can also dissociate at a rate $R_- = K_{off}$, which solely depends on the properties of the terminus. Polymerization keeps consuming free actin monomers in solution until the equilibrium between polymerization and depolymerization ($R_+ = R_-$) is reached. At the equilibrium state, there is no net conversion from monomers to filaments or vice versa, as the concentration of monomers is just equal to the critical concentration $Cc = K_{off}/K_{on}$.

Nucleotide exchange can strongly influence actin polymerization, as the critical concentration of ATP-actin is much lower than that of ADP-actin. G-actin is not very active in hydrolyzing its bound ATP by itself, but the hydrolysis occurs rapidly after monomer assembly, which is also faster than the subsequent release of phosphate (Pi). Therefore, as for a fast growing filament, a short cap with ATP can be usually found at the growing end, followed by the consecutive fragments containing ADP + Pi and ADP only. ATP hydrolysis reduces the stability of actin filament as ADP-actin is more prone to depolymerization than ATP-actin[9].

Solvent conditions are also important regulators of polymerization rate and critical concentration. Binding of magnesium ion favors polymerization by decreasing the critical concentration while calcium ion favors depolymerization. High ion strength, high temperature and medium pH (6.5-7.5) are also favorable conditions for polymerization[14].

1.1.3.3 Treadmilling

The orientation of actin subunits gives rise to filament polarity, as the two opposite ends are different in both structures and dynamics. Barbed end has a lower critical concentration, and is hence the favorite side of polymerization (plus end) compared to pointed end (minus end). In fact, the barbed end is of more dynamic nature, as both of its association (K_{on}^+) and dissociation (K_{off}^+) constants are higher. Its lower critical concentration is resulted from the dominance of association constant over dissociation constant, as given by $Cc+ = K_{off}^+ / K_{on}^+$, where $Cc+$ is the critical concentration (Cc) at plus end.

Actin polymerization will gradually reduce the concentration of G-actin and finally lead to the equilibrium between G-actin and F-actin at critical concentration. However, because Cc+ and Cc- (Cc at minus end) are very different, the overall critical concentration (Cc) should fall in-between Cc+ and Cc- (Cc+ < Cc < Cc-), as the filament elongates at barbed end while shrinks from pointed end, as illustrated in Figure 1.1.2. This process is named 'Treadmilling', an important feature of actin dynamics in equilibrium. Though the average length of actin filaments may not appear to change, actin subunits are kept being recycled. ATP-actin subunits continuously join the barbed end, while ADP-actin subunits keep dissociating from the other side. The released G-actin, then, can exchange its bound ADP for ATP and become ready for polymerization again. These properties may contribute to actin retrograde flow in cells and some other dynamic phenomena of actin cytoskeleton.
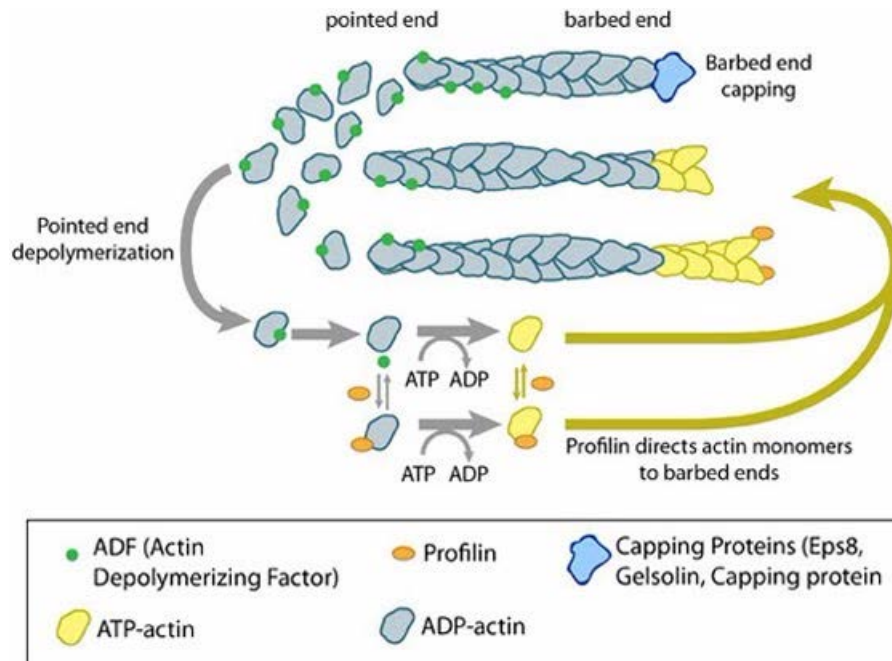
Figure 1.1.2 Actin polymerization, depolymerization and treadmilling.

This figure is reprinted from http://www.mechanobio.info/figure/1385022688553.jpg

1.1.4 Actin regulatory proteins

Pure actin proteins can spontaneously form a homogeneous gel at equilibrium state, which is very different from the diverse structures in cells. So how is the heterogeneous distribution and dynamics of actin cytoskeleton achieved? The answer is very likely to be actin regulatory proteins, a population of more than 100 members that have been discovered in eukaryotes. In Figure 1.1.3, some categories are classified according to their main functions.
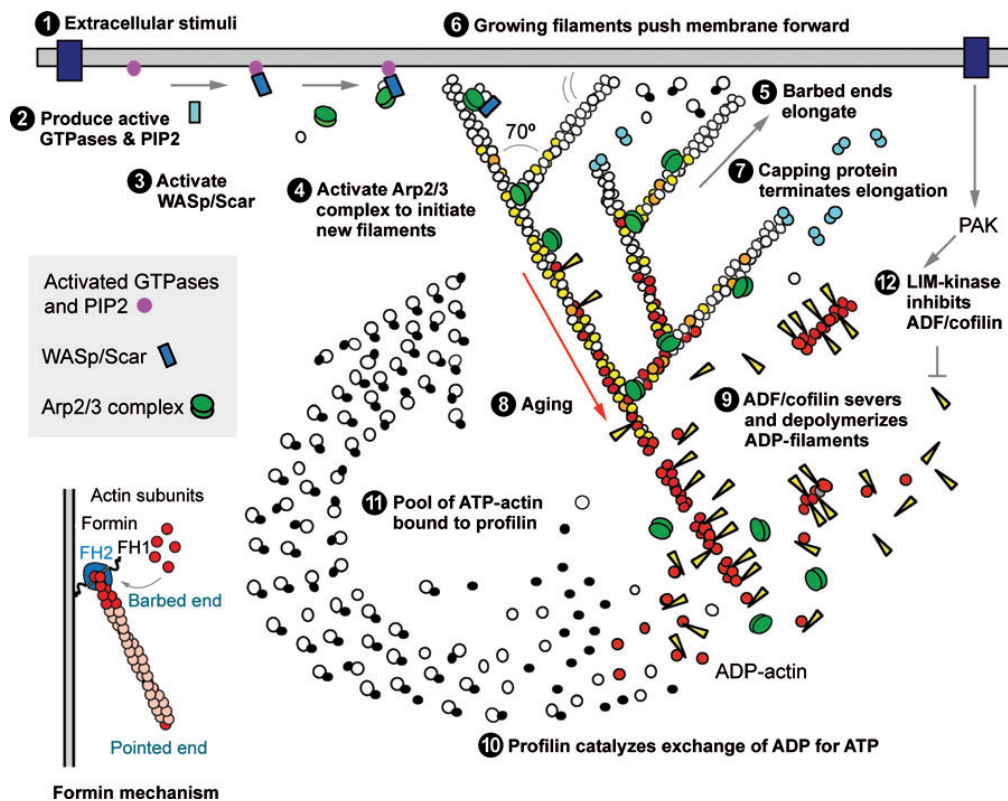
Figure 1.1.3 Regulation of actin dynamics by actin regulatory proteins.

It is described as a series of functional processes in actin assembly and recycling in a typical actin network in lamellipodium. This figure is reprinted from Pollard, T.D. 2007 [15].

Nucleation and polymerization: In many cases, because spontaneous nucleation is not energetically efficient, nucleation factors are needed to facilitate nucleation promptly upon stimulation. Two families of regulatory proteins WASP and formin, have been identified as nucleation promoting factors[16]. WASP induces actin nucleation on the side of existing filaments via the activation and assembly of Arp2/3 complex, which leads to the formation of branched network[17]. Formin proteins can also induce nucleation but in a manner independent of existing filaments[18]. Some formins may be activated at specific sites, by which the location of actin assembly

can be regulated. After nucleation, rapid elongation may occur to form branched network or long straight fibers, and serve as the driving forces of many dynamic processes like lamellipodium extension and filopodia protrusion. The process of polymerization is also under the precise regulation of different kinds of polymerization factors, such as formin and VASP[19]. In particular, both of them function to accelerate elongation.

Disassembly: Disassembly is also an important process, which recycles the assembled subunits into a pool of monomers. Two mechanisms are mainly involved: depolymerization and severing. ADF/cofilin is a family of ARPs that promotes the depolymerization of ADP-actin from pointed end. Some of them also function to sever ADP-F-actin into short fragments, by which to increase the number of barbed ends and promote recycling[20,21].

Stabilization: In many cases, there are needs to stabilize existing actin filaments. This function can be achieved by capping proteins, e.g. capZ directly caps barbed end, while tropomodulin caps pointed end. Such capping protects the terminus from both unexpected assembly and disassembly[22,23]. Tropomyosin is also a kind of stabilizer, which wraps around actin filaments in a polymerized form, to prevent their depolymerization and regulate the binding of ARPs[24,25].

G-actin binding: The concentration of cytoplasmic G-actin is much higher than critical concentration, which enables fast reaction to polymerization signals. However, such a concentrated pool of G-actin would not be homeostatic if without any other regulatory factors. Profilin is such a regulator that binds G-actin in 1:1 ratio and

protects the monomers by inhibiting both spontaneous nucleation and pointed-end polymerization. In addition, it also promotes the exchange of ADP to ATP in G-actin, which may help to maintain a pool of active monomers[26]. However, in the presence of formin or VASP, profilin can dramatically accelerate polymerization and exhibit its multifaceted roles in the regulation of actin dynamics[27]. In contrast, thymosin-β4, another G-actin binding protein, was found to sequester G-actin and prevent assembly[28]. Therefore, the balance between profilin and thymosin-β4 has been thought to be important to the maintenance of an active G-actin reservoir[29].

Crosslinking and bundling: Many actin-based subcellular structures are built by actin crosslinking and bundling proteins. Several kinds of such proteins have been identified with their specific roles, like the bundling funtions of α-actinin in stress fibers, fascin in filopodia and the crosslinking functions of filamin-A in actin networks[30].

Overall, it can be seen that the large variety of actin regulatory proteins are key to the regulation of actin organization and dynamics. However, besides these biochemical factors, many studies in the past decade have also highlighted the involvement of mechanical factors in actin regulation. It seems difficult to explain many phenomena of highly spatial and temporal dynamics if not taking mechanical forces into account. Therefore, discovery of potential responses to mechanical signals and the cooperation between biochemical and mechanical factors is critical to understanding the regulation of actin dynamics and functions.

1.2 Mechanical regulation of actin cytoskeleton

In multicellular organisms, cells are organized into tissues via their physical connections with neighbouring cells and matrix, in which they are subject to mechanical forces almost at any time. Studies during the past decade have revealed mechanical forces as active regulators of many biological functions[31]. For examples, cell differentiation has been found to be guided by substrate rigidity[32]. The migration of fibroblast is strengthened by stiff substrates rather than soft ones. Antigen presenting to T cells may involve physical interactions and be regulated by mechanical forces[33]. Some diseases may also be caused by defects in mechanotransduction[34,35].

Meanwhile, it has also been well accepted that actin cytoskeleton and related subcellular organelles play central roles in cell mechanotransduction[36]. In this chapter, how actin cytoskeleton experiences, transduces and reacts to mechanical forces will be discussed from the level of cells to individual molecules.

1.2.1 Mechanosensing of cells

In some aspects, cells can be simply considered as a collection of soft materials that are enclosed by lipid membrane. Extracellular matrix and cytoskeleton is key in protecting them from mechanical perturbation and destruction. Via cell-matrix adhesions and cell-cell contacts, cells establish connections with their surrounding environments. These contacts are also linked to the cytoskeleton network inside cell boundaries, by which mechanical forces can be effectively generated and transmitted[37].

According to the sources, forces experienced by cells can be mainly classified into two categories: outside-in (external) and inside-out (internal). The forces applied by environment, including shearing, pressure and those from matrix and neighbouring cells can be transmitted into cells via membrane and mechanical receptors. Meanwhile, the internal forces generated by actomyosin contractility and some other mechanisms can be transmitted outwards to resist tension, pressure and shearing, as well as to modulate surroundings.

1.2.2 Cytoskeleton as a key player in mechanosensing

The transduction of mechanical forces requires appropriate medium. Instead of being a homogeneous fluid, cytoplasm contains a variety of well-organized and pre-stressed cytoskeletal architectures, which are of high elasticity or high stiffness. The distinction of stiffness between cytoskeleton and cytosol enables force transduction over a long distance (about tens of micrometers) without significant decay[38]. Compared to the transmission of biochemical signals via diffusion and directional transport, mechanical signals can be transmitted much faster over a long range (in the scale of milliseconds).

The essence of mechanosensing is to convert mechanical signals into biochemical effects and downstream responses. As revealed in many studies, most of the conversion can be attributed to force dependent conformational changes. In general, mechanical forces applied on biomolecules or complexes may change their conformations by altering their energy landscape. The shift of chemical potential or energy barrier may lead to certain kinds of reactions, such as the extension of polypeptide chains, domain folding, unfolding, and ligand binding and dissociation.

1.2.3 Force dependent stability of actin

Considering the irreplaceable roles that actin cytoskeleton plays in mechanotransduction, the variety of actin machineries and regulatory proteins seems important to the diversity of mechanical responses[34]. These machineries, made of either networks or bundles, should be stiff enough to resist tensile and contractile forces, or elastic enough to buffer sudden stroke and store the elastic energy imposed by pressure, bending or stretching. Actin cytoskeleton should also be of rapid dynamics, allowing immediate responses to mechanical signals.

1.2.3.1 Actin mechanics

As a flexible polymer, actin filament can be mechanically characterized by its persistence length (Lp), an indicator of its worm like chain (WLC) flexibility. The Lp of ATP and ADP-Pi F-actin was both measured to be about 15μm[39], indicating a rigidity ibetween DNA and microtubule. This rigidity allows actin filament to resist a certain magnitude of pressure. In theory, because buckling force is predicted to be inversely proportional to the length squared as $F = \pi^2(Lp/k_BT/L^2)$, where k_B is boltzmann constant and T is absolute temperature, a pressing force of 1pN is enough to buckle a filament longer than 1μm[40]. In this case, to withstand large pressure and generate pushing forces, short actin filaments in a densely crosslinked network (e.g. in lamellipodium) and filament bundles (e.g. in filopodia) are favoured. In contrast, actin filaments behave much stronger against tension. A single actin filament can sustain the tension of several hundred piconewtons without being ruptured[41]. The terminal subunit may also form a catch-slip bond as the maximum lifetime was found

at 20pN[42]. However, even the strength is high in longitude direction, bundling seems still necessary for the long-range traveling of tension, e.g. in stress fibers.

1.2.3.2 Actin related force generation

In general, effective force generation and transduction requires the medium to be continuous and rigid. As discussed above, actin cytoskeleton is an appropriate candidate. Actin filaments themselves can withstand significant constrains via direct contacts with substrates[37]. Besides, many actin regulatory proteins, such as the end capping and tracking proteins, may serve as the bridges of force transduction between actin filaments and substrates. Many molecular sources have been found responsible for actin related force generation, such as myosin-II contraction, actin polymerization and depolymerization, and possibly myosin-X translocation[43,44,45].

1.2.3.3 Actin as a mechanosensor

The players that mediate mechanical regulation of actin dynamics have long been of great interest. Many evidences have suggested that actin may function as a mechanosensor by itself[36,46]. For example, compression forces exerted on actin filaments can generate curvature and possibly consequent mechanosensing reactions. When a filament is locally bent, breaking may occur easily in comparison to the rupturing in longitude direction, which is possibly a mechanism to produce polymerizing ends in response to the compression on lamellipodia[47]. In 2012, Risca et al. reported that Arp2/3 complex favored to initiate nucleation on the convex side of a

compressed mother filament, probably by which can the branched network expand against leading membrane tension[48].

In recent years, more and more attention has been given to the structural polymorphism of F-actin. Novel techniques and protocols based on cryo-EM and fluorescent microscopy helped to uncover the structural heterogeneity of F-actin under different circumstances, such as shearing forces and tension[46]. In 2009, a cutting-edge experiment which pulled tetramethylrhodamine labeled actin filaments using optical tweezers revealed a decrease of fluorescence intensity by increased tension[49]. It suggested that tension might shift the states of filamentous actin towards globular state, as the fluorescence of labeled actin was normally brighter in filamentous form.

1.2.3.4 Actin associated proteins in mechanosensing

Many actin regulatory proteins are physically linked to actin filaments and substrates such as membrane, nucleus and focal adhesions. Some of them have been identified as mechanosensors, as they directly sense and convert mechanical signals into biochemical outputs. For example, the auto-inhibitory state of α-catenin can be opened by physiological range of forces to expose its vinculin binding sites[50]; Filamin A, a molecule that crosslinks actin filaments, is sensitive to the mechanical strain within actin network, which can regulate its domain unfolding and recruitment of signalling molecules[51].

In summary, various kinds of biochemical cascades may occur upon the force induced conformational changes. However, at the beginning of this study, none of

them has been directly linked to the core process of actin dynamics - actin polymerization. Little evidence has been shown on how actin polymerization is regulated by mechanical tension, and relatively, whether actin polymerization factors such as formins are involved.

1.2.4 Force dependent actin polymerization

It has long been predicted that an exponential decrease of polymerization rate may occur when the polymerizing end experiences opposing force. It was supported by a measurement with branched actin network in vitro and an evidence that lamellipodium extension can be slowed down by tension[52,53]. Then, by simultaneously anchoring the two ends of single actin filaments on glass surface, Kovar, et al. made direct observation and showed that the barbed-end polymerization mediated by mDia1 was inhibited by accumulating tension with an estimated stall force of 1.3pN[43].

However, at the beginning of this study, whether a pulling force can induce actin polymerization was still a mystery. Different from pushing a growing filament, it seems hard to apply direct tension on the dynamic terminal of an actin filament. Therefore, it becomes necessary to include an end tracking protein such as formin (or VASP), and anchor it as well as the actin filament at the same time, which is probably the situation in physiological conditions. Then, it becomes a question how formin senses mechanical tension and transduces the effects to actin polymerization.

1.3 Formin dependent regulation of actin polymerization

As discussed above, actin polymerization is a key process in actin dynamics. Formin, a large family of regulators marked by their conserved formin homology 2 (FH2) domains, have been identified to promote actin nucleation, polymerization and the formation of long unbranched actin fibers. Studies in details have revealed that formin processively tracks the barbed end of an actin filament, promotes actin polymerization in a profilin dependent manner and prevent the barbed ends from capping[27,54]. Besides, formin proteins are very likely the candidates to anchor actin barbed ends to other subcellular components and mediate the mechanical regulation of actin polymerization. This section will give an introduction to formins' features, activation and regulatory functions, and discuss its hypothesized roles in mechanosensing.

1.3.1 The features and biochemical activation of formin

Formin was first known in early 1980s from the mouse limb deformity (ld) mutants that caused severe defects in limb formation[55,56]. In 1990, the name 'formin' was given to describe the limb deformity gene[57]. After four years, a Drosophila gene required by cytokinesis, diaphanous, was found to be a homolog of formin[58]. Comparison between diaphanous, ld gene and Bni1 from S.cerevisiae gave rise to the identification of two regions of homolog, FH1 and FH2[58]. FH2 is the domain of highest sequence homology. FH2 and proline-rich FH1 domains are characterized as the defining feature of the formin family. In 1997, yeast Bni1 was first identified to function in actin assembly[59]. Afterwards, varies kinds of functions have been attributed to different formin members, as briefly summarized in figure 1.3.1. Up to

date, at least 15 formin genes have been identified in mammals, which are classified into 8 subfamilies according to their FH2 homology[60].
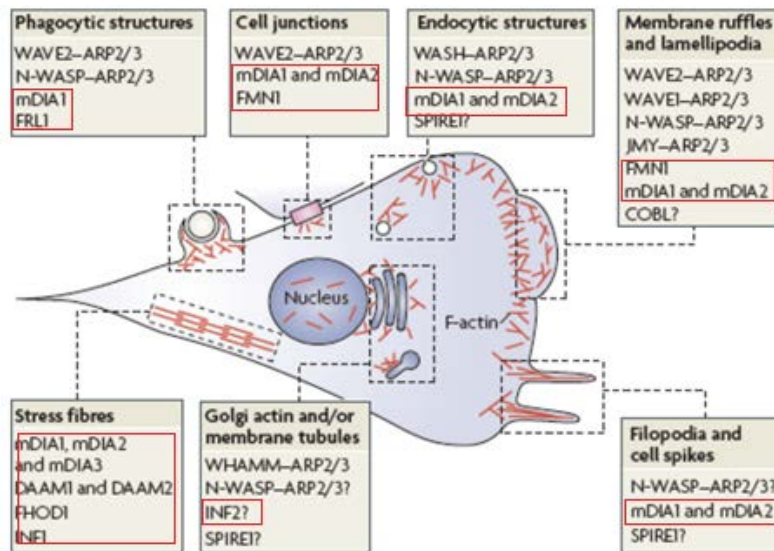
Figure 1.3.1 Formin proteins are involved in many actin based subcellular structures. Formin family members are highlighted in red boxes. This figure is adapted from Campellone, K.G. and Welch, M.D. 2010 [16].

Conventional formins are large multi-domain proteins (120-220kD), as shown in Figure 1.3.2. Taking the typical mammalian Diaphanous-related formins (DRFs) as examples, they are defined by their C-terminal auto-regulation domain (DAD), which include the subfamilies of Dia, Daam, FMNL and FHOD[61]. FH1 and FH2 domains precede DAD and function as the core modules for actin nucleation and polymerization. There is always an FH3 region at the N-terminus to FH1-FH2 element, which can also be described as Diaphanous inhibitory domain (DID) according to its autoinhibitory interaction with DAD domain[62]. Adjacent to the N-terminal of DID is a GTPase binding domain (GBD). The binding of small GTPases to GBD can activate formin by disrupting the autoinhibitory interactions[63,64].

18
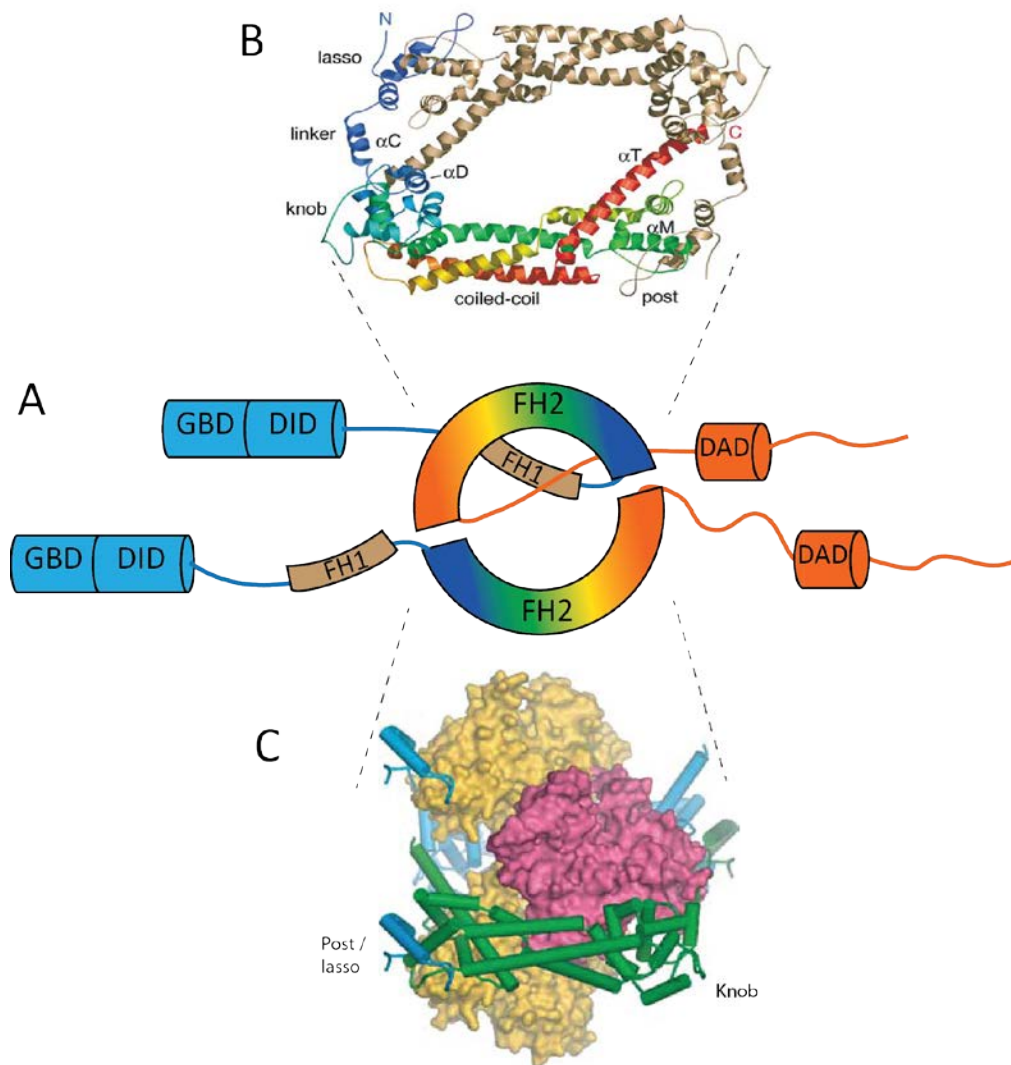
Figure 1.3.2 Formin domain organization.
(A) Formin domain organization. (B) The crystal structure of dimerized FH2 domains.
(C) The structure of co-crystalized FH2 dimers and actin monomers. Sub-figure B
and C are adapted from Xu et al. 2004 and Otomo et al. 2005 respectively[65,66].

After the FH2 domain is exposed, it can directly bind actin monomers, nucleate new

filaments for elongation and remain binding to the barbed ends during polymerization.

This tracking helps to maintain processive polymerization and prevents the access of capping proteins, which enables the formation of long unbranched actin filament[67].

FH2 domains are believed to be functionally active in form of dimer[68,69,70]. By now, FH2 dimeric structures of three different formins yeast Bni1, murine mDia1 and human Daam1 have been resolved[65,70,71,72]. Bni1 FH2 dimers were also co-crystalized with TMR-labeled actin, providing deep insights into the mechanisms of FH2 functions[66]. As shown in Figure 1.3.2 B, dimeric FH2 domains form a 'doughnut' shape with a head to tail orientation between each other. Both subunits are of arch shape, giving the 'doughnut' ring structure a diameter of about 11nm, just suitable to accommodate the barbed end with a diameter of 8nm. Each subunit can be divided into several regions from N- to C-terminal: a "lasso" subdomain, an extended linker region, a spherical "knob" subdomain, a coiled-coil region and a "post" subdomain. Each "lasso" binds the other "post" subdomain to form the ring. This "lasso" region, together with the post, coiled-coil and knob subdomains of the other subunit, is regarded as a structural hemidimer. Each hemidimer probably contains two actin-binding sites. Therefore, four sites are available for the interactions with two actin monomers, which permit FH2 nucleation and processive tracking.

FH1 domain usually contains several polyproline tracks, the number and length of which varies largely in different formins[73]. These tracks have affinity to profilin as well as the profilin:G-actin complex[63,74]. Some evidences have shown that profilin strongly inhibits the nucleation activity of FH2 domain alone as well as in the presence of FH1[75,76]. However, as for the stage of elongation, FH1 domain functions to recruit profilin:G-actin complex to the barbed end and drastically accelerate FH2 mediated actin polymerization[73].

FH3 domains share low sequence identity between different formins, but the ones of mDia1 and FHOD1 have been shown to share a helical armadillo repeat fold[77,78]. DAD domain comprises a conserved MDxLL motif and a polybasic region, both of which together function to recognize the N-terminal FH3 domain and lead to the outcome of autoinhibition[79].

Considering the adjacent localization of GBD to FH3 domain, binding of specific active GTPases can displace DAD from FH3, due to their higher affinity to GBD-FH3 element[80]. It is worth noting that different GBDs have specific affinity to small GTPases, by which formin activities can be precisely regulated[81].

1.3.2 Formin's functions in actin nucleation and polymerization

1.3.2.1 Formin nucleation activity

FH2 nucleation activity is one important mechanism of new filament generation. The FH2 dimer can directly bind and stabilize two or three actin monomers to form a nucleus, which is hard to form by themselves[66]. Interestingly, the binding of profilin to G-actin further inhibits spontaneous nucleation as well as pointed end elongation, which, however, can be rescued by the presence of FH1 domain[76]. Therefore in cells, formin is established to be prominent in selective and prompt actin nucleation from a high concentration reservoir[82,83,84].

1.3.2.2 Formin processivity

In complex intracellular environments, new-born actin filaments may be subject to different fates. The filament nucleated by Arp2/3 complex, for example, can be capped by capping proteins after a short elongation, which frequently occurs for the formation of a highly branched network of short filaments at cell leading edge[85]. In contrast to Arp2/3 complex, formin proteins function to generate long and unbranched actin cables for diverse subcellular structures, thanks to their abilities of processive elongation. In 2004, Higashida et al. found that the constitutive active form of mouse mDia1 can translocate as fast as 2.0 µm/s (740 subunits/s) for over tens of micrometers through the cytoplasm of fibroblasts[86]. Similarly in vitro, rapid growth of actin filaments from anchored FH2 molecules was observed, as they kept remaining on the fast growing ends during hundred rounds of monomer addition[43].

Three factors may be essential for formin processivity. First, FH2 domain protects the barbed ends from being blocked by capping proteins[69,54,68,87] or annealed to the pointed ends of other filaments[88]. Second, the dissociation rates of FH2 on barbed ends should be low enough. Third, FH2 domain must keep interacting with new actin subunits for processive translocation[89].

Crystal structures provided some insight into the mechanisms of FH2 processivity. As suggested by Figure 1.3.2 C, the circular shaped FH2 dimer wrapped around two pioneering actin monomers with each hemidimer bridging both on one side. The two "knob" and "lasso-post" subdomains totally contributed four actin binding sites. The linker regions in-between each pairs of subdomains were suggested to be unstructured and flexible, by which elastic energy can be stored[66]. When all of the four binding

sites were engaged for terminal binding, the linker regions were likely to be fully extended.

Based on the structural information, some models have been proposed to explain FH2 processive tracking. Because the lagging actin subunit was suggested to be blocked in the state of full association, it may be regarded as a "close" state in which the addition of new monomer was prevented. The strength of these interactions, however, may not be so strong that individual bond may dissociate spontaneously to expose the access to both FH2 hemidimer and terminal actin. The dissociation was supposed to happen more frequently from the lagging subunit, due to the potential to release tension within linker region. Such dissociation may lead to the switch to "open" state, in which a new actin monomer can be inserted and form interactions with the lagging subunit as well as the exposed FH2 hemidimer. It would be one step of elongation as the FH2 dimer moved one step forward and the state was changed from "open" to "close" again. Thousands of such cycles gave rise to the elongation over micrometers. Because FH2 moved on the barbed end in a manner of stair-stepping, it was named "stair-stepping" mode[65,66].

A "step-second" mode was also proposed based on the "flat" arrangement of terminal actin[76]. In the co-crystals with FH2 dimer, the two terminal actin subunits were arranged opposite to each other with a turn of 180°, which was different from 167° inside filaments. If this evidence was true, it may be the reason of barbed end recognition, as the FH2 dimer may favour terminal flat arrangement than filamentous fragment. In the step-second mode, new actin monomer was supposed to be recruited prior to FH2 translocation. Upon monomer addition, the lagging subunit may change itself towards the conformation of filament body, which increased the energy of FH2

binding. In this case, FH2 may be energetically driven to dissociate from the lagging subunit and form interactions with new terminal monomer.

1.3.2.3 Formin polymerization activity

When profilin or FH1 domain is absent, FH2 domain alone, in fact, inhibits actin polymerization to some extent, as FH2 capping may increase the energy barrier for monomer addition. The inhibition can be described using a "gating factor", which reflects the equilibrium between "open" and "close" states. It is defined to be the speed ratio between FH2 mediated polymerization and spontaneous polymerization (ranging from 0 to 1), as what a portion of polymerization is allowed under FH2 capping[73].

It is worth noting that though different FH2 domains share highly conserved core structures, their polymerization activities may differ a lot. Systematic comparison has been done among several formins: mDia1, mDia2, yeast Bni1p and cdc12p, whose inhibitory effects are very diverse. Their individual gating factors were reported to be: mDia1 (~0.9) > Bni1p (~0.7) > mDia2 (~0.3) > cdc12p (~0.0), ranging from weak (mDia1) to complete inhibition (cdc12p)[73]. Therefore, even if they shared similar mechanism of polymerization, their functions in cells may be very different.

Their functional diversity is very likely a result of the difference in primary sequences. Recent studies implicated an interesting correlation between polymerization activities and the length of linker regions. The mDia1 has the longest linker among those formins, while Bni1p and mDia2 in the middle and cdc12p the shortest. Shortening of the linker region led to the loss of assembly activity[71]. This correlation supports the

hypothesis that linker region is needed to be extended to accommodate terminal subunits, and longer linker may be more flexible to lower the barrier for monomer addition[65,66].

Besides, the dissociation of FH2 – another parameter related to formin processivity – is highly correlated with polymerization. The off-rates of FH2 dimers ranged over two orders of magnitude as mDia1 (1.2×10^{-3}/s) > Bni1p and mDia2 (1.3×10^{-4}/s) > cdc12p (6.0×10^{-5}/s)[73]. This significant correlation suggests some mechanistic links between polymerization and FH2 dissociation.

1.3.3 The involvement of formin in mechanical responses

As shown in Figure 1.3.1, formin proteins exist in a large variety of force related cytoskeletal structures, in which they are very likely to experience mechanical forces[16]. At the tips of filopodia, some formins like mDia2 and DAAM1 may experience periodic compression and tension during protrusion and retraction[90,91]. In stress fibers and contractile rings, formins are likely subject to contraction forces dependent or independent of myosin[92,93]. Some formins are also needed for actin assembly in cell adhesions, which serve as the mechanical bridges between neighbouring cells[94], and lamellipodia, the major machinery of cell motility[94,95]. In addition, many diaphanous related formins are involved in phagocytosis and endocytosis, the processes that are under mechanical regulation[96,97].

Some connections between formin and mechanical forces were obtained by cell manipulation. In 2001, Riveline et al. reported the induction of focal contacts by scratching cell membrane using micropipette[98]. They found that the external forces

strengthened focal contacts by mimicing and substituting actomyosin contraction, but still requiring formin activities. Active forms of formin mDia1 were able to rescue the mechanical induction of focal contacts in Rho inactive cells, in which neither myosin nor endogenous mDia1 was active (Figure 1.3.3). These evidences suggested that mDia1 was involved in mechanical strengthening of actin assembly in cell-matrix adhesions and probably can sense and response to mechanical signals.
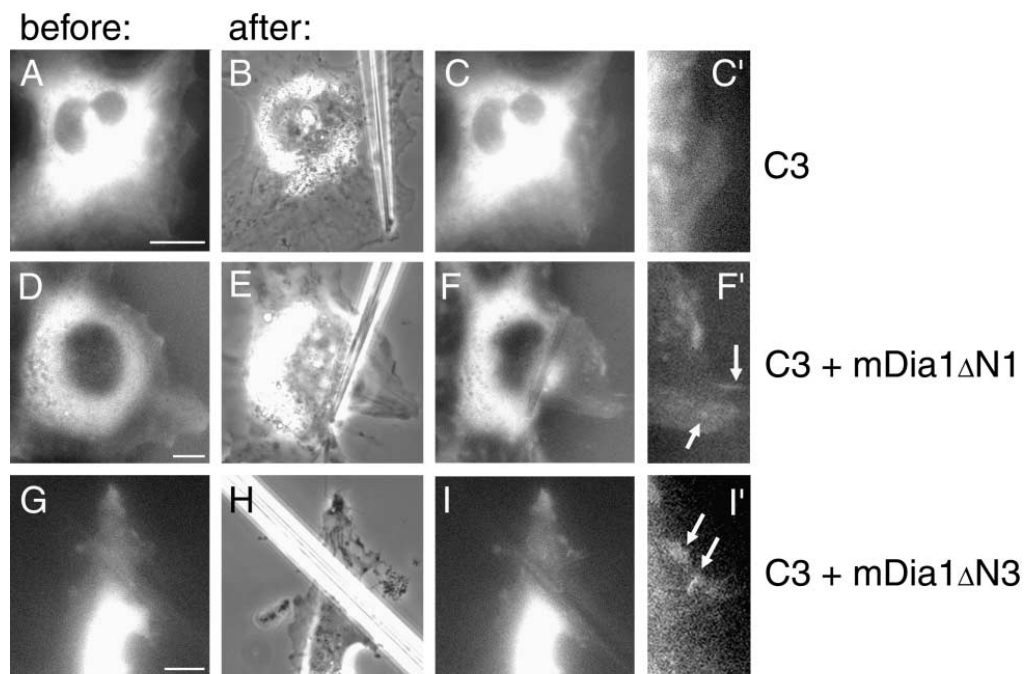
Figure 1.3.3 Formin mDia1 mediated the strengthening of focal contacts by mechanical stretching. (A-C') In the C3 cells whose Rho activities were inhibited, very few focal contacts can be found before and after micropipette scraping of the cell body. (D-F') In the cells that overexpressed constitutively active mDia1-ΔN1, focal contacts were strengthened after scraping. (G-I') Similar effects were observed for mDia1-ΔN3 construct. This figure is adapted from Riveline, D. and Bershadsky, A.D., 2001, originally published in *The Journal of Cell Biology*, doi: 10.1083/jcb.153.6.1175 [98].

1.3.4 Pulling forces are predicted to facilitate actin polymerization mediated by FH2

The above in-vivo and structural evidence suggests a potential mechanosensing role of formin that mediates the promotion of actin polymerization by tension. Several theoretical models have been proposed to predict the behaviours of FH2 dimer in response to pulling. In 2004, Kozlov and Bershadsky proposed that a pulling force on FH2 dimer may energetically favour actin polymerization, in terms of decreasing critical concentration and increasing polymerization rate[99].

This hypothesis was proposed based on "stair-stepping" mode, a classic model of FH2 processivity, as illustrated by figure 1.3.4A. The information of crystal structures suggests that an FH2 dimer can form several contacts with terminal actin subunits. Full engagement of these contacts may lead to the accumulation of intramolecular elastic energy, which facilitates the dissociation of a hemidimer from the recessed subunit to enter open state (a1). This state allows an actin monomer to be incorporated via associating with both dissociated hemidimer and exposed subunit. The incorporation deforms FH2 dimer and makes it enter closed state with with stored elastic energy (a2). This energy may then drive the dissociation of the other hemidimer as the begining of a new polymerization cycle (a3). In a polymerization event, the energy change can be expressed as:

$$\Delta E_{tot} = E_{AB} - k_B T \cdot \ln Cv \qquad (1)$$

where E_{AB} is binding energy, k_B is Boltzmann constant, T is absolute temperature and $\ln Cv$ represents the entropy change of consuming an actin monomer.
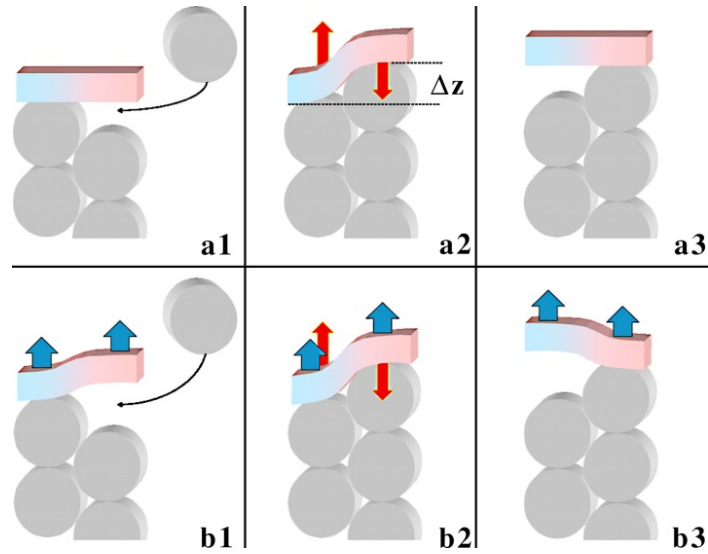
Figure 1.3.4 Stair-stepping mode – a model of formin mechanosensing.
The bar of blue and red color represents a formin FH2 dimer and the gray balls represent actin subunit. Blue arrows indicate the application of force. This figure is adopted from Kozlov, M.M. and Bershadsky, A.D., 2004, originally published in *The Journal of Cell Biology*, doi: 10.1083/jcb.200410017 [99].

According to this model, the pulling force exerted on FH2 dimer is very likely to drive all processes energetically. First, as illustrated in sub-figure b1, a force f (half of the total force $F = 2f$) on the recessed hemidimer may impose an energy of $-f\delta$ during the transition to open state, where δ denotes the transition distance. Second, as a new actin subunit is inserted, force f may provide an additional energy of $-f\zeta$, upon the protrusion of ζ. Considering the axial symmetry of filamentous actin, it is reasonable to think the δ and ζ to be roughly of the same value - half of the monomer size ($1/2\ \Delta z$). Therefore, the total energy change ΔE_{tot} of a polymerization cycle in the presence of tension can be expressed as:

$$\Delta E'_{tot} = E_{AB} - k_B T \cdot \ln Cv - f \cdot 2\Delta z = E_{AB} - k_B T \cdot \ln Cv - F \cdot \Delta z \quad (2)$$

where $F = 2f$ is the total pulling force on FH2 dimer and $\Delta z = (\delta + \zeta) / 2 = 2.7\text{nm}$ is the protrusion of monomer addition.

In principle, ΔE_{tot} reflects the feasibility of actin polymerization. At the equilibrium state when no net polymerization occurs at barbed end, ΔE_{tot} should equal to zero. The actin concentration at this estate is critical concentration C*.

Therefore, by combining equation (1) and (2) at equilibrium state,

$$E_{AB} - k_B T \cdot \ln C_f^* v - f \cdot 2\Delta z = E_{AB} - k_B T \cdot \ln C_0^* v \quad (3)$$

we can obtain a relationship between pulling force and critical concentration:

$$C_f^* = C_0^* \cdot e^{-F \cdot \Delta z / k_B T} \quad (4)$$

This equation suggests that a pulling force F may exponentially decrease the critical concentration by a factor of $F \cdot \Delta z / k_B T$. Taking $k_B T$ as 4.1 pN·nm and Δz to be 2.7nm, a pulling force of about 3.5pN may be able to reduce the critical concentration by a factor of 10.

It can be seen that this model describes how pulling force applied on formin dimer can shift the equilibrium state of actin polymerization. However, this assumption can be made in a more general way beyond any particular model of formin behaviors. In principle, a tensile force given to barbed-end formin should be sensed by the entire filament. Therefore, the force F should be able to reduce the chemical potentials of all polymerized actin subunits (μ_p), as given by:

$$\mu_p(f) = \mu_p(0) - F \cdot L / N \quad (5)$$

where F is the tension along the entire actin filament, L is filament length and N is the number of actin subunits. Here, the term L/N equals to the step size of each monomer $\Delta z = 2.7$nm.

Meanwhile, the principle of polymer physics also tells us that actin polymerization is a reversible reaction driven by the difference between the chemical potentials of G-actin and F-actin. In a steady solution where G-actin is of critical concentration, the chemical potential of polymerized form should equal to that of monomeric form plus entropy decrease, as shown in the equation:

$$\mu_p(0) = \mu_m + k_B T \cdot \ln C_0^* v \quad (6)$$

Similarly, for a filament under tension F, its chemical potential can be expressed as:

$$\mu_p(f) = \mu_m + k_B T \cdot \ln C_f^* v \quad (7)$$

By combining the equations of (5), (6) and (7), we can obtain a relationship between C_0^* and C_f^*:

$$C_f^* = C_0^* \cdot e^{-F \cdot \Delta z / k_B T} \quad (8)$$

which is as same as equation (4), indicating that tension energetically favors actin polymerization in a formin independent manner.

Besides critical concentration, force is also likely to influence polymerization rate. The hypothesized decrease of critical concentration by tension, in principle, corresponds to an increase of polymerization rate at original equilibrium state. This probably because both of the on- and off-rates at barbed end are mechanosensitive.

This phenomenon can be interpreted from the gating function of FH2 dimer. Many studies have shown that FH2 capping to some extent inhibits the spontaneous polymerization that is limited by diffusion, probably because FH2 may partially block the barbed end from monomer access. The rigidity of FH2 dimer may be a significant factor that influences the ratio of 'open' state, by setting an energy barrier for the partial dissociation and forward translocation of recessed hemidimer.

In this scenario, external pulling force can be supposed to trigger its dissociation and forward displacement for the recruitment of new actin subunit. The total transition distance in a polymerization cycle can be postulated to be a monomer size ~$2\Delta z$. As such, a total work of $f \cdot 2\Delta z = F \cdot \Delta z$ may be done to overcome the energy barrier and accordingly increase the association constant by: $k_{on}(f) = k_{on}(0) \cdot \alpha$, where $\alpha > 1$ is a force dependent coefficient.   (9)

Similarly, dissociation constant may also be influenced. In the presence of tension, dissociation of an actin monomer requires the corresponding hemidimer to overcome a work of $-f \cdot 2\Delta z = -F \cdot \Delta z$ to re-establish its contacts with recessed actin subunit. In this case, the dissociation constant may be changed to: $k_{off}(f) = k_{off}(0) \cdot \beta$, where $\beta < 1$ is also a force dependent coefficient.   (10)

Considering (9) and (10) together, the polymerization rate may be changed to:

$$v = k_{on}(0) \cdot \alpha \cdot C - k_{off}(0) \cdot \beta.$$

Here, β can be directly measured from the force dependent depolymerization rates, while α can then be known from the polymerization rates. It can be seen that a pulling force may accelerate FH2 mediated actin polymerization in a complex relationship.

Overall, the above theoretical analysis suggests that mechanical pulling force applied on FH2 dimer may decrease barbed-end critical concentration and shift equilibrium towards polymerization. It may also influence the kinetics of polymerization, in terms of increasing polymerization rate. These potential mechanosensing functions support the hypothesis that actin polymerization may be enhanced by local tensile forces in cells. In general, most of the actin monomers in cytosol are sequestered by G-actin binding proteins, leaving only a few of free monomers of about critical concentration. The effect of decreasing critical concentration by force may break the balance and promote actin polymerization as a mechanical response. Meanwhile, for the microfilaments of rapid dynamics, like those in filopodia and contractile rings, pulling force may promote their elongation and inhibit their shrinkage. On the other hand, cells may use similar mechanism to generate forces via formin, as actin polymerization may provide the power to push mechanical loads, e.g. in lamellipodia, while actin depolymerization may produce retracting forces to pull substrates and cargos. Importantly, it is worth noting that the above mechanosensing mechanism is hypothesized to be the functions of FH2 domain only, which is independent of FH1 domain and profilin.

1.4 Single molecule manipulation techniques

Over the past two decades, single molecule study became a cutting-edge research field along with the inspiring outburst of single molecule manipulation technologies. This realm is very different from traditional biochemistry, in that it focuses on the behaviors of individual molecules to provide direct information about mechanics,

reaction, interaction and motility. These abilities greatly boost our understanding of the fundamental processes in biological functions.

Up to date, several kinds of single molecule manipulation technologies have been developed, including optical tweezers, magnetic tweezers, hydrodynamic flow, atom force microscopy and micropipette manipulation[100]. In this chapter, I will discuss the first three technologies that have been involved in this study.

1.4.1 Hydrodynamic flow

Hydrodynamic flow has long been used to study biological phenomena at microscopic level. As illustrated in Figure 1.4.1, the directional hydrodynamic flow can align and stretch tethered materials, e.g. microspheres or polymer chains by viscous friction. As early as in 1994, Perkins et al. began to use flow to stretch single DNA molecules to explore their mechanics[101,102]. From then, hydrodynamic flow has become a powerful single molecule tool in studying DNA mechanics and dynamics of DNA binding proteins, especially after fluorescent microscopy is incorporated[103]. In comparison with other single molecule techniques, this way of force application is intrinsically of high-throughput nature, especially with a high yield of complex assemblies and high efficiency of data collection.
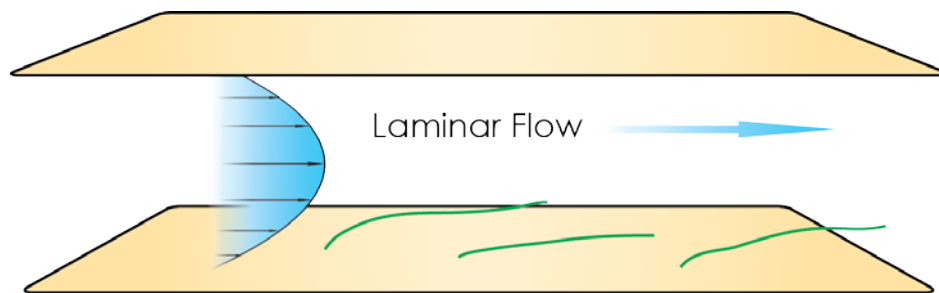
Figure 1.4.1 Hydrodynamic flow applies drag forces on single molecules.
In a microfluidic chamber, the polymers with one end anchored on bottom surface are subject to frictional forces given by laminar flow. The flow speed is maximum in the middle and approximately zero on surface.

Another apparent advantage is laminar flow, which is available with microfluidic device. As for a microfluidic channel in the scale of hundreds of micrometers, the fluid mainly behaves in the form of laminar flow, in which the mixing between two adjacent layers is largely limited to diffusion. This feature significantly benefits the control of fluidic properties and delivery of materials, allowing the studies of highly dynamic processes such as DNA-protein interactions, for example[104].

However, though the microfluidic method has been extensively used to explore DNA properties and reactions, only in a few cases was it related to single molecule studies of actin dynamics. In a paper published recently, Jegou et al. first reported the use of laminar flow to align tethered actin filaments, whereas no stretching force was applied on the polymerizing ends[105]. Later in 2013, based on the microfluidic method, two groups reported their studies on the activities of formin under force, and found that mechanical stretching can promote formin mediated actin polymerization in the presence of profilin[44,106]. However, there are still many challenges, which will be discussed in section 1.4.4.

1.4.2 Optical tweezers

In 1980s, Arthur Ashkin and his colleagues found that a highly focused beam of light can trap and hold dielectric particles in its focus by imposing restoring forces in all dimensions[107]. Optical tweezers was then built based on this principle and has become a powerful tool of manipulation and single molecule force spectroscopy.

As shown in Figure 1.4.2, an objective of high numerical aperture is needed to generate a steep gradient of electric field by tightly focusing the beam of light. Dielectric particle trapped in the gradient experiences attraction forces in the direction of increasing strength towards the center of the focus where the light density is highest. Within a short range (<150nm), the attraction force is always proportional to the displacement from balanced position (center of focus)[100]. As the gradient always tends to keep dielectric objects inside, a trapped particle can be freely moved just by controlling the movement of beam focus, like being clamped by a tweezers.

Optical tweezers can be used to capture many kinds of bio-particles including bacteria and mammalian cells. Single molecule can also be manipulated by linking one of its ends to a microsphere. In order to apply mechanical force, the other end of the molecule is usually linked to a surface or a second microsphere.
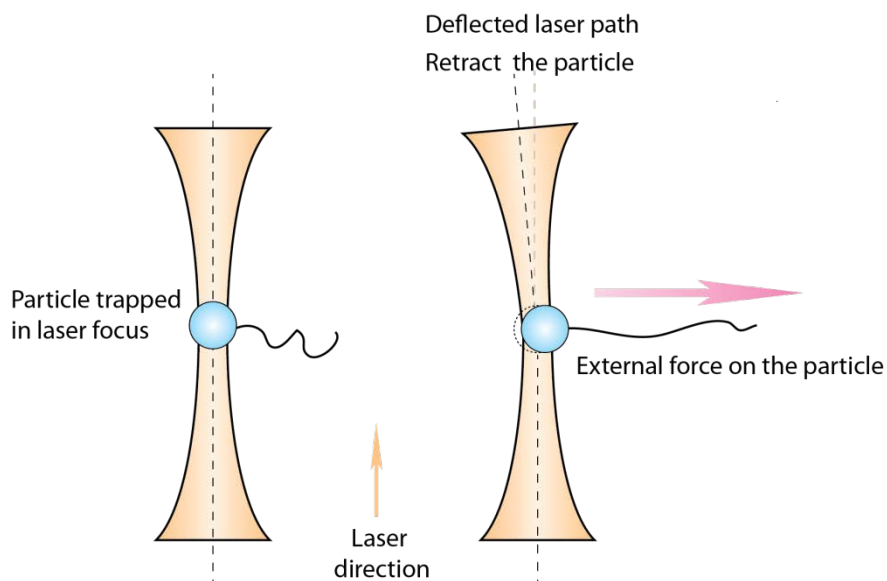
Figure 1.4.2 Illustration of the working principle of optical tweezers.
A highly focused laser beam can trap dielectric particles in the center of focus. Any displacement of the particle from its balanced position will cause beam refraction, which in turn generates a restoring force in the opposite direction. The restoring force can be used to stretch single molecules and manipulate them in three-dimensional space.

Optical tweezers is exceptional in manipulation, as it can move objects freely in three-dimensional space, and in some circumstances can manipulate multiple objects simultaneously. It is also an instrument of high precision, with spatial resolution of sub-nanometer and temporal resolution of sub-millisecond[100]. However, despite these unique advantages, some shortcomings limit its usage in certain conditions. First, it is not an intrinsic source of constant force, unless some special feedback mechanism is incorporated. Second, the lower limit of trap stiffness and thermal fluctuation limits the minimal force that the instrument can apply. Third, effects of photo-damaging and heating may cause severe problems due to the use of high power laser. Forth, because the optical trap does not distinguish dielectric objects from each other, it is very

sensitive to sample purity, which largely limits its application in handling many samples of multiple components or high density.

Optical tweezers has been used to study the mechanics of filamentous actin and actin associated proteins for over 20 years. For example, by holding actin filament as a track, the mechanical properties of myosin movement have systematically investigated[108]. Also, the force dependent severing activity of cofilin has been revealed on tensed actin filaments as templates[109]. However, very few of single molecule experiments have been done to explore the mechanical regulation of actin dynamics, especially by pulling forces. It seems that some creative improvement must be done to overcome the weakness of optical tweezers in pulling dynamic tethers.

1.4.3 Magnetic tweezers

During the past ten years, magnetic tweezers has been frequently used to study DNA and protein mechanics. The instrument is relatively simple compared to other single molecule techniques, comprising mainly a motorized or electric magnet and an inverted microscope.
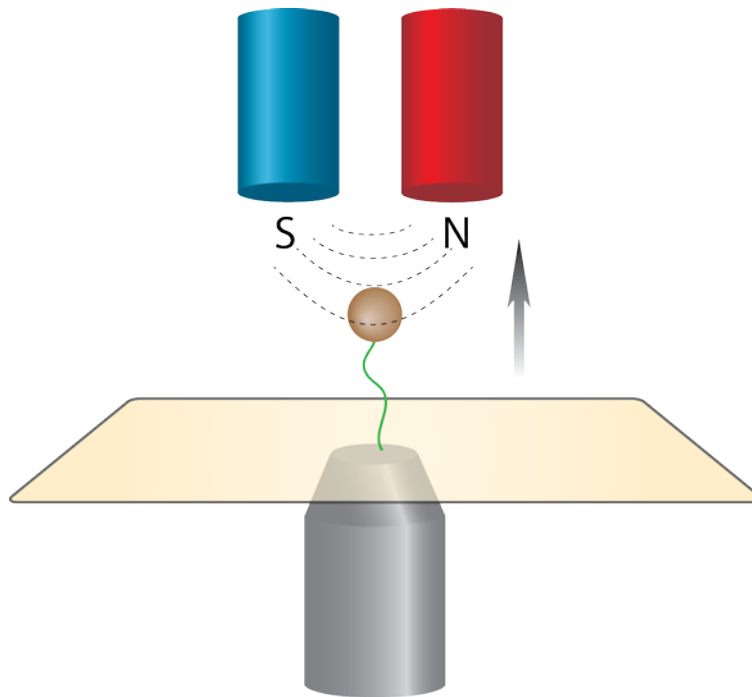
Figure 1.4.3 Illustration of the setup of magnetic tweezers.
In magnetic field, a super-paramagnetic bead will be magnetized and experience attracting force towards the increase of gradient. The magnetic force can be used to stretch single molecules tethered in-between the magnetic bead and substrate. Force magnitude can be adjusted simply by changing the positions of magnet.

As illustrated in Figure 1.4.3, the molecule of interest is usually tethered between a super-paramagnetic bead and substrate. In a given magnetic field, the bead is magnetized and subject to a pulling force, with its magnetic moment $\vec{m}$ aligned in the direction of magnetic field $\vec{B}$. The force is directed along the gradient of increasing field strength, while its magnitude is proportional to the local magnetic flux density $\vec{B}$ as well as the magnetic moment $\vec{m}$ as described by the relationship:

$$\vec{F} = \frac{1}{2}\,\vec{\nabla}\,(\vec{m}\cdot\vec{B})$$

There are many advantages over other single molecule techniques. First, force can be simply controlled by tuning electrical current or the positions of magnets. Because the displacement of bead is neglectable in comparison to the scale of magnetic field, it is in nature a perfect force clamp to maintain a constant force for a long time. Second, The range of magnetic forces is wide and continuous from 0 to 1nN[100]. Third, it is a manipulation technique free from heating, flow and photo-damaging, as the force is applied over a long distance. Forth, because the magnetic moments of beads are aligned with magnetic field, it is easy to achieve bead rotation for studying torque and rotational processes. However, magnetic tweezers may still have some weakness in comparison to optical tweezers, e.g. the weakness in multi-axis manipulation, which may limit its usage in some situations.

In spite of the weakness, magnetic tweezers has been demonstrated powerful in many single molecule studies, including the mechanics of protein unfolding[50], DNA-protein interactions[110], DNA overstretching[111] and DNA supercoiling[112]. However, it was rarely used in studying actin mechanics, probably because of the dynamic nature of actin. The traditional targets of magnetic tweezers are mostly single molecules tethered by covalent bonds or strong pairs like biotin-streptavitin, rather than weak protein complexes like formin capped actin filaments. It strongly implies that some special improvements are necessary to expand the usability of this technique.

1.4.4 Single molecule study of actin dynamics

Single molecule studies of actin dynamics have long been of great interest due to the needs to understand complicated behaviors of cytoskeletal dynamics. The observation of single actin filaments was achieved first by heavy meromyosin (HMM) decoration,

and then the use of fluorescent phalloidin[113,114]. The first manipulation of single actin filaments were done by Kishino et al. in 1988, who stretched fluorescent filaments using glass microneedles[115]. Later, the introduction of optical tweezers provided researchers a powerful tool, which soon became the most popular technique to manipulate single actin filaments with high efficiency, precision and maneuverability. For example, single actin filaments trapped using optical tweezers have been frequently used to explore the kinetics of myosin motors and activities of actin binding proteins such as cofilin and β-catenin[108]. The mechanics of F-actin have also been well studied using optical tweezers.

However, few of these manipulation approaches have been used to study actin dynamics. An exception is the demonstration of the inhibitory effects of mechanical load on actin polymerization. It was done by Footer et al. in 2007, who confined growing actin bundles in-between a trapped bead and a barrier[116]. However, it is worth noting that the objects put under constraint were actin bundles instead of single actin filaments. More importantly, in comparison to compression forces, it seems more challenging to apply tension on the end of a polymerizing filament. An end binding protein is needed to anchor the barbed end while allowing actin polymerization and sustaining force application.

A method that overcomes these challenges is the use of hydrodynamic flow. Drag forces can be applied on the body of filaments in a natural way without any need to build apparatus of force application. In addition, the high-throughput nature of fluidic method ensures high yield of data even when dynamic and weak tethers are pulled.

However, it was only recently that the hydrodynamic flow has been utilized to study actin dynamics at single molecule level. Jegou et al. first published their work that

utilized laminar flow to align actin filaments on TIRF microscopy, but no effect of force was considered at that time[105]. Then in 2013, almost at the same time, two research groups presented their studies that took advantage of the flow drag to study the mechanosensing of formin mediated actin polymerization[44,106]. Both of them reported that in the presence of profilin, the stretching forces applied by laminar flow were able to accelerate formin mediated polymerization. These results supported that formin mediated the mechanosensing of actin polymerization. However, the involvement of profilin may confuse the understanding of underlying mechanisms. It is still unclear which formin domain was involved in force sensing and how these signals were converted into acceleration. Meanwhile, whether these effects were dependent on profilin should be well considered.

Courtemanche et al. also reported an inhibitory effect of force on Bni1 mediated actin polymerization in the absence of profilin[106]. The effect seemed very strong as the polymerization rate was almost inhibited at only 0.3pN. However, it is unclear whether this inhibition was specific to yeast formin Bni1 or due to some particular experimental settings like the use of barrier. This result is simply not consistent with the effects of forces in polymer physics as discussed above, while more proof is needed to explain how profilin can rescue the strong inhibitory effects under very low stretching forces. Meanwhile, the critical concentration – another parameter that was supposed to be influenced by stretching, was not discussed in these studies.

Furthermore, as for the technique, force application by hydrodynamic flow is still far from perfection. First, different from other single molecule technologies, the magnitude of drag force can only be estimated but not directly measured. Large force uncertainty may limit the accuracy of results. Second, since all of the polymerizing

41

filaments were aligned very close to surface, surface interaction may be a problem that interferes filament growth. Third, the medium must undergo fast flow for force generation, which was different from many conventional polymerization assays. It is unknown whether flow could alter the dynamics of polymerization, especially through changing the local concentration around barbed ends. Fourth, because the elongation of filaments can only be determined by fluorescent imaging, it was not easy to obtain high resolution in either spatial or temporal dimension. The spatial resolution is limited by thermal fluctuation and diffraction limit to only several hundreds of nanometers, while the temporal resolution may not be kept higher than several frames per second for long time due to photobleaching and photo-damage. Overall, the weakness of flow method largely limits its usage in investigating many sensitive and weak effects, as well as slow polymerizing events at critical concentration.

In summary, hydrodynamic flow is a high-throughput method powerful in dealing with unstable tethers and fluorescent imaging. It is one of the ideal ways to pull single actin filaments mediated by formin, and provide an early insight into the mysteries of mechanical responses. Other single molecule manipulation techniques such as optical tweezers and magnetic tweezers, should be more powerful with higher precision and reliability. They are especially suitable for investigating slow elongation processes and sensitive responses to stretching, which is hard to be addressed by the methods of microfluidics.

1.5 Objective of this study

As discussed above, pulling forces have been predicted to promote formin mediated actin polymerization, as a part of actin mechanosensing. However, the prediction were made mainly based on in-vivo studies and theoretical analysis, which were insufficient to provide definite evidence. The complex biochemical and mechanical environment in cells largely confuse the understanding of individual processes. Fortunately, the technologies of single molecule manipulation may enable us to manipulate and observe the behaviours of single actin filaments in clean and simplified systems. However, at present, most of them have their own limitations. None of them can meet our needs to stretch single actin filaments and detect their responses accurately.

In consideration of these limitations, my Ph.D research aims to establish proper experimental tools to study the mechanosensing of formin mediated actin polymerization, with high yield, precision and reliability. It will be based on three conventional methods of single molecule manipulation: hydrodynamic flow, optical tweezers and magnetic tweezers. I plan to achieve the goals by modifying these methods, overcoming their individual challenges and creating novel experimental strategies.

Novel tools will enable us to elucidate the mechanical regulation of actin polymerization and the roles of formin in mechanosensing. High spacial and temporal resolution is necessary for studying the effects of weak forces and the influence on critical concentration. These tools can also serve as experimental platforms for many other topics such as the regulators of actin polymerization, the behaviours of other

end tracking proteins and the mechanosensing of microtubule dynamics.These results

will deepen our understanding of mechanotransduction and cytoskeleton organization.

CHAPTER 2 Materials and Methods

2.1 Protein purification

GST-mDia1-ΔN3 purification

Human formin mDia1-ΔN3 (FH1-FH2 domains) was originally cloned in pGEX-4T-1 expression vector (GE Healthcare) with an N-terminal GST tag. Protein purification was performed in Rosetta 2 competent cells (Novagen). At the beginning, the cells were cultured at 37°C in 2L terrific broth medium containing ampicillin and chloramphenicol (Sigma). After O.D. 0.8 was reached, 0.5mM IPTG was added to induce expression during a 18-hour shaking at 16°C. Cells were then harvested by centrifugation and suspended in cold buffer A (50mM Tris, pH 8.0, 200mM NaCl, 5mM EDTA, 5mM DTT and Roche protease inhibitor cocktails). From then, all steps must be done on ice or at 4°C. Cell lysis was collected by sonication and clarified by high-speed centrifugation (12000rpm for 1h). The suspension was then incubated with 2ml glutathione sepharose 4B (GE Healthcare) for 1h, followed by a wash with at least 20ml buffer B (buffer A plus 0.05% thesit from Sigma). Proteins were then eluted using 3ml buffer C (50mM Tris, pH 8.0, 50mM NaCl, 1mM EDTA, 1mM DTT, 50mM reduced glutathione and 0.05% Thesit), and dialyzed against buffer D (50mM Tris, pH 7.0, 50mM KCl, 1mM EGTA, 5% glycerol, 1mM DTT and 0.01% NaN_3) for 24h. After determining concentration using Pierce assay (Thermo Fisher Scientific), the proteins were aliquoted, snap frozen in liquid nitrogen and stored at -80°C. After being thawed, the mDia1 proteins would be used within one week.

Biotinylated-mDia1-ΔN3 purification

In order to produce biotinylated mDia1- ΔN3 protein, a DNA sequence that encoded Avitag (CGTGGATCCGGTGGCGGTCTGAACGACATCTTCGAGGCTCAGAAAATCG AATGGCACGAAGGTCGACTCG) was inserted into GST-mDia1-ΔN3 sequence between the restriction sites of BamHI and SalI. The Avitag was then located in-between the N-terminal GST-tag and FH1 domain. There was also a thrombin cutting site between the GST tag and Avitag.

Biotin-mDia1-ΔN3 was prepared according to the purification of GST-mDia1-ΔN3, except for GST cleavage and biotinylation. After column wash, Avitag-mDia1-ΔN3 was cleaved from GST tag by overnight incubation with thrombin (Sigma) in buffer C without glutathione at 4°C. The cleavage step should release avitag-mDia1-ΔN3 into suspension, which was then eluted using buffer C without glutathione. After determining protein concentration, the solution was changed to buffer R (10mM Tris, pH8.0, 10mM NaCl) using ultrafiltration (30k, Millipore) for biotin labeling. Biotinylation reaction was started by mixing the protein with BirA enzyme (biotin protein ligase), biotin and biomix buffers (Avidity, LLC). After 0.5-hour incubation at 30°C, the proteins were changed to buffer D using ultrafiltration and stored at -80°C in small aliquots.

2.2 Actin polymerization

Actin polymerization

G-actin was purified from rabbit muscle acetone powder (Pel-Freez Biologicals) according to Pardee et al.[117], and kept in cold G-Ca buffer (2mM Tris, pH 8.0, 0.1mM $CaCl_2$, 0.01% NaN_3 with freshly added 0.5mM DTT and 0.2mM ATP). F-actin was prepared by mixing G-actin with polymerization buffers, according to Kovar et al.[43,118]. In general, G-actin is diluted into G-Mg buffer (basic G-Ca buffer containing 0.1mM $MgCl_2$ instead of $CaCl_2$) 5 minutes before polymerization. Then polymerization can be started by adding 1/10 volume of 10×KMEI buffer (100mM imidazole, pH7.0, 500mM KCl, 10mM $MgCl_2$ and 10mM EGTA). Polymerization is allowed at RT for 20-30min to prepare F-actin. After that, phalloidin of the same concentration can be added to label and stabilize F-actin. The F-actin will be kept on ice and used within two hours if formin is added.

Pyrene polymerization assay

Pyrene labeled actin was purchased from Cytoskeleton, Inc. Pyrene polymerization assay is especially sensitive to protein quality and procedure. Freshly prepared G-actin was used and mixed with 10% pyrene-G-actin in G-Ca buffer. The mixture should be 2× of the final actin concentration, which allowed the future addition of formin in 1:1 ratio. Capping proteins (10nM) can be added as optional to inhibit spontaneous polymerization and test the exclusion effects of formin. At the same time, formin mDia1 proteins should be diluted to 2× of the final concentration in polymerization buffer (1×KMEI + 0.5mM DTT and 0.2mM ATP). Before the assay,

the fluorimeter must be switched on and all buffers should be warmed to RT. At 2 minutes before polymerization, 0.1 volume of 10×ME buffer (10mM EGTA and 1mM $MgCl_2$) was added to G-actin to allow ion exchange. Polymerization was started by the addtion of 0.1 volume of 10×KMEI to G-actin, which was immediately followed by the mixture with mDia1 or control buffer. The solution was mixed rapidly without bubble and then loaded into the wells of fluorimeter (Tecan Infinite M200) with illumination at 360nm and recording at 405nm. Data was collected every 20 seconds until the plateau was reached. The lag time before recording was not accounted.

Polymerize actin filaments from microspheres

In the flow chamber, biotin-mDia1-ΔN3 proteins were first coated on the immobilized streptavidin microspheres. G-actin mix was prepared by mixing Alexa-568 actin (Life technologies) and unlabeled G-actin in a ratio of 3:7. After adding ME buffer, the mixture was diluted in imaging buffer (polymerization buffer plus 3mg/ml glucose, 100μg/ml glucose oxidase and 18μg/ml catalase) to a final concentration of 1μM (30% labeled with Alexa568). This solution was then immediately flushed into the chamber for polymerization on microspheres. Filament growth from bead surface was observed for 10 minutes in red channel on Zeiss confocal microscope at 15s/frame.

Prepare actin filaments for single molecule experiments

Fluorescent actin filaments with biotin-mDia1-ΔN3 was prepared according to the basic protocols, except for the addition of mDia1. At the beginning, G-actin was first mixed with biotinylated mDia1 in G-Mg buffer. Then 10×KMEI was added to start polymerization. After 20-minute incubation at RT, alexa-488 phalloidin was added for to label and stabilize the filaments. The solution will be kept on ice until use. In particular, a final volume of 50ul was always prepared, which contained 2μM F-actin, 2μM alexa-488 phalloidin and 50nM biotin-mDia1-ΔN3. The concentration of mDia1 and phalloidin may be different depending on particular requirements. Dilution was always made before imaging. As for the polymerization on streptavidin microspheres, 1/10 dilution was normally used.

As for GST-mDia1-ΔN3, however, a step of incubation with anti-GST antibody was needed before polymerization. Normally, GST-mDia1 was mixed with the antibody in a molar ratio of 5:1 in G-Mg buffer. After 1h incubation on ice, the mixture of mDia1 can be added to G-actin to a final concentration similar to the above. Polymerization can then be initiated with the addition of 10×KMEI and stabilized with phalloidin. If biotin labeling is needed, biotin-G-actin can be added to unlabeled G-actin in a final ratio of 10%. Finally, a ten-times dilution was always used to obtain anchored filaments on protein A-coated coverslip surface.

2.3 Surface treatment

Glass surface functionalization with APTES

APTES treatment can fully cover the glass surface with a layer of amino groups. Before treatment, the coverslips (20×30mm, No. 1.5, VWR) have to be cleaned by several steps. First, they were sonicated in Decon 90 detergent for at least 2 hours, followed by two consecutive 15-minute sonication in methanol and acetone. The coverslips were washed with MilliQ water after each sonication. After that, they were treated with plasma to remove any superficial organic residue. Then, the clean surface were immediately sinked in methanol containing 1% APTES for coating. After 40 min stand at RT, the coverslips have to be thoroughly washed with methanol and MilliQ water and dried for storage.

Biotin-PEG surface

PEG molecules can be covalently linked to superficial amino groups via their terminal NHS ester groups SC (succinimidyl carbonate) or SVA (succinimidyl valerate). If so, the other ends of the molecules can be exposed out of the PEG layer for ligand binding. In practice, a mixture of methyl-PEG and biotin-PEG was used to provide a hydrophobic surface with superficial biotin. For each pair of the APTES coverslips, a mixture of 4 mg methyl-PEG-SVA (MW 2000, Laysan Bio, Inc.) and 0.1mg biotin-PEG-SC (MW 3400, Laysan Bio, Inc.) was used with a final ratio of ~2.5% biotin-PEG in weight. The PEG powder can be dissolved in 40ml freshly prepared buffer that contains 100mM $NaHCO_3$. The solution should then be dropped onto the glass surface immediately after dissolution (within 1 min) to avoid

hydrolysis. By covering the other piece of glass onto this coverslip, a sandwich was formed with the PEG solution in between. After a 4-hour functionalization, the coverslips can be washed and air-dried for storage.

COOH-PEG surface and protein coating

COOH-PEG-SC (MW 3400, Laysan Bio, Inc.) can be coated on APTES glass surface as biotin-PEG-SC, and gave a hydrophobic surface with exposed carboxylate groups. These groups, upon activation, can be used to link proteins via their amino groups. The activation was always done after making flow chamber. Normally, 2mg EDC (E7750, Sigma) and 3mg NHS (130672, Sigma) was used to functionalize four chambers. After being dissolved in 120μl MES buffer (100mM MES, pH 6.0), they must be immediately added into the chambers. After 15min incubation at RT, the chambers were intensively washed with PBS, which was followed by the addition of 30ul 0.05mg/ml Protein A. After 4-hour incubation, the chamber can be washed with PBS again to remove free protein A.

2.4 Flow chamber assembly

Our flow chamber mainly consists of three layers. The top layer is mainly a piece of acrylic with three holes for tubing connection. The bottom is a piece of functionalized coverslip. In the middle there is a layer of parafilm with patterned microfluidic lines. The parafilm has to be melted in-between the top and bottom for 15 seconds at 85°C. It is worth noting that the parafilm should be attached gently to avoid the change of

pattern size. After that the chamber can be sealed with silicone gel as optional to avoid leaking. Finally, the height of parafilm was measured to be 130µm.

The Y-shape microfluidic lines can be made using a cutting plotter (Graphtec). The parafilm is of 36mm in length and 18mm in width, which is slightly smaller than the coverslip (40×22mm). The main stream line is 12mm long and 1.5mm wide. The three ends of the Y-shape pattern are designed to fit the holes on acrylic top. Buffer will be input via the two arms of the Y-shape and form laminar stream in the main line. In particular, one of the inlets was designed to be a reservoir for buffer exchange, while the other inlet and the outlet was connected to syringe pumps with hard tubing. All connections on the chamber were fixed using epoxy. The rate of pump withdrawing at outlet should be faster than that of pushing at inlet, whose difference defined the rate of flow entering from reservoir.

2.5 Force calibration

The magnetic force was calibrated using a lambda DNA which is 48502bp long. Both of its two ends were labelled with biotin, for being tethered in-between a magnetic bead and coverslip surface. Due to thermal fluctuation, the bead underwent Brownian motion like a fluctuating pendulum. According to equipartition theorem, the force can be measured as a function of the transverse fluctuation δ_y^2 along the direction of magnetic field[119]:

$$\frac{f}{l} = \frac{k_B T}{< \delta_y^2 >}$$

where l is the average extension of DNA in the direction of force.

At a certain magnet position, the pulling force can be calculated from l and δ_y^2. The minimal time that is needed for accurate δ_y^2 determination can be known from $\tau = \frac{3\pi\eta r}{k_B T}\delta_y^2$, where η = 10^{-3} kgm^{-1}s^{-1} is dynamic viscosity and r is bead radius. Considering that the lambda DNA was of 16491nm in contour length and the bead was of 1.4μm in radius, we can know that the τ ranged from 1.19 to 0.01 seconds at the forces between 0.1 and 20 pN. In practice, at least 30 seconds were used for measurement at each force.

Then a set of force f and extension l was obtained. These data were used to fit the worm like chain (WLC) model of DNA force extension, as given by Marko – Siggia formula[120]:

$$\frac{fA}{k_B T} = \frac{l}{L} + \frac{1}{4(1 - \frac{l}{L})^2} - \frac{1}{4}$$

where L is the contour length of the DNA and A is persistence length. When force is larger than 0.1pN, an approximation can be used:

$$\frac{l}{L} = 1 - \sqrt{\frac{k_B T}{4Af}}$$

Fitting this formula will return the persistence length A. By comparing the measured A with known value, we can know the quality of the force extension curve and the effectiveness of force application. In normal conditions, the persistence length of B-form DNA was reported to be 50nm[121,120].

CHAPTER 3 Stretching Polymerizing Actin Filaments Using Hydrodynamic Flow

3.1 Introduction

Hydrodynamic flow is an intrinsic high-throughput method that can stretch multiple filaments simultaneously. It is especially efficient in obtaining statistical data. Here, a setup of dual flow line was used to provide a reliable control of buffer exchange and actin concentration. TIRF microscopy was also used to detect the elongation of single actin filaments in high contrast.

Before measurement, quality of the home made proteins including G-actin and biotin-mDia1-ΔN3 (FH1-FH2) was first tested. The purified mDia1 was proven to be active in actin nucleation and polymerization. It was also shown that the binding and polymerization of F-actin on microspheres was specific to mDia1 proteins.

At first, local flow velocity was determined by calibration of laminar flow profile, by which drag forces can be estimated as a function of filament lengths and flow velocities. Considering the promoting effects of profilin, we first examined actin polymerization in the presence of profilin and found that the polymerization rates gradually increased as the filaments became longer, which was probably a result of force increase. Then the effect of stretching was tested by changing flow speed. In the absence of profilin, some effects of acceleration in response to force increase were found. To quantify this effect statistically, a group of data was collected from independent experiments, with stretching forces estimated from 0 - 1.8pN. However, it was hard to conclude any significant force dependent change of polymerization rates, simply because of the large statistical errors. Finally, tests were also done with

low level of G-actin to investigate critical concentration. It was found that polymerization was accelerated slightly with low concentration of G-actin and even occurred at critical concentration. This result was in principle equivalent to a decrease of critical concentration. However, it seems not easy to validate these findings due to the large variation of force and elongation rates, especially when polymerization was slow.

In summary, the result with profilin indicates that the method of hydrodynamic flow is effective in applying forces on polymerizing filaments. The promotion may be mediated by FH1 domain and profilin in a mechanism different from FH2 activity, but suggests a potential pathway to remodel actin cytoskeleton in vivo. The effects on profilin independent polymerization may be too weak to be detected with current system. Some methods of higher resolution and accurate forces are needed to provide reliable results.

3.2 Strategy and methods

It has been known that actin filaments are highly prone to mDia1 dissociation because of their low affinity[73]. This factor may limit data collection for statistics. Hydrodynamic flow may solve this problem as a high-yield method. The flow chamber can provide large surface area for binding of multiple filaments. Simple setup also reduces the time of sample preparation, which allows more time of measurement before dissociation.

Figure 3.1 illustrates the design of the microfluidic chamber and the strategy to stretch single actin filaments. The Y-shape chamber allows fast buffer exchange

between two flow lines. The reservoir is used to deliver different materials, which is important to protein complex construction. The flow speed can be precisely controlled using two syringe pumps. The flow speed of the reservoir is equal to the difference between the two pumps.

Actin filaments are needed to be anchored via mDia1 for force application. Biotinylated mDia1 can be anchored on streptavidin microspheres which are immobilized on bottom surface. The beads help to mark the barbed ends of actin filaments and reduce non-specific interactions by levelling the filaments up. The filaments may be aligned more straight in laminar flow and experience more uniform drag forces in comparison with surface anchoring.
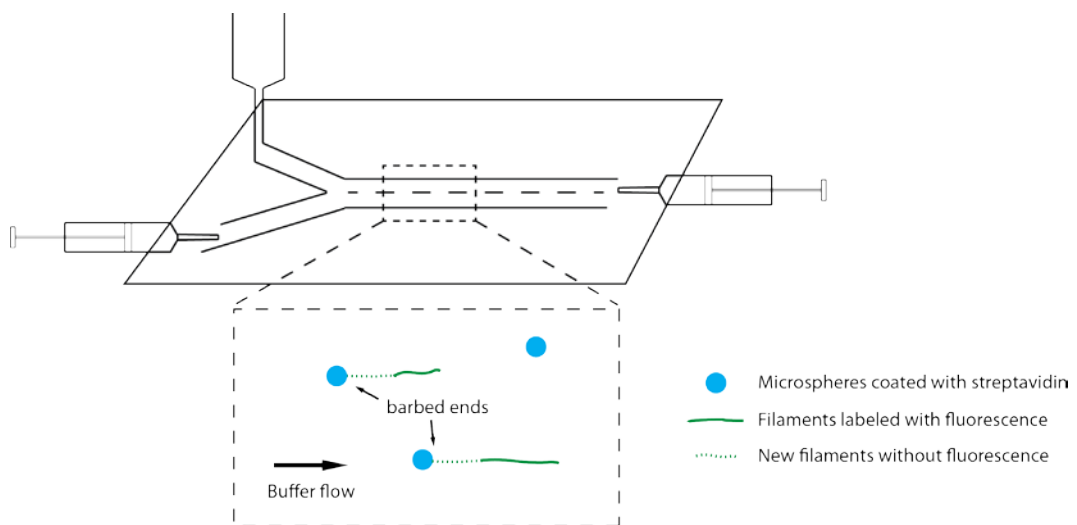
Figure 3.1 Illustration of the flow chamber and experimental strategy

In summary, the experimental procedures are designed as:

1. Assembly the flow chamber with functionalized coverslip for bead immobilization. Actin filaments labelled with biotinylated mDia1 proteins may have chance to bind the surface of microspheres.

2. F-actin is polymerized with biotin-mDia1-ΔN3 in Eppendorf tube, and then stained and stabilized with Alexa-488 phalloidin.

3. Flush prepared F-actin into the chamber. Some filaments are able to be trapped on bead via their barbed end mDia1 proteins. The density of anchored filaments is observed in real-time using TIRF microscopy.

4. When an optimal density is reached, the buffer will be immediately changed to unlabelled G-actin of interested concentration.

5. The bulk flow speed can be kept constant for force application. Time-lapse images are recorded for the analysis of polymerization rates.

3.3 Results

3.3.1 Preparation of formin, G-actin and F-actin

Diaphanous related formin (DRF) mDia1 is of our interests because it is a well-studied mammalian formin that has evidence in mediating the mechanosensing of focal contacts. A constitutively active mDia1 that contains only FH1 and FH2 domains (mDia1-ΔN3) is used as in many in-vitro polymerization assays. GST tagged mDia1-ΔN3 was purified according to Kovar et al[43]. In order to increase the

efficiency of immobilization, an Avitag that can be biotinylated was inserted into the GST-mDia1 construct in-between the N-terminal GST-tag and FH1 domain. The GST-tag was finally removed during purification, and biotin was labelled on Avitag via in-vitro biotinylation assay.

The activities of purified proteins must be examined. Using pyrene polymerization assay, the nucleation activities of the biotin-mDia1-ΔN3 were first tested. As shown in figure 3.2, spontaneous nucleation and polymerization in the sample of control occurred slowly as the fluorescence gradually increased. Capping proteins were added to further inhibit spontaneous polymerization but not formin mediated actin nucleation and polymerization. It can be seen that the addition of biotin-mDia1-ΔN3 dramatically accelerated the formation of new actin filaments, indicating that the purified protein was active in nucleation.

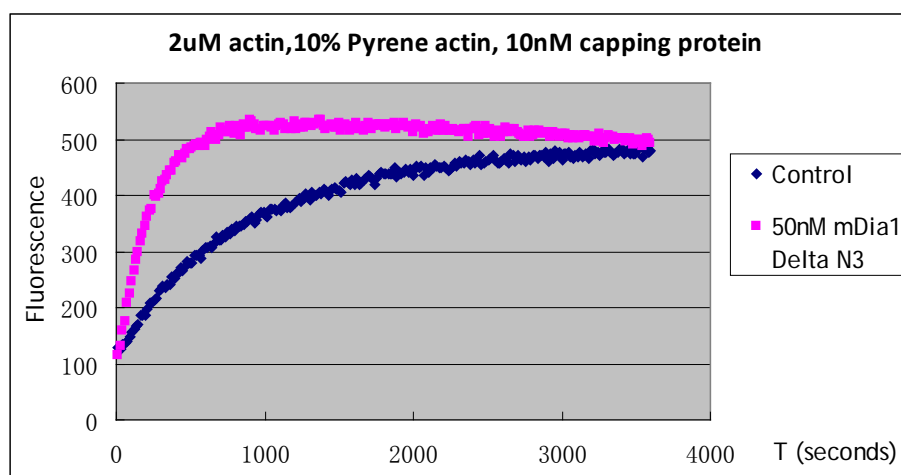**Figure 3.2 Purified biotin- mDia1-ΔN3 was active in actin nucleation.**
Blue curve represents the sample of control with 2μM G-actin and 10nM capping protein. 10% G-actin was labelled with pyrene fluorophores. The sample of pink curve contained 50nM biotin-mDia1-ΔN3 proteins. Active formin mDia1 dramatically increased the rate of actin nucleation, with a time of half increase ≈ 160 seconds compared to ~720 seconds.

Since actin filaments are needed to be anchored via mDia1, its coating on streptavidin bead surface was tested. Figure 3.3 shows the binding of biotin-mDia1-ΔN3 proteins which was detected by immunostaining against mDia1 FH2 domain. This result indicates that biotin was indeed labelled on the Avitag of mDia1 and can mediate its surface anchoring.

Green   Bright   Overlay
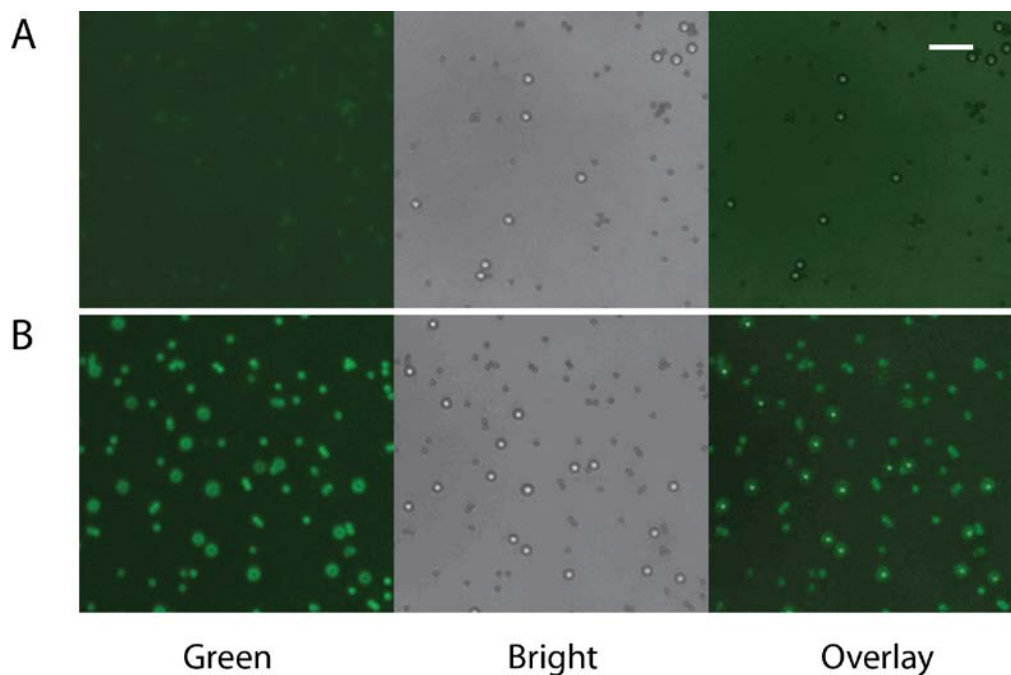
Figure 3.3 Biotin-mDia1-ΔN3 proteins can be coated on streptavidin microspheres. The effectiveness of coating was examined by immuno-fluorescence staining. The beads without mDia1 coating (A) were used as the control for treated beads (B). Both groups contained 3µm polystyrene beads and 1µm magnetic beads. (A) The polystyrene beads showed no fluorescence, while the magnetic beads exhibited weak auto-fluorescence. (B) Both kinds of beads were stained with strong fluorescence. Scale bar = 10 µm.

However, even the mDia1 proteins were able to be immobilized, whether they were still active in actin polymerization was still unclear. To confirm this issue, the specificity of actin filaments to superficial biotin-mDia1-ΔN3 was first examined. By in-vitro polymerization reaction, a mixture of actin filaments was prepared and

stained with Alexa-488 phalloidin. The F-actin exhibited filamentous appearance in green fluorescence as shown in Figure 3.4. For the microspheres coated with mDia1, actin filaments were preferentially accumulated around its surface (Figure 3.4 A). In contrast, the filaments had an even distribution around the streptavidin microspheres without mDia1, indicating a high specificity between actin filaments and superficial biotin-mDia1-ΔN3 (Figure 3.4 B). Non-specific interaction between actin and the microspheres can be neglected.
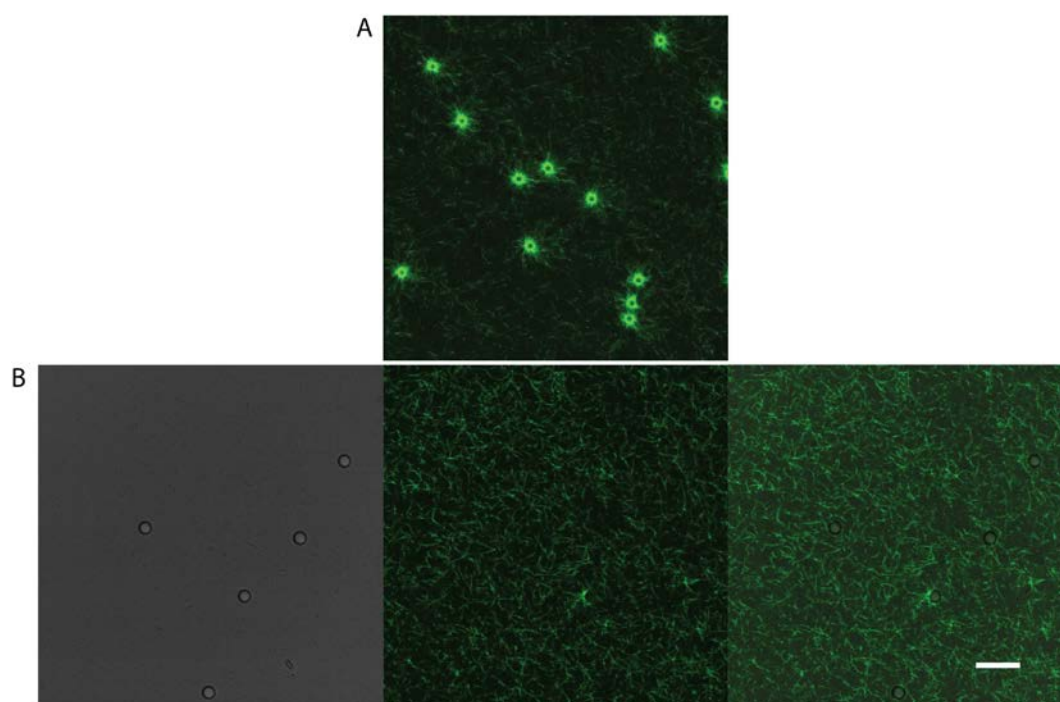
Figure 3.4 Actin filaments selectively bound the microspheres coated with biotin-mDia1-ΔN3. (A) Confocal image of fluorescent filaments around the microsphere coated with mDia1. The F-actin in solution was of 1μM and stained with 1μM Alexa-488 phallodin. (B) From left to right: bright field image of the control microspheres, confocal image of F-actin around, overlay of microspheres and F-actin. Scale bar = 10 μm.

Since the specificity has been established, real-time observation of polymerization was needed to confirm mDia1 polymerization activity. In a chamber that contained some microspheres with mDia1 coating, G-actin proteins were added in the condition of polymerization. 30% of the G-actin was labelled with Alexa-568 fluorophore, and hence can show the elongation of filaments in real time. It can be seen from Figure 3.5 that fluorescent actin filaments accumulated around the beads and gradually became longer as a process of polymerization. Considering the specific interactions between F-actin and microspheres, it is reasonable to think that the polymerization was mediated by mDia1 on microspheres.
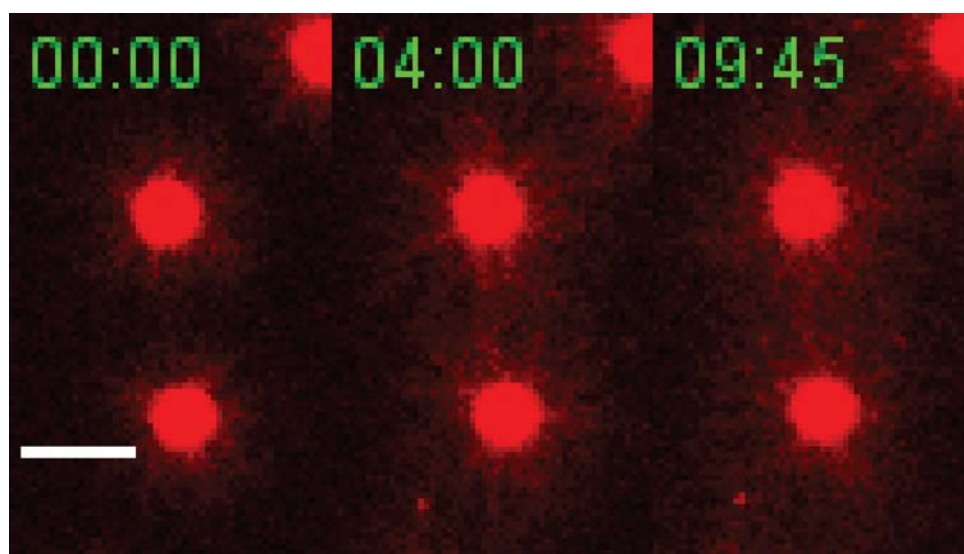
Figure 3.5 Biotin-mDia1-ΔN3 coated on microspheres was active of actin polymerization. The images were taken using confocal microscope, with 1µM actin and 30% Alexa-568 actin, 15s per frame, 10min duration. Scale bar = 10µm.

3.3.2 Actin filaments were subject to stretching forces in laminar flow

In our strategy, laminar flow was used to pull single actin filaments whose barbed ends were anchored via biotin-mDia1-ΔN3. In order to obtain single actin filaments in an efficient and well-controlled way, the filaments were first nucleated and polymerized in solution by incubating G-actin with mDia1 together. The length and density of F-actin can be tuned simply by controlling the ratio between mDia1 and actin. After polymerization, Alexa-488 phalloidin was added to stabilize and stain the filaments. In this solution, the majority of F-actin would be in single form due to the lack of bundling proteins, and many of them were likely to have mDia1 remaining on their barbed ends as products of mDia1 nucleation.

It now became convenient to obtain single tethers on microspheres by flushing in the prepared actin filaments. Simply by diffusion, some actin filaments with biotinylated mDia1 capping can be anchored on the microspheres via their barbed ends. The amount of anchored filaments kept increasing along incubation time and was related to F-actin concentration and microsphere density. Overlong incubation was likely to produce multiple tethers on a single microsphere. Therefore, in order to obtain an optimal experimental condition, the process of anchorage was monitored by TIRF in real time. In my experiments, in a field of view ($130 \times 130 \mu m^2$) that contained ~20 microspheres, a density of no more than eight tethers was chosen. In this condition, there were normally only a few cases of multiple tethers, which can be further removed by image analysis. If there is a requirement of high yield, multi-field imaging mode can be taken for data acquisition.

For the tethers linked to beads, most of them were able to polymerize in the buffer of G-actin. The G-actin proteins for elongation were not labelled, and hence gave rise to

a dark gap between the fluorescent fragment and the microsphere, as shown in figure

3.6A. From the kymograph of a single polymerizing filament, we can clearly see its

displacement from the anchoring point on bead surface. The polymerization rate in

flow direction can be quantified by tracking either its fluorescent fragment or

unlabelled gap.
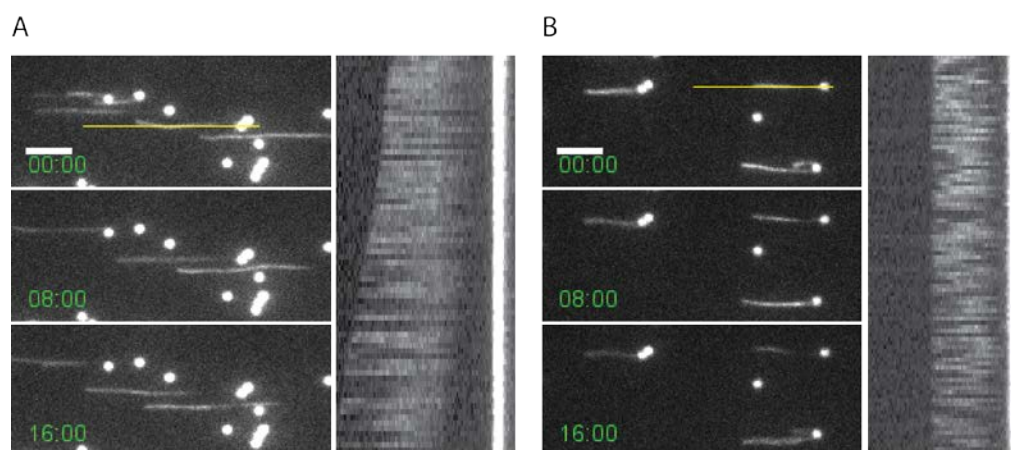
Figure 3.6 Polymerization of single actin filaments in laminar flow.
The actin filaments were prepared in tube with biotin-mDia1-ΔN3 and stained with
Alexa-488 phalloidin. The filaments were stretched in the buffer containing (A)
0.3µM G-actin; (B): 0.3µM G-actin and 0.2µM cytochalasin D. The bright dots were
1µm streptavidin magnetic beads with auto-fluorescence. Scale bar = 5µm.

To validate that the emerging of dark fragment was a result of actin polymerization,

cytochalasin D – a drug selectively inhibiting actin polymerization at barbed ends

was added as a negative control. Figure 3.6B shows that the inhibition of filament

growth by 0.2µM cytochalasin D, indicating the specificity of actin polymerization.

3.3.3 Determine the profile of flow velocity and calculate drag force

Different from other single molecule manipulation technologies, it is hard to directly measure the drag forces applied by hydrodynamic flow in a well-established way. However, based on the principle of frictional force, its magnitude should be approximately proportional to the factors including viscosity, local velocity and the length of molecules, as given by the formula:

$$F = \gamma v = \frac{2\pi\eta L}{\ln\left(\frac{L}{2r}\right) - 0.2} v$$

Where γ is denoted as parallel drag coefficient, η is fluid viscosity, 2r is the diameter of the rod-like molecule, L is its longitude length, and v is the local fluidic velocity[40]. The stretching force sensed by an anchoring end, in fact, is an integral of the drag forces along the whole filament. Here, because of its uniformity and large persistent length, a tensed actin filament can be approximated to be a cylinder-like rod that is considerably straight in the scale of ten micrometers. Local flow velocity is also likely to be uniform because of the laminar feature of the fluid. Therefore, it seems reasonable to obtain an approximate force from filament length and local flow velocity. Considering that the length can be measured by fluorescent imaging, a strong need is arised to determine local flow rates.

According to the principles of fluidic mechanics, laminar flow is the major form of fluid in the chamber of centimetre scale. The flow speed v is in theory a parabolic function of height h, as given by the function: $v\,(h) = 6\,h\,(H - h)R/(H^3 w)$, where H is the height of the chamber, w is the width and R is the bulk flow rate.
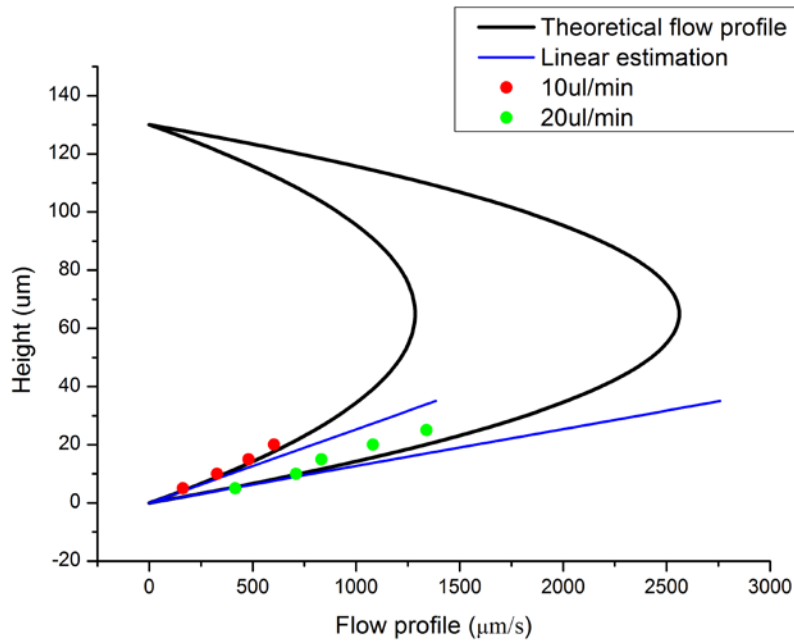
Figure 3.7 Calibration of the flow profile in microfluidic chamber.
Bulk flow speeds of 10 and 20 µl/min are plotted in red and green, respectively. The black curve is the theoretical flow profile, while blue curve is linear approximation.

As illustrated in figure 3.7, the flow speed is supposed to be highest in the middle of the chamber, while approximately zero at boundary due to the friction with surface. Especially, in the layers very close to surface, the increase of flow speed can be considered to be linear: $v(h) = 6 h R/(H^2 w)$, which largely simplifies the determination of flow speed at the sample level of filament stretching. The blue line in figure 3.7 is the linear approximation. It can be seen that the linear approximation well coincides with the parabolic estimation under 10µm, and thus, can be used to calculate the velocity above surface.

Flow profile was determined by tracking 100nm fluorescent microspheres at different flow layers. The objective can be focused at different heights from bottom surface precisely using a piezo controller. In practise, the speeds of fluorescent microspheres

in a flow of 10µl/min were tracked at the heights of 5, 10, 15 and 20µm respectively, as shown in red dots in Figure 3.7. It can be seen that these data basically fitted the predicted flow profile. As for the data of 5 and 10µm high, linear approximation was also well fitted with a slope of 32.8µm/s per micrometer of height increase.

As given by the formula of flow profile, local flow velocity is a linearly dependent on bulk flow speed. Therefore, the flow profile was also measured in another bulk flow speed. In figure 3.7, as for 20µl/min, the local flow rate in proximity to surface can be fitted by parabolic formula, though the data at 15, 20 and 25µm deviated from theoretical curve, probably because the microspheres flew too fast to be accurately tracked. In contrast, the data of 5 and 10µm fits both parabolic and linear curves well, supporting the accuracy of flow determination above surface. The speed increment of 20µl/min is fitted to be 70.9µm/s per micrometer, which was just about two-fold of 10µl/min.

Therefore, we can now assume the flow velocities of different bulk flow speed. Calculation of force was benefited from the use of microspheres, as the anchored filaments are likely to be aligned in parallel to surface. Considering the fluctuation of the height of individual filaments, an average value of 0.5µm – half of the microsphere size was taken for force calculation. It is to some extent reasonable because 0.5µm should be the average height of formin and fluctuating fragments in statistics. It was also supported by the similar fluorescent intensities of actin filaments in TIRF imaging.

Based on the theoretical formula, drag force can be calculated by multiplying length and velocity. Taking the local flow velocity v of 0.5µm high to be 16µm/s per 10 µl/min, viscosity η as 1×10^{-3} kg/(m·s) and 2r as 8nm, we can obtain a viscous drag of

about L*v/1000pN (assume $\frac{2\pi}{\ln\left(\frac{L}{2r}\right)-0.2} \approx 1$, then $F \approx \eta L v$, L and v are value in micrometers).

3.3.4 Polymerization was accelerated by flow drag in the presence of profilin

Using this system of microfluidics, the effects of stretching forces on actin polymerization were first examined in the presence of profilin, taking advantage of its functions of acceleration. Figure 3.8 presents the polymerization event of an actin filament under stretching forces. Elongation occurred in the buffer containing 1μM G-actin and 1μM profilin, in a constant flow of 5μl/min. The original length was 5μm.
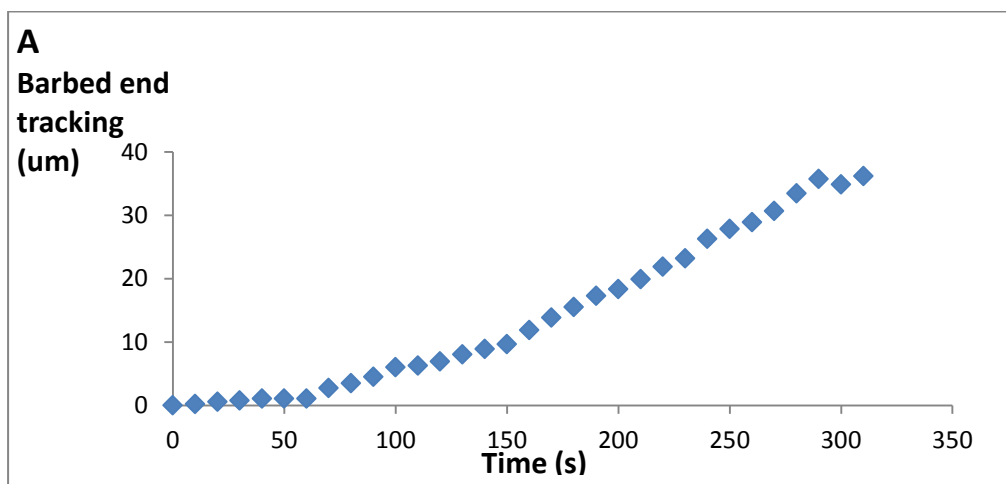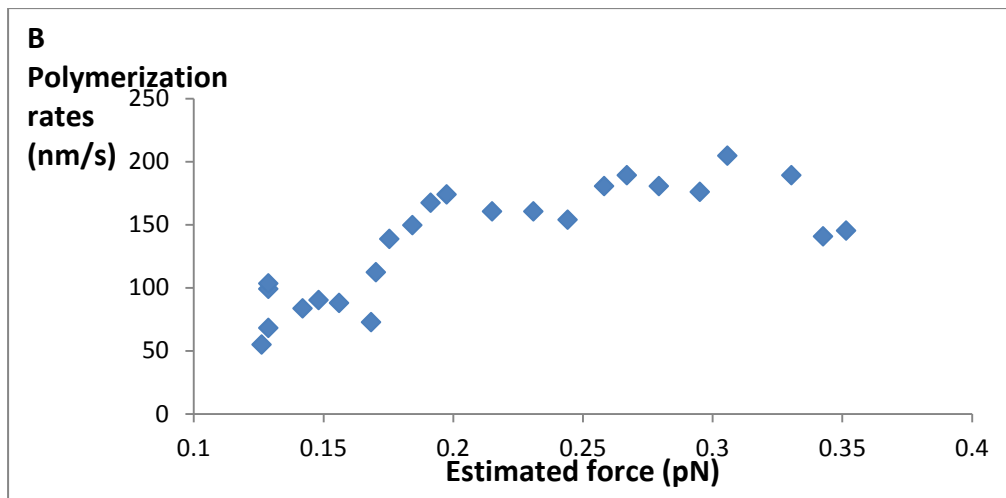
Figure 3.8 Actin polymerization was accelerated as filaments elongated in the presence of profilin. (A) The elongation of a filament is shown. Its barbed end is being tracked due to low fluctuation (B) The polymerization rate of the filament is plotted against estimated force. Linear fitting was done for this set of data.

From the elongation curve, it can be seen that the polymerization rate gradually became faster as the length became longer. Because stretching force was approximately proportional to the length of filament and length was the only property appearing to change during polymerization, the increase of polymerization rates was very likely resulted from force increase. When polymerization rates were plotted against the calculated forces, as shown in figure 3.8B, a positive relationship can be obtained between polymerization rate and force, which suggested that stretching forces promoted mDia1 mediated actin polymerization in the presence of profilin.

This observation supports the mechanosensing roles of formin in mediating actin polymerization in cells. It is also consistent with the observation made by two other teams. However, the underlying mechanism is still unclear, because profilin is able to trigger actin ATP exchange and promote the recruitment of G-actin to FH1 domain. Involvement of profilin and its partner FH1 domain may complicate the

understanding of the mechanical responses – which player among FH2 dimer, FH1 domains and actin itself is responsible?

Interestingly, FH1 domain has been predicted to be unstructured, and mechanical force may has significant influence on its conformation[122]. It is unclear how large does this kind of conformational change contribute to the force induced acceleration. In addition, profilin needs to dissociate from terminal actin to complete a cycle of polymerization. Therefore, it may also be possible that the stretching forces promote actin polymerization by accelerating profilin dissociation. In this case, it is still unclear how FH2 domain and F-actin behaves in this mechanosensing event. Therefore, it seems necessary to investigate the effects of stretching forces in the absence of profilin.

3.3.5 Stretching force may promote actin polymerization in the absence of profilin

Formin-mediated polymerization from G-actin alone is apparently slower than from profilin-G-actin complexes by a fold of 3-6 times, which may cause a problem to force application. In the presence of profilin, the filaments can elongate very fast, resulting in a significant length increase during observation. The polymerization without profilin, however, may not give a so large length increase for the filament to experience different drag forcces in a constant flow. Therefore, force change was done by tuning the flow speed.

Figure 3.9 shows the elongation of an actin filament in different flow speeds. The solution contained 0.4μM G-actin. The filament experienced bulk flow speeds of

10µl/min for 400 seconds, 40µl/min for 120 seconds and 10µl/min for 100 seconds consecutively. Linear fitting was done for each speed and gave the individual polymerization rates of 11.7, 16.6 and 8.7 nm/s. It can be seen that the elongation rates increased as the flow speed was increased by 4 times, and then decreased when the flow was slowed down. This result suggests that stretching forces may promote the mDia1-mediated polymerization even in the absence of profilin.

Though both of the two rates measured under the flow of 10µl/min were slower than that of 40µl/min, the last rate with a longer filament length was shown even slower than the first one. This is probably resulted from the low accuracy of quantification. Considering the large fluctuation of filament in buffer flow, the spatial resolution may be only of several hundreds of micrometers. As such, the growth rate may not be well measured by the automated image analysis, especially when the number of data is limited and photobleaching occurs.
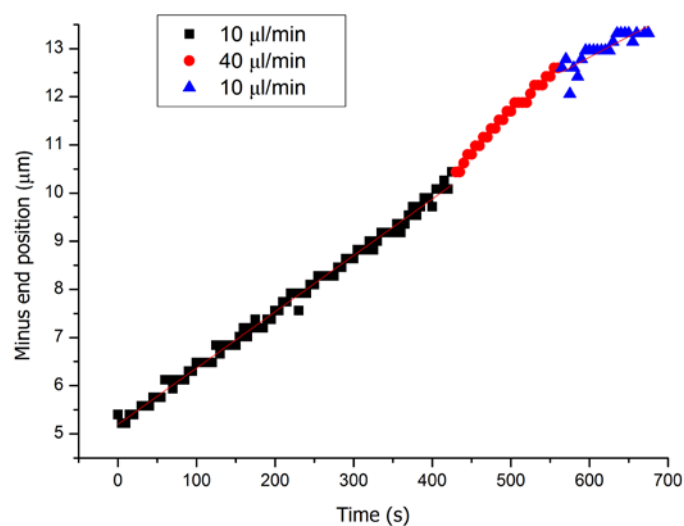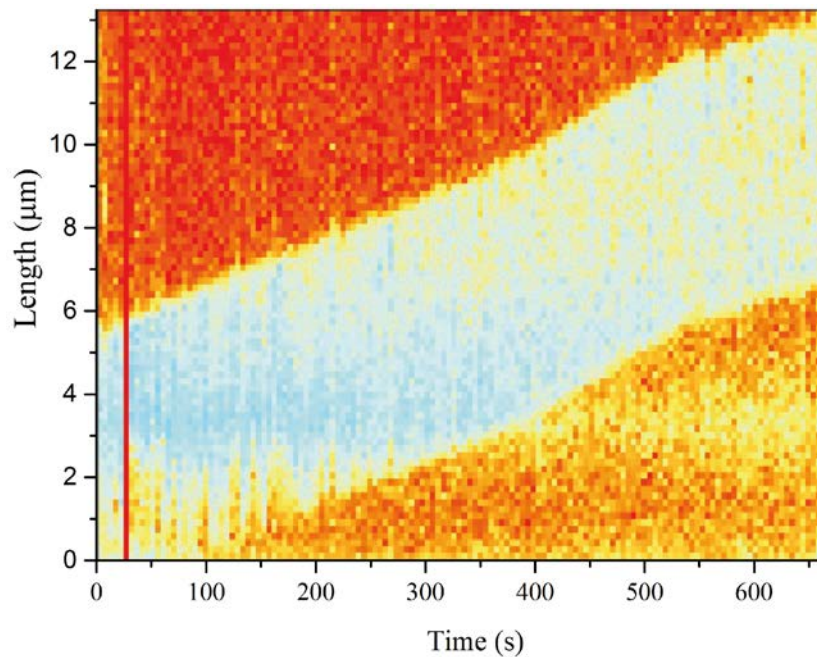
Figure 3.9 Growth of an actin filament was accelerated by the increase of flow speeds. (A) The elongation curve of an actin filament under different flow rates. The concentration of G-actin is 0.4μM. The black, red and blue curves represent the bulk flow rates of 10, 40 and 10μl/min, respectively. Linear fitting was done for each flow rate. (B) Kymograph of the elongating filament. The fragment labeled with fluorescence is shown in bright yellow. The filament is shown to grow from bottom to top.

Therefore, the results obtained from individual filaments must be validated by statistical analysis with a broader range of filament lengths and flow speeds. In order to have a better quality of image analysis, a higher concentration of 0.6μM was used to increase polymerization rates. Figure 3.10 shows an example of statistical data, which plots the polymerization rates of 12 individual filaments against their calculated forces. The data were obtained from three independent experiments, which are presented in blue, black and green circles respectively.
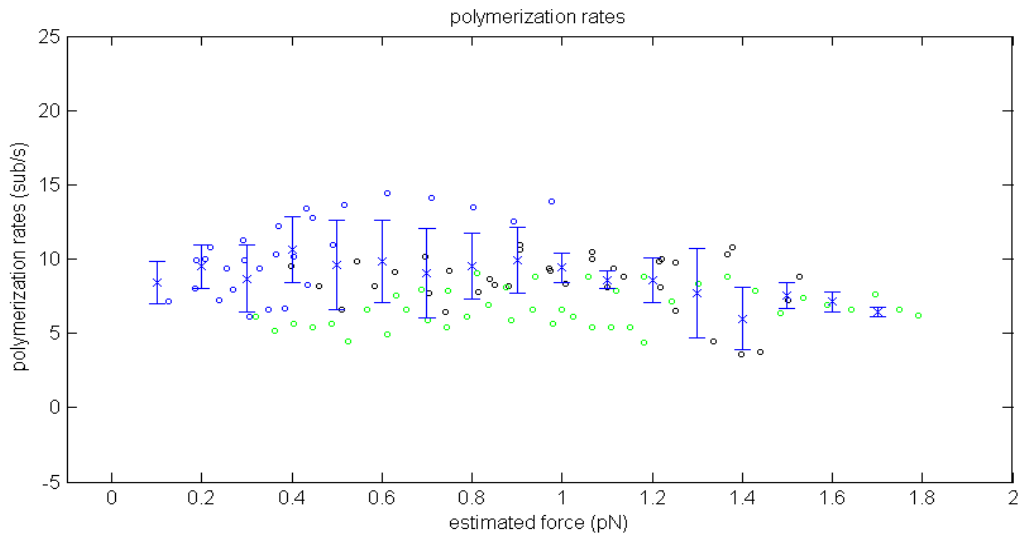
Figure 3.10 The statistics of polymerization rates as a function of estimated forces. Black, blue and green circles represent the data from three independent experiments, each of which contains four filaments (total n=12). Actin concentration was 0.6μM in all experiments and two bulk flow speeds (10 and 40μl/min) were used to obtain a broad range of forces. Error bars of the polymerization rates are given for every force increment of 0.1pN.

In figure 3.10, it can be seen that plotting the data of different experiments together gives a big variation of polymerization rates, which is much larger than that of individual experiments. It seems hard to draw conclusion from the current statistical data due to large variation. However, when paying attention to each individual groups, it can be found that the rates of polymerization do not change much in response to stretching, though there is probably a slight increase within the force range less than 1pN.

This set of data is not of good quality, simply because (1) the forces and polymerization rates are not accurately quantified; (2) The results obtained from different experiments are too diverse to be combined.

Because the magnitude of stretching forces were calculated based on filament length and local flow speed, any errors of these two factors will lead to inaccuracy. The filament length was obtained from image analysis, whose accuracy was limited by optical resolution and fluctuation. In principle, the error of measurement can be extremely high for short filament. The other factor, flow speed, was controlled by syringe pump. In this case, it seems hard to completely prevent the accumulation of system errors, if the speed was not directly measured for each individual experiment. Overall, these errors made it difficult to determine the pulling forces accurately. Similarly, the errors of polymerization rates may also be large, as limited by the low spatial and temporal resolution.

It is obvious that the pulling forces applied by hydrodynamic flow did not have strong effect in a profilin-free environment, compared with the above experiments with profilin. It seems reasonable because FH1 domain, the intrinsic unstructured domain responsible for profilin binding, may be more sensitive to stretching than FH2 domain. This difference probably means that the current approach based on hydrodynamic flow may only be sensitive enough to study the force responses of profilin dependent polymerization.

It is worth noting that, though no promoting effect can be concluded from this statistical data, there was also no significant inhibition, which was different from the observation in Courtemanche, et al.'s fluid-based experiment. This difference may be attributed to the difference in experimental setup. Our microfluidic system was basically similar to that setup, except for the use of microspheres instead of lipid bilayer and barrier. It may be possible that the barrier used to align actin filaments may hinder polymerization when stretching forces were applied.

3.3.6 Critical concentration may be lowered in response to flow stretching

Theory of polymer physics has implied that the tension applied on actin filament may decrease its chemical potential and promote the conversion from monomers to polymers[99]. This process is equivalent to the decrease of critical concentration in response to tension. In order to test this hypothesis, experiments were done in the conditions with low G-actin concentrations.

If no force is involved, actin polymerization rate should normally follow a linear dependence of G-actin concentration, as suggested by the kinetics of polymerization. The rate should be about zero at critical concentration. However, when pulling forces were applied on the polymerizing actin filaments, the acceleration at critical concentration was probably observed. As shown in figure 3.11, actin elongation rates were examined in the buffer flow of different G-actin concentration, ranging from 0.1- 0.5μM. The bulk flow speed was kept to be 10μl/min, which applied the forces of 0.2-0.6pN, depending on the length of filaments. It can be seen that the five measured rates did not well match a linear trend towards ~0.1μM, the critical concentration of Mg-ATP-G-actin at barbed end, while the rates at 0.1 and 0.2μM were slightly higher than theoretical values. This result probably indicates an effect of acceleration at low G-actin concentration by stretching forces, which corresponds to a possible decrease of critical concentration by tension.
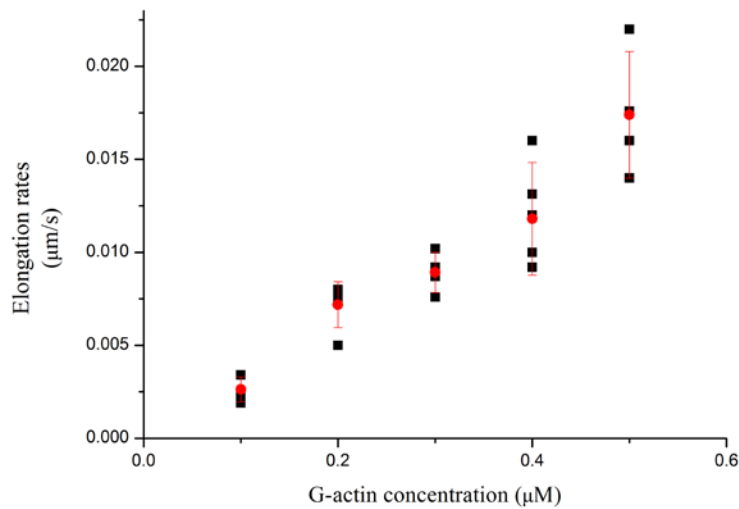
Figure 3.11 Polymerization from low concentration of actin in laminar flow.
Black dots represent the measured growth rates of individual actin filaments. Red
dots are the averaged values at each force. Each group contains 4 or 5 filaments.

If this result is true, it may indicate a higher mechanical sensitivity of critical

concentration than polymerization rates. That is possible because its decrease may

contribute more to the acceleration of slow polymerization.

However, more data are still needed to support these results. First, it is unclear

whether buffer flow can influence the measurement of critical concentration. More

control experiments are needed to exclude any side effect. Second, since the growth

at critical concentration was very slow, the accuracy of position measurement may

not be satisfying. Third, the wish to apply larger forces was largely limited by long

sampling duration, which was used to gain polymerization rates. Therefore, a new

method of higher sensitivity is strongly needed to investigate critical concentration.

CHAPTER 4 Stretching Single Actin Filaments via mDia1 Using Optical Tweezers

4.1 Introduction

Optical tweezers' advantages in detection and manipulation make it broadly used in manipulating single actin filaments. In principle, it can detect small force change, by which the drag forces in our study may be directly measured instead of being estimated. Furthermore, if the single actin filaments can be trapped in-between a pair of beads, spatial resolution can be dramatically increased as well. Therefore, in view of the previous studies with laminar flow, a combination of optical tweezers and dual-line microfluidics was designed to facilitate the manipulation of F-actin via mDia1.

Here, actin filaments were prepared with biotin-mDia1-ΔN3 in a similar way. These filaments were able to bind the streptavidin microspheres in laser trap and polymerize from them, as shown by epi-fluorescent imaging. The growing filaments were found to experience frictional forces in laminar flow, and the elongation led to an increase of stretching force that can be detected by laser trap. This increase basically correlates with the dependence of force on polymer length. However unfortunately, the measured force may not be accurate due to the large noises in this system. Meanwhile, the contrast of epi-fluorescent imaging was not high enough to determine whether only a single filament was tethered on bead.

4.2 Strategy and methods

The optical tweezers used here is NanoTracker, a commercial product of JPK, Inc. It is equipped with two infrared laser beams of 1064nm. The two beams are separated from a single one by polarization beam splitter, and controlled using piezoelectric mirror and acoustic optic deflector, respectively. Laser deflection can be detected using photodiode in nanometer resolution.
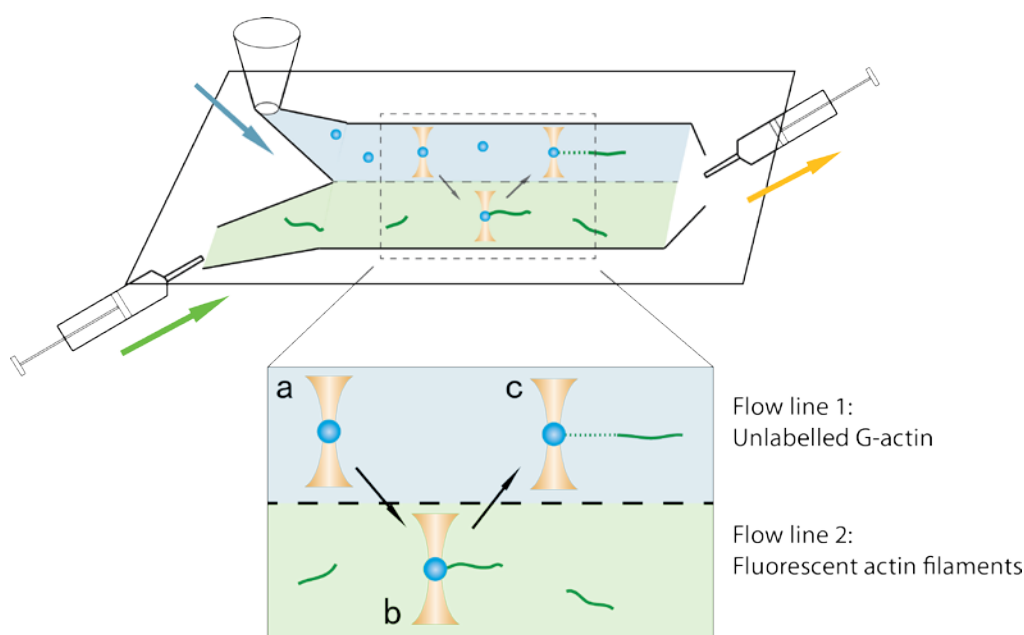
Figure 4.1 Illustration of the strategy to manipulate polymerizing actin filaments using optical tweezers. The blue flow line contains G-actin and streptavidin coated microspheres, while the green line contains fluorescent F-actin prepared with formin. The microspheres were moved sequentially from a to c to capture actin filaments and perform elongation.

The dual-line microfluidic chamber is similar to that of flow method except for the use of bottom surface without functionalization. Some 1µm microspheres with streptavidin coating were added together with G-actin for laser trapping. As shown in Figure 4.1, a bead should first be trapped in flow line 1 (a) and then moved to flow

line 2 for the binding of F-actin capped by biotin-mDia1-ΔN3 (b). Once a filament was found, it would be moved back to line 1, where polymerization may occur in laminar flow (c). Here, force can be directly measured from laser deflection and the number as well as growth of filaments is planned to be tracked by epi-fluorescent imaging.

In principle, the force measured by laser should be the total friction forces experienced by bead and filaments. The force on bead is only dependent on flow velocity, as given by $F_{bead} = 6\pi\eta rv$, which should be constant in a steady flow. Then the drag force on tethers can be obtained by: $F_{filament} = F_{trap} - F_{bead}$. Using these parameters, a relationship between elongation and stretching forces may be established.

4.3 Results

4.3.1 Stretch actin filaments using optical tweezers

The process of obtaining tethers is shown in Figure 4.2. First, a microsphere coated with streptavidin was trapped and moved from flow line 1 to line 2. Then, it was kept for some time until an actin filament can be found. In laminar flow, the filaments linked to the microsphere can be observed as an aligned polymer, with unbound filaments flowing around. Finally, after a filament was found, it would be moved back to line 1, which contained G-actin for polymerization. The contrast was dramatically increased due to the low background (Sub-figure C).
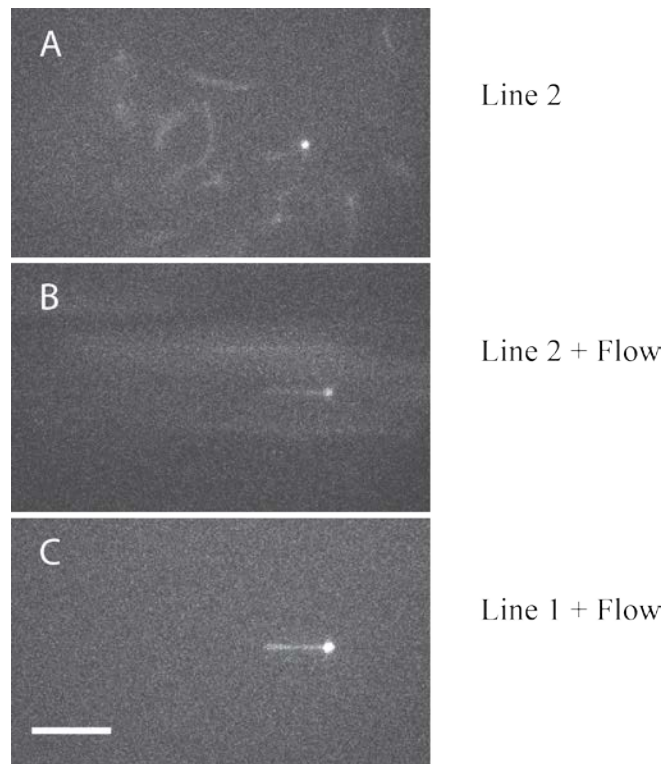
Figure 4.2 Laminar flow applied tension on trapped actin filaments.
(A) A streptavidin bead was held by laser trapping and placed in the flow of actin filaments. (B) Actin filaments were found linked to the microsphere and aligned in flow. (C) The microsphere in flow line 1 can be imaged with a higher contrast. Scale bar = 10 µm.

4.3.2 Determine the relationship between drag force and polymerization

Using optical tweezers, the force exerted on the microsphere and actin filaments can be directly measured. In principle, the total force should be the accumulation of the drag forces on microsphere and actin filaments. In a steady flow, it should be constant for a stable tether. However if the length of filament changes, the drag force should change in a corresponding way. Figure 4.3 shows an example of force measurement. An actin filament was polymerizing in the direction of flow, whose elongation is plotted in blue points (B). Pink curve is the force measured from bead displacement.
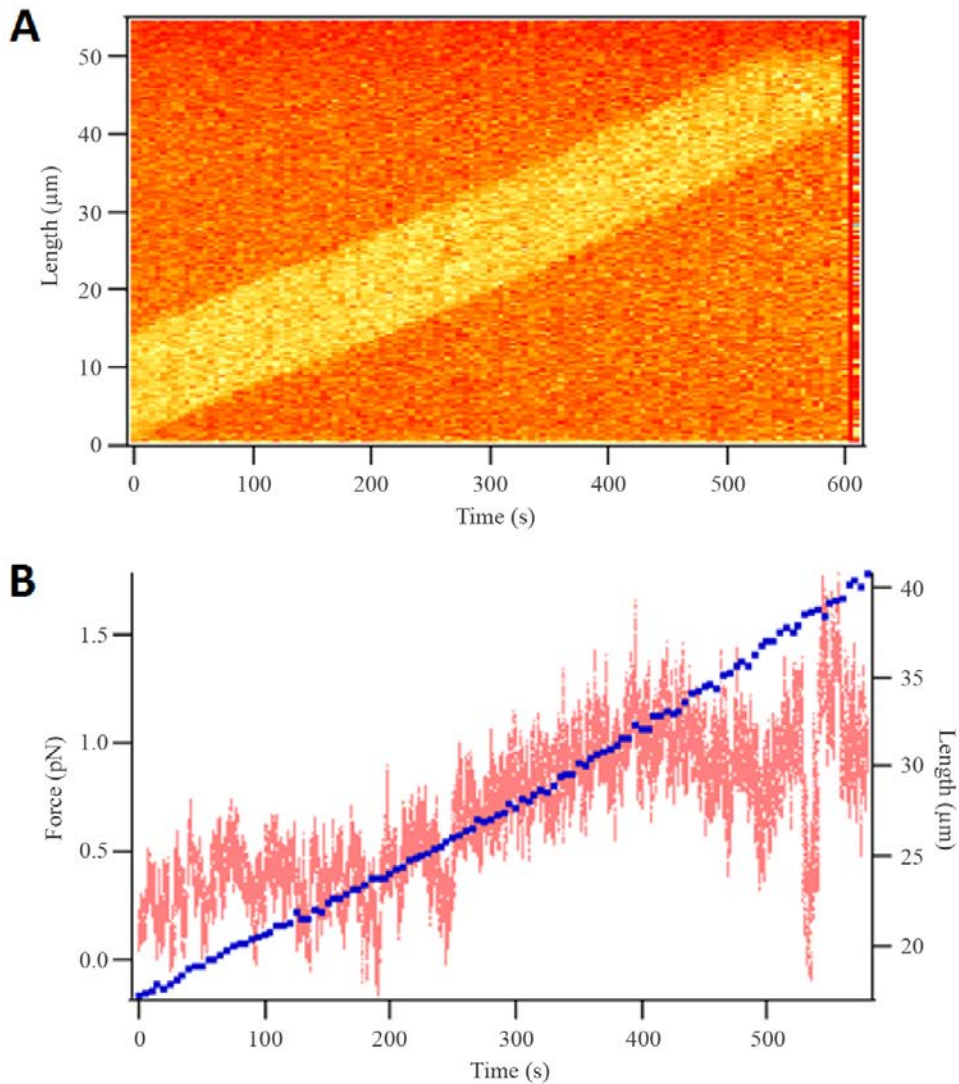
Figure 4.3 The measured force increase was partly correlated with filament elongation. (A) Kymograph of a polymerizing actin filament. The fragment labeled with fluorescence is shown in bright yellow. The filament is shown to grow from bottom to top. (B) Measured force (pink) and the plus end of the fluorescent filament (blue) was plotted as a function of time.

It can be seen that the filament of ~15µm long elongated for ~40µm during 600s. The

average rate was ~ 66nm/s (25 subunits /s), in the same scale of the conditions with

1µM G-actin plus 1µM profilin. Drag force was also measured to be increasing, but

only in correlation with polymerization between 150 and 400s, giving an increment of 0.75 pN / 250s.

However, the force did not follow the growth of actin in the range below 0.5pN as well as over 1pN. There seemed to be a large noise in low force regime, probably because: (1) precision was not high enough to detect the force less than 0.5pN; (2) the drag force on actin was concealed by the force fluctuation of microsphere. The large noise may be generated by several deficiencies in the system, such as mechanical drift of optical trapping and instability of the microfluidic system. Overall, in current conditions, it seems difficult to obtain an absolute value of drag force.

Meanwhile, a large drop of force can be found over 1pN in figure 4.3B. The sudden drop was possibly resulted from (1) sudden change of flow speed and (2) dissociation of a filament from the microsphere. The second factor is reasonable because multiple filaments and dissociation can always be found in practise. In the current system of epi-fluorescent imaging, it was difficult to identify single actin filament on a microsphere. This problem may impede the single molecular study of formin mediated actin mechanosensing.

CHAPTER 5 Magnetic Tweezers That Manipulate Single Actin Filaments

5.1 Introduction

Although the method of hydrodynamic flow can be used to stretch single actin filaments and track their polymerization, its low spatial and temporal resolution largely limits the detection of small changes in polymerization rates. In contrast, the method of magnetic tweezers is one of the advanced single molecule techniques that can apply constant pulling force with high resolution of detection. Therefore, in order to investigate the potent mechanosensing behavior of FH2 dimer, I set up a novel method that combines magnetic tweezers with hydrodynamic flow and TIRF microscopy to take their respective advantages.

Importantly, the magnetic tweezers used here are built with a tilted angle to avoid spatial obstruction, which is different from conventional ones. This setup allows us to manipulate long tethers together with TIRF imaging. The magnitude of force is known from magnet position, based on the calibration of DNA force extension curve.

Pulling force is applied on the polymerizing barbed end via a single actin filament, which is anchored in-between GST-formin-mDia1 and a streptavidin magnetic bead. Surface treatment has been optimized to increase the specificity and yield of single actin filaments, which enables further bead attachment in an efficient way. After identifying effective tethers, pulling force can be applied by moving the magnet. Using bright field imaging, polymerization events can be tracked with high spatial and temporal resolution. In summary, this novel method makes it possible to apply constant pulling force on single polymerizing actin filaments even through weak

linkage. Also, even slow polymerization process and small change of growth rate can be detected, as required by the studies of critical concentration.

5.2 Strategy and methods

In general, there are mainly two types of conventional magnetic tweezers: vertical and transverse magnetic tweezers. Vertical tweezers are suitable for stretching short tethers like single-strand DNA and polypeptide chain, while transverse tweezers are good at stretching long tethers such as lambda DNA molecules. Although actin filaments are also long tethers, the transverse tweezers is still not the first choice as it seems difficult to allow simultaneous TIRF imaging. Meanwhile, actin tethers are normally of uncertain length, which makes it difficult to know the force directly from thermal fluctuation.

To solve these problems, the magnetic tweezers can be implemented with a tilted angle, as illustrated in figure 5.1. It can be seen that a specially designed dual-flow chamber is also included to facilitate the assembly of stretchable tethers. In this design, the actin filaments with biotin labelling are first prepared in a tube and stained with fluorescent phalloidin, which will then be immobilized on surface via their barbed end GST-mDia1. Their biotin labelling makes it possible to attach streptavidin magnetic beads to the side of them. After that, magnetic pulling force can be applied from the side of the chamber. Since the pulling force is given with a tilted angle, these tethers will be elevated from bottom surface, by which some unexpected surface interaction can be avoided.
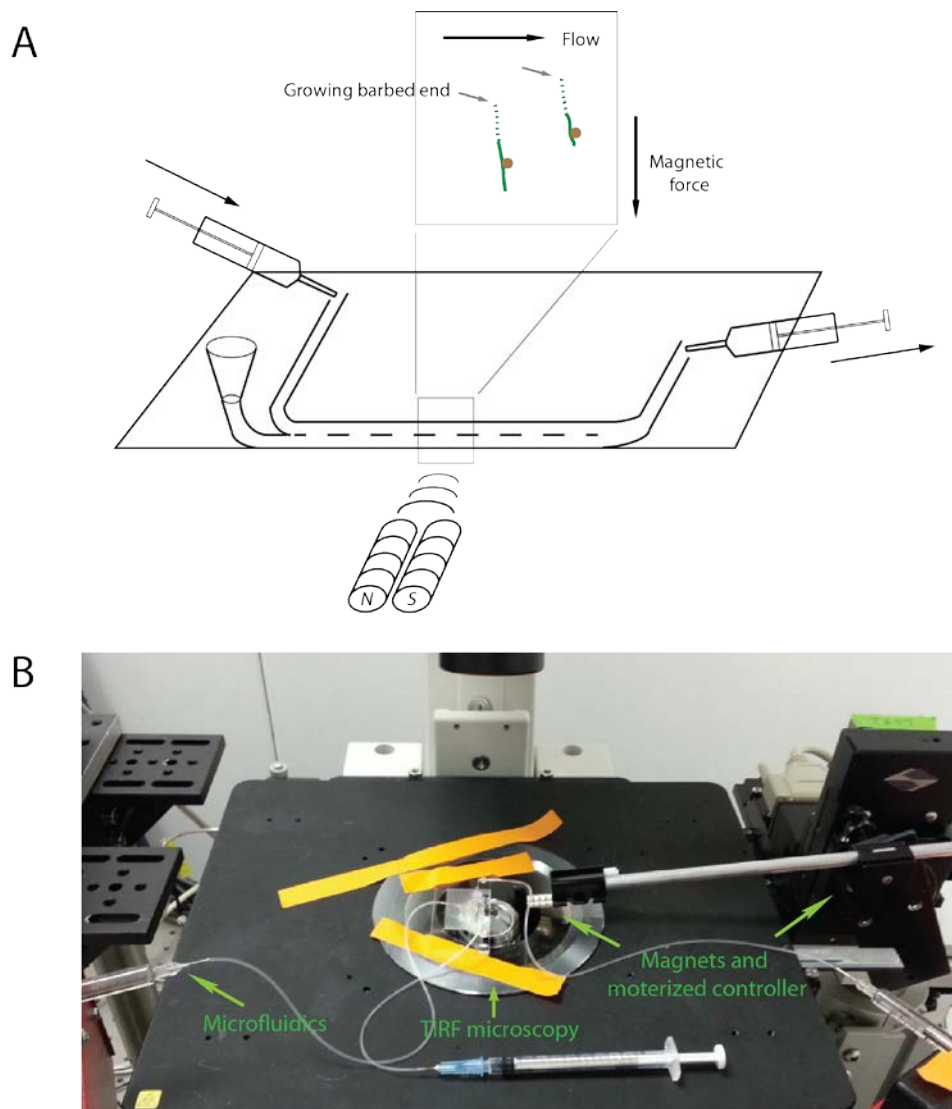
Figure 5.1 Illustration of the magnetic tweezers in combination with microfluidics and TIRF microscopy. (A) The polymerizing filaments (green) and magnetic beads (brown) are shown in the enlarged window. (B) The real instrumentation.

Here, the procedures to anchor mDia1-capped actin filaments are similar to those in chapter 3. The next steps are:

1. Obtain a proper density of immobilized single actin filaments. These filaments are pre-labelled with biotin-actin during preparation (referred to chapter 2 and 3).

2. Deliver streptavidin magnetic beads into the chamber via laminar flow. This step also helps to remove unbound filaments and free phalloidin in solution.

3. Monitor the binding of magnetic beads by real-time TIRF imaging. After finding a proper density of tethers, the buffer containing G-actin of interested concentration will be delivered to remove unbound magnetic beads and start polymerization.

4. Stop buffer flow and apply force by moving close the permanent magnets.

5. Examine the process of polymerization by tracking the movement of magnetic beads using bright field imaging. The movie can be analyzed afterwards using Matlab program.

5.3 Results

5.3.1 Experimental instrumentation

5.3.1.1 Flow chamber design and preparation

A microfluidic chamber was designed for the use on tilted magnetic tweezers. Flow lines were made by melting a layer of patterned parafilm in-between a functionalized coverslip and an acrylate top. The pattern of microfluidics is similar to the one used in hydrodynamic method, except that the main flow line is located by the side of the chamber to allow force application. As shown in figure 5.2, the main flow line is of 15mm in length and 2.5mm in width. Its front margin is designed as narrow as 0.6mm in width to make the stretching force as large as possible.
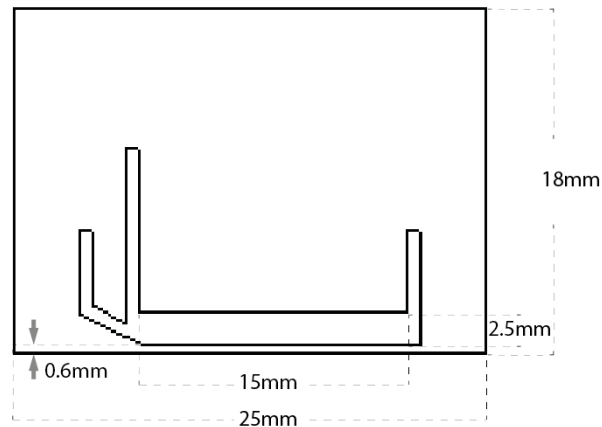
Figure 5.2 Design of the flow channel.
The main flow line is about 15mm × 2.5mm. Its front edge is about 0.6mm in width, which allows force application from this side.

The pattern is cut using Graphtec cutting plotter. The chamber is made by heating the parafilm in the middle of a sandwich structure and sealing with silicone gel. A small reservoir is fixed at one inlet to facilitate buffer addition and exchange, while the other inlet and the outlet are connected to hard tubing (Tygon) to reduce flow vibration. Buffer delivery is controlled by two syringe pumps (AL-1000, World Precision Instruments), with one injecting buffer and the other one withdrawing waste.

5.3.1.2 The setup of magnetic tweezers

In our system, the magnetic tweezers are combined with TIRF microscopy and microfluidics. Figure 5.1B shows the appearance of the instruments. An MP285 manipulator (Sutter Instruments) is placed on the side of the Nikon TIRF microscope to impose magnetic forces through moving a pair of permanent magnets. The manipulator is mounted on a holder in 30°, with its X-axis pointed to the objective.

86

This tilted angle is required to prevent spatial expulsion of the magnets from high-NA TIRF objective and elevate magnetic beads away from surface. In order to apply magnetic forces, the chamber is needed to be fixed on the stage with its narrow margin faced to magnet. Based on this setup, the tethers of interest can be first assembled and observed in the microfluidic chamber and then stretched using magnetic tweezers.

In regard to the tilted angle, alignment of the magnets is to some extent different from conventional transverse or vertical magnetic tweezers. In practice, Z-position of the TIRF objective is first defined by focusing on the functionalized surface. Then a 10× objective is selected and kept in the same focal plane. By controlling the manipulator, the pair of magnets can be precisely placed at the position where the central point of its front surface is located at the center of the focused field of view. Because this position can be considered as the place of the tether of interest, it can be set as the origin of magnet movement. Based on this setting, the manipulator's position in X-axis can be directly used as the distance of magnet.

5.3.2 Force calibration of tilted magnetic tweezers

Tilted magnetic tweezers is a new setup to be used for the first time. Therefore, calibration must be done to ensure the accuracy of force application. As for conventional magnetic tweezers, force can be known in two ways: (1) for a stable tether of known contour length such as DNA and polypeptide, force can be obtained from the transverse fluctuation of bead, as given by $\frac{f}{l} = \frac{k_B T}{<\delta_y^2>}$,

where l is extension and $< \delta_y^2 >$ is transverse fluctuation[119]; (2) force can be known from the positions of magnet, as the magnitude of force is mainly related to bead magnetization and magnetic field, which can be calibrated as a function of the distance between bead and magnet[123].

In our case, the first method seems not to be applicable, because the actin filaments capped by formin are neither of certain contour length nor stable enough to sustain long-time calibration. In contrast, the second method provides a very convenient way of force measurement. One of the two factors that determine force magnitude is bead magnetization, which has been found to be quite uniform for commercial magnetic beads[123]. This knowledge supports a monotonic relationship between force and the positions of permanent magnet. The effectivity of force application can be determined by force calibration using DNA as a template.
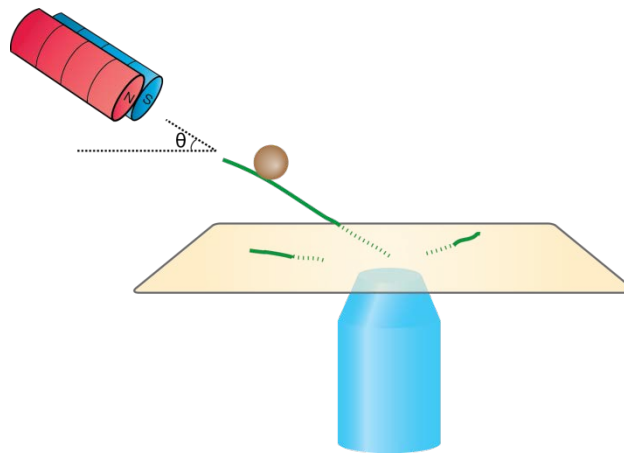
Figure 5.3 Illustration of the tilted force application.

Figure 5.3 illustrates the application of magnetic force with an angle θ. Direction of the magnet must be aligned very well with the sample of target by following the

procedures described in the above session. The effectivity of alignment can be seen

from DNA force extension curve.

Figure 5.4 presents the force extension curve of a lambda-DNA tethered in-between

bottom surface and a magnetic bead. The force was applied with an angle of

30°. Extension of the molecule was extracted from its projection on x-axis according

to $l = $ x $/$ cos30°. The tilted angle should not influence the accuracy of force

measurement as the term δ_y^2 was independent of this angle.
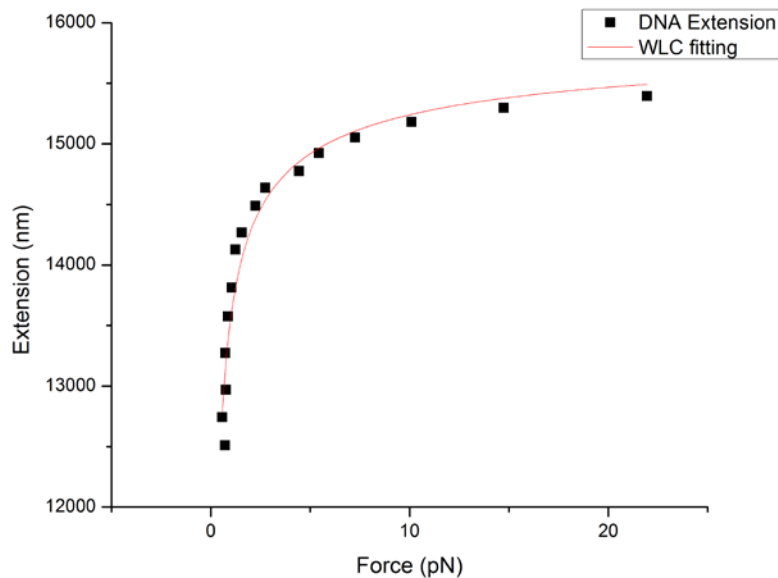
Figure 5.4 DNA force extension curve by tilted magnetic tweezers of 30°.

It can be seen that the data was fitted to worm like chain model with a persistent

length of 45nm, in comparison with the known value of 50nm. This result indicates

that the magnitude of force was basically accurate based on the current method of

alignment. Later, the correlation between force and magnet positions can be obtained, by which the force can be known and changed simply by moving the magnet.

5.3.3 Surface treatment for high specificity and efficiency

Although in the methods of microfluidics, we have succeeded in anchoring a population of actin filaments on surface via biotin-mDia1, some changes are needed for the method of magnetic tweezers. Here, because the biotin-streptavidin pair is assigned for the attachment of magnetic beads regarding its fast on-rate, the pair of GST and its antibody is chosen for formin surface immobilization. In this case, the peptide of formin mDia1 FH1-FH2 is conjugated with N-terminus GST tag, and about 5%-10% biotin-actin is introduced during filament preparation.

There are several ways to coat protein on glass surface. However, these methods may give various readouts, mainly different in two aspects: efficiency and specificity. The later one is especially important to this experiment because any non-specific interaction between the surface and filamentous actin will result in the failure of polymerization. Thus, different conditions and materials of surface functionalization, including glutaraldehyde, PEG, BSA blocking and so on, have been tested for an optimal outcome of surface specificity.

Among them, PEG coating has been found to the best way of surface passivation. As shown in figure 5.5A, a combination of a methyl- and carboxylate-PEG is coated on the glass treated with APTES. The terminal carboxylate groups are available for covalent protein immobilization upon carbodiimide activation. Figure 5.5B compares the situations of non-specific binding on the surface under different treatment. The

left image shows an example in which about 10-20 actin filaments can be found on the surface treated with plasma and BSA blocking in a field of view (100×100μm). In contrast, generally no filament can be found on the surface coated with PEG. This result suggests that PEG coating largely reduces undesired interaction between actin filaments and glass bottom, which is necessary for further manipulation. In addition, this high specificity makes it possible to achieve a high density of anchored filaments on surface and long manipulation time without significant interference.

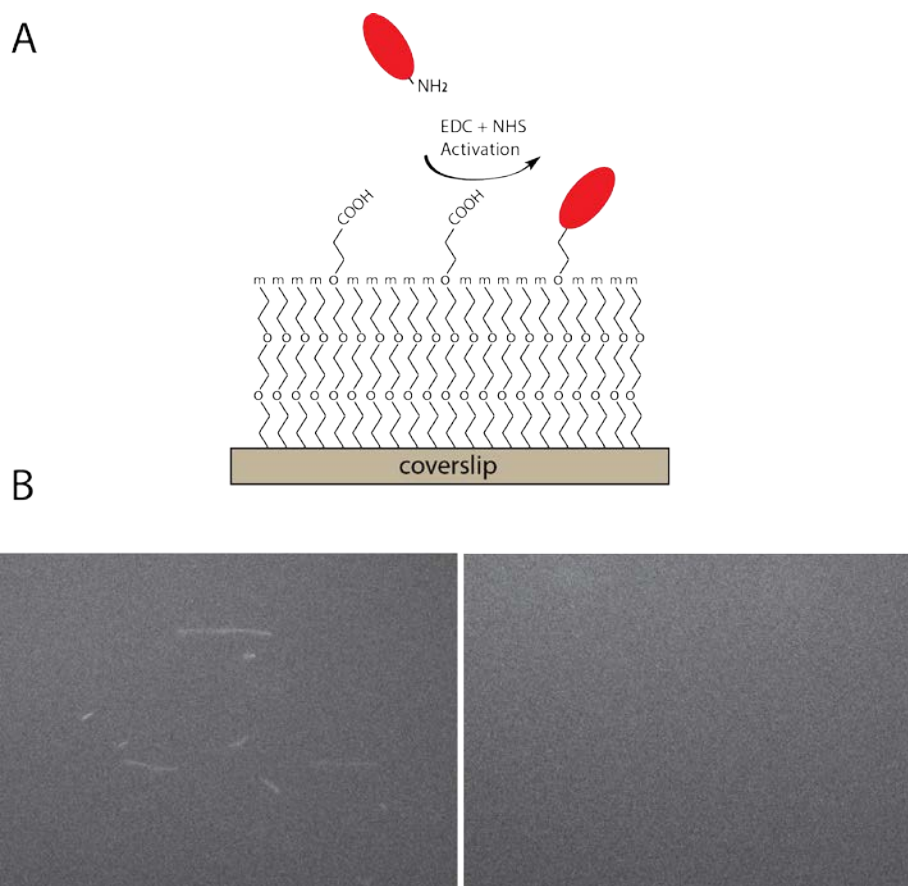**Figure 5.5 PEG functionalization reduced actin non-specific binding on surface.**
(A) Illustration of the PEG functionalization. The COOH-PEG molecules are supposed to form a curtain with carboxylate groups on top. Red objects are proteins of interest, which can be covalently linked to the carboxylate groups via carbodiimide and NHS activation. (B) Comparison between the surface blocked with BSA (Left)

and functionalized with PEG (Right). The images (part of a field of view) were taken 2 minutes after adding actin filaments (~1μM) into the chamber.

Besides specificity, efficiency is another important parameter worth being concerned. Since the attachment of magnetic beads is a relatively inefficient process due to the limited number of biotin-actin in filaments, the density of specifically anchored filaments seems to be critical to success. High filament density can drastically increase the chance of bead attachment as well as reducing the incubation time that is required. This is especially beneficial as the life-time of mDia1 on actin barbed end is short compared with conventional targets of magnetic tweezers such as DNA and polypeptide[73].

Therefore, some efforts were then made to improve the efficiency of anchoring. At first, GST-antibody was directly immobilized via carboxylate group. However, it was then found that some filaments can be trapped via their side rather than barbed end formin, indicating a possible undesired interaction between GST-antibody and actin. Any such interaction may cause severe interference, because the amount of actin subunits that are exposed to receptors is far more than the amount of GST-formin. In order to solve this problem, the GST-antibody was first incubated with excess GST-formin for at least 1h before preparing actin filaments, which drove the majority of antibody to be stably engaged by GST-formin.

Accordingly, protein-A was then introduced as a receptor to anchor the barbed end capping complex. Figure 5.6 illustrates how the molecular complex is assembled on PEG surface. Upon activation, protein-A can be linked to the carboxylate PEG molecules via its amino group, which can then capture GST-antibody as well as the filaments capped by GST-formin via its binding to antibody Fc fragment.
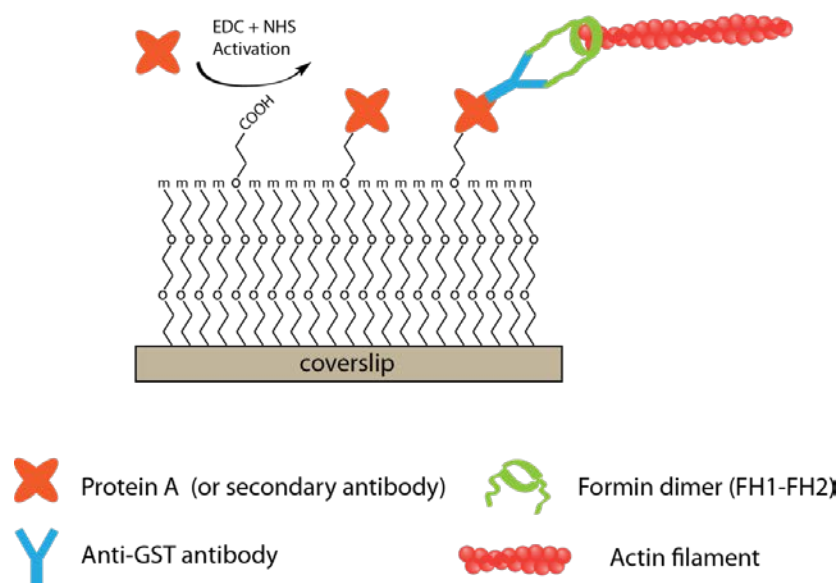
Figure 5.6 Illustration of the barbed-end molecular assembly of an actin filament. Protein A was used to capture the complex of GST-antibody, GST-mDia1-ΔN3 and actin filament.

Figure 5.7 shows the elongation of actin filaments from PEG surface. It can be seen that about 5~6 filaments can be found in a field of 54×27µm, most of which were elongating from their anchored terminus in the direction of flow. The density of immobilized filaments depends on several factors, including surface capacity, filament density, incubation time and association rate. This result clearly shows that a high efficiency has been achieved after the procedures of optimization without sacrificing high specificity.

Meanwhile, it can be seen that three dissociation events have occurred within 4 minutes, probably because of the instability of FH2 capping. The fast dissociation rate further emphasizes the importance of high density, which ensures the gain of target tethers before applying magnetic forces.
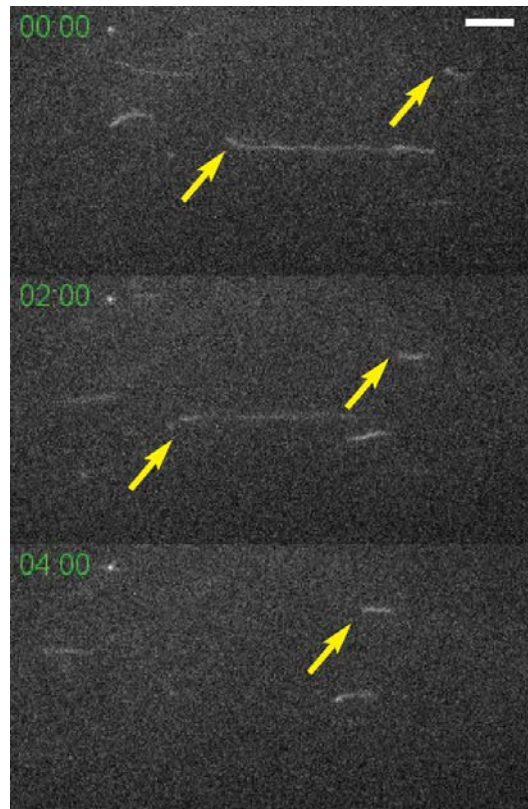
Figure 5.7 High specificity and density of polymerizing filaments on PEG surface. Yellow arrows indicate the elongation of two single actin filaments. The other filaments in this figure were also polymerizing. Scale bar = 5µm.

5.3.4 Assemble and identify tethers of interest

After observing a population of single filaments on PEG surface, magnetic beads can be added to form tethers for manipulation. In practice, MyOne magnetic beads with streptavidin coating (Dynabeads, Thermo Fisher Scientific) are flowed into the chamber after a short wash of unbound filaments. Due to the high affinity of streptavidin to biotin-actin, the number of beads attached to actin filaments gradually increases. This process is monitored by real-time TIRF imaging until an optimal density of tethers can be found.

Because these magnetic beads always bind to surface in a non-specific manner, the number of stuck beads also increases during incubation. Meanwhile, the beads that have already bound to filaments also have the chance to interact with bottom. Therefore, we can normally obtain a combination of several kinds of tethers including the interested ones and undesired ones.

Here, a set of criteria have been settled to determine what kind of tethers can be selected for further manipulation. Figure 5.8 shows some typical kinds of tethers that are observable after adding magnetic beads, including:

(1) A single actin filament with one or more magnetic beads binding to its side, which is fluctuating around the anchoring end and extended towards the direction of flow;

(2) A single actin filament with one or more magnetic bead binding to its side, which are also stuck to the surface;

(3) Two or more actin filaments anchored to surface via their individual ends, but crosslinked by the same magnetic bead;

(4) One or more actin filaments that bind to stuck magnetic beads but not the surface.
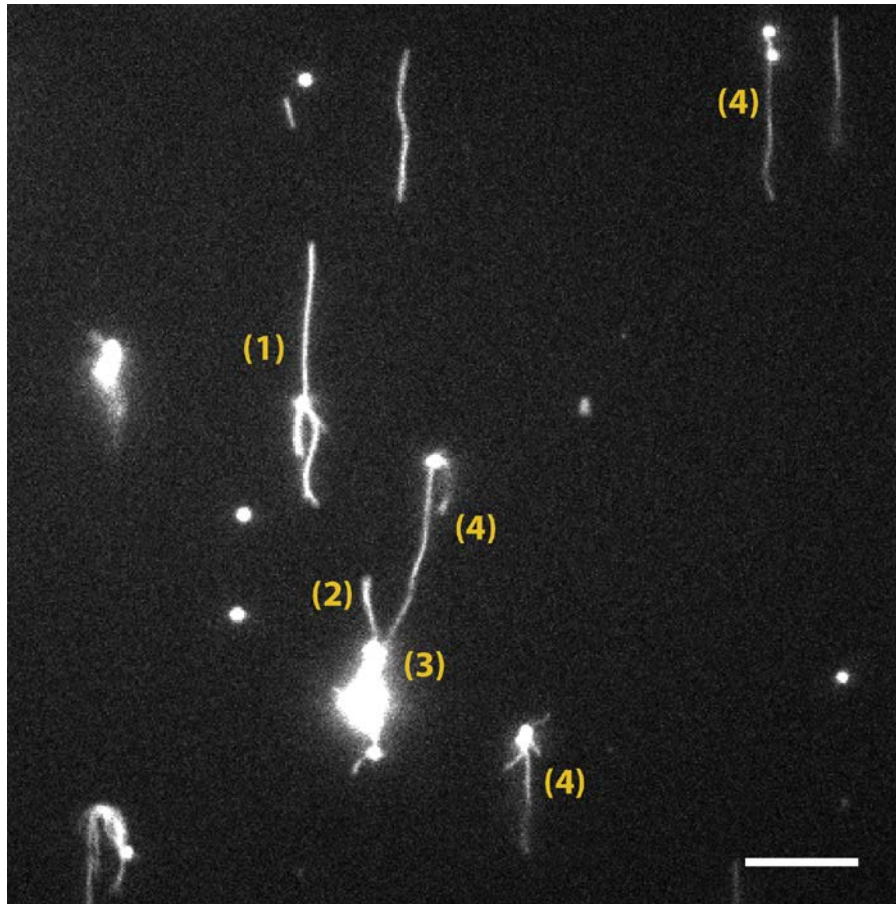
Figure 5.8 A TIRF image showing different types of tethers.
(1) An active tether undergoing polymerization and fluctuation. (2) A filament which
was polymerizing but trapped by immobilized beads. (3) Two filaments that were
bundled by beads. (4) Some filaments binding to the beads that were stuck on surface.
Scale bar = 10µm.

In principle, the filament in case 2 is not able to be stretched due to the
immobilization of magnetic beads. The filaments in case 3 are obviously not single
tethers. In case 4, the filaments are trapped via their bodies but not the antibody-
protein-A interaction. Therefore, only the filament in case 1 is the tether of our
interest. It is a single tether whose barbed end is anchored via formin mDia1. It can
also be stretched because the magnetic bead can sense and transduce magnetic force
along the body of filament to barbed end.

It is worth noting that the position of bead attachment does not affect manipulation much, because the magnitude of pulling force is independent of bead position and is exerted on the entire fragment between barbed end and the magnetic bead. Besides, in some rare cases, the tethers may have more than one bead binding on their side. They can also be used for further manipulation just as the force is multiplied.

Importantly, the chance of getting proper tethers is highly relative to the density of filaments and beads, as well as the time of incubation. If filament density is not high, it may be difficult to find specific tethers, due to the low probability of those beads to encounter actin filaments. On the other hand, overcrowded actin filaments may lead to a severe crosslinking mediated by those streptavidin beads. Therefore, in addition to the optimization of material concentration, a proper control of density by real-time observation is also important to success. As for our experimental conditions including 0.2μM diluted filaments and 0.1mg/ml MyOne magnetic beads, a density of 10-15 actin filaments in a view-field of $130 \times 130 \mu m^2$ was found to be proper for further bead attachment.

Figure 5.9 presents an example of a single actin filament with a magnetic bead. Here, the tether can be found elongating in the direction of flow as a result of mDia1 mediated actin polymerization. This assembled structure represents the tether to be manipulated in the next step.
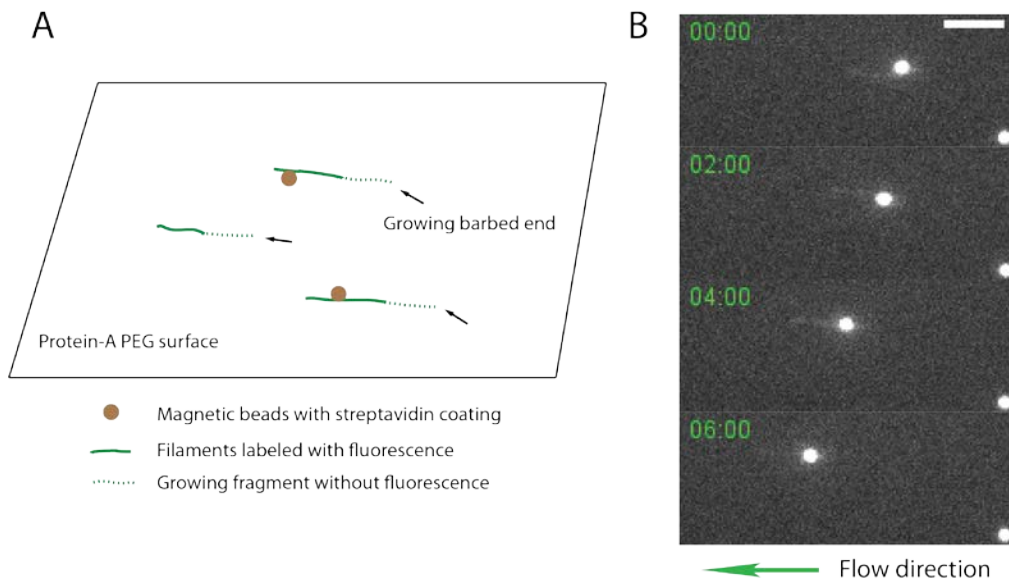
Figure 5.9 Binding of magnetic beads on the side of polymerizing actin filaments. (A) Illustration of the attachment of magnetic beads. (B) A bead was translocating on a single actin filament in the direction of flow. Scale bar = 5µm.

5.3.5 Pull a single polymerizing actin filament

Since the attachment of magnetic beads has been achieved, magnetic forces can now be applied to pull single actin filaments that are polymerizing. This process includes several steps:

(1) Remove unbound magnetic beads by flowing in the polymerization buffer containing G-actin of interested concentration;

(2) After the chamber is filled with the solution containing G-actin, stop buffer flow;

(3) Move the magnet close to the chamber to apply pulling force;

(4) Switch the imaging mode from TIRF to bright field for observing the magnetic bead;

(5) Record time-lapse images of the bead that is translocating under pulling force. The force can be changed by controlling magnet positions in X-axis.

Figure 5.10 shows the processes of stretching a single actin filament. At the beginning, the filament was extended towards the direction of laminar flow. Stop of the flow resulted in a larger fluctuation of the tether. Then a magnetic force was applied from left, which caused the tether to turn to the direction of the magnet. It can be seen that the turning occurred around the polymerizing end of the filament, which indicated that the barbed end was subject to pulling.

In this figure, it can also be seen that there were some short filaments associated with the bead of target. It is normal because all of the preformed filaments have affinity to magnetic beads via biotin-streptavidin interaction. In principle, these by-products will not interfere with stretching and polymerization, because they rarely have interactions with the bottom and barbed ends, and should not have much influence on magnetization and thermal fluctuation.

Since the bead is 1µm in diameter and pulled with a tilted angle, TIRF imaging is not applicable to track its movement. Instead, bright field imaging can be used for tracking as a rapid and stable method. In addition, illumination with transmitting light enables a very broad range of observation in Z-direction, which is especially beneficial to this kind of experiment that involves tilted manipulation and long tethers of uncertain and dynamic length.
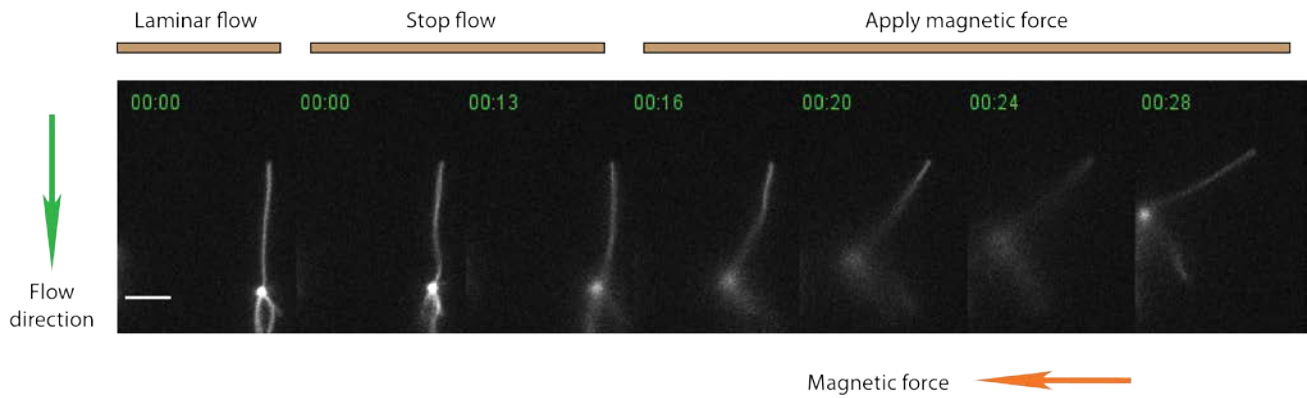
Figure 5.10 The filament can be aligned towards the direction of magnetic force. In this video clip, buffer flowed towards bottom, while the magnet was placed on the left side. In the 1st frame, the filament was extended by laminar flow. In the 2nd and 3rd frames, flow was stopped. Then in the other frames, magnetic force was applied by moving close the magnet, which aligned the filament towards left. Scale bar = 5μm.
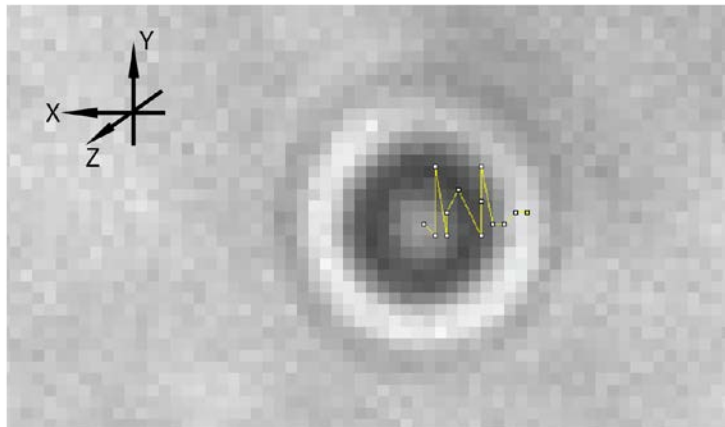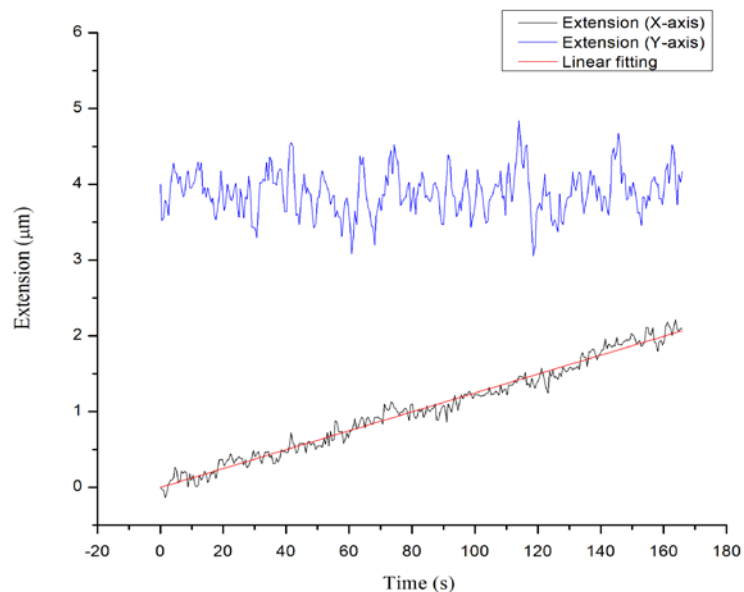
Figure 5.11 Data analysis of a polymerization event under tension.
(A) Trajectory of magnetic bead by bright-field imaging. (B) The x and y trajectories of an elongation event. Black and blue curves are the positions of the magnetic beads in x and y axis, respectively. An average elongation rate is given to be ~12.4nm/s by linear fitting of the black curve.

Figure 5.11A shows the trajectory of a magnetic bead attached to a polymerizing filament. Here, the magnitude of pulling force was constant and less than 0.2pN. Positions of the bead were obtained using a Matlab program that determines its centroid and plotted against time as shown in figure 5.11B, where black and blue curves represent the positions in X and Y coordinates, respectively. In fact, the bead was fluctuating in all three coordinates, all of which were decreased as pulling force increased. However, only the positions in X-axis were directly related to the change of filament length during polymerization. The fluctuation in Z-axis was small compared to the length of filament, and hence had little influence on length determination upon averaging over time.

It can be seen in figure 5.11B that the bead was translocating along X-axis in a linear manner, while there was no significant change in Y-axis, which indicates that the polymerization occurred only in X coordinate. During the time window of 170 seconds, the filament elongated about 2 µm at an almost constant rate. Linear fitting of the curve gave an elongation rate of 12.4nm/s, which was consistent with the reported value of 0.4µM actin in the absence of force, suggesting that a single actin filament anchored by mDia1 can effectively polymerize when being stretched using magnetic tweezers and a pulling force less than 0.2pN may not have significant effect on FH2 mediated polymerization.

In summary, these observations demonstrate that the method of magnetic tweezers in combination with TIRF and microfluidics is effective in manipulating single actin filaments that are polymerizing. It is capable of applying constant pulling forces of definite magnitude. In addition, the temporal resolution of tracking can reach up to 0.013s (at the imaging speed of 80 frames/second), which is important to the capture of fast dynamics and short-term events. The spatial resolution can be narrowed to about 10nm, which is far more precise than conventional approaches based on fluorescent imaging[124]. Overall, these abilities make this method effective in studying actin dynamics beyond optical limit and mechanosensing of actin dynamics to pulling forces.

CHAPTER 6   Investigating mDia1-Mediated Actin Polymerization under Tension

6.1 Low stretching forces did not accelerate polymerization

As discussed in chapter 5, with the newly developed magnetic tweezers, we are able to study the influence of stretching forces on actin polymerization.

As shown in figure 6.1, three different stretching forces (0.1pN, 0.2pN and 0.4pN) were applied consecutively on a polymerizing single actin filament. It can be seen that the magnitude of bead fluctuation was consistent under the same force, but much different from the others. This observation accords with the principle that force can reduce the fluctuation of tethered polymer.

As for the responses of polymerization rates, however, no significant change was found. By assuming the polymerization rate to be constant within a short duration, linear fitting was done to fit the curve of each individual force. The polymerization rates obtained were 22.0, 21.4 and 22.2nm/s, respectively. These rates are similar to each other and consistent with the force-free speed of mDia1-mediated barbed-end polymerization with 700nM G-actin. This result indicates that the pulling forces below 0.4pN may not have significant effect on the actin polymerization mediated by mDia1 FH2 domain.

Though no significant effect has been found yet, this result shows the possibility to probe the effects of larger forces. It can be seen that the bead fluctuation was reduced to a very small degree by the force as low as only 0.4pN. In other words, this force can drastically decrease the noise of length measurement. Therefore, for the studies

under larger forces, only a short sampling time is needed for measuring speed. This advantage is especially beneficial to formin studies, as FH2 domain may be subject to fast barbed end dissociation under large forces [44].
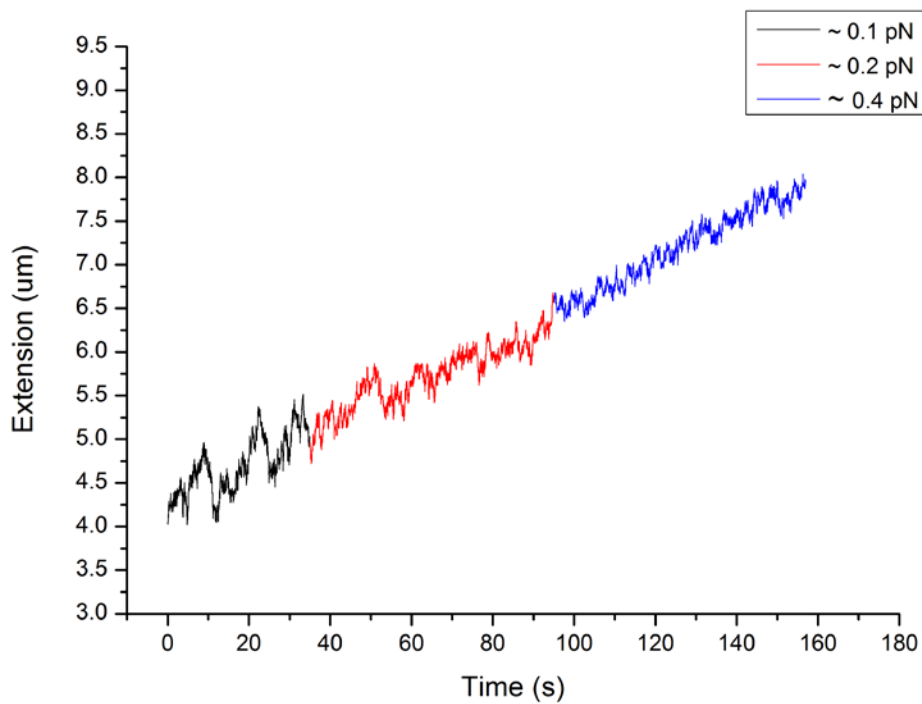
Figure 6.1 Polymerization curve of a single actin filament in response to different stretching forces. The events of elongation under the stretching forces of 0.1, 0.2 and 0.4pN are presented in black, red and blue color, respectively.

6.2 Discussion

The essence of this study is to discover possible regulation of actin polymerization by forces, to deepen our understanding of in-vivo mechanotransduction and polymer physics. The weak effect observed below 0.4pN is not very surprising, as it can be explained by the influence of thermal fluctuation. Thermal fluctuation exists everywhere as a function of temperature and drives all molecules to undergo random

walk. This randomness, as a kind of noise, may override weak signals of directionality.

The formin FH2 dimer is also prone to thermal fluctuation when associating with barbed end, which may contribute to the noise of polymerization speed. In contrast, pulling forces are thought to directionally shift the energy states of both formin and F-actin towards polymerization. However, whether the effect of pulling is significant depends on the magnitude of force in comparison with thermal fluctuation. Thermal fluctuation is associated with an energy state of $\sim k_B T$, which is approximate 4.1pN·nm at room temperature. During actin polymerization, adding a new actin monomer results in an extension increase of ~2.7nm. This leads to a characteristic force of ~ 1.4pN, which is several folds larger than the maximal force that I could applied to the tether by the time. In this case, the influence of directional force is possibly concealed by thermal fluctuation.

Meanwhile, it is worth noting that the temperature in vivo is slightly higher than room temperature, which corresponds to a larger randomness. Therefore, higher pulling forces may be required to overcome fluctuation.

Fortunately, it may not be a problem in cells, thanks to the internal tensile forces that are large enough. Myosin II is the major player of tension maintenance in cells, which is able to generate pulling force of 3-4pN [108]. This magnitude is higher than 1.5pN and was predicted to be able to reduce critical concentration drastically. In addition, Myosin II may work in a cooperative manner and impose even higher forces on actin filaments.

As for this study, only the forces less than 0.4pN have been tested due to the limitation of time. It is possible to achieve higher pulling forces by using stronger magnet. Therefore, future plan includes the increase of pulling force to 3pN.

Meanwhile, our current observation is different from the results obtained using hydrodynamic flow. In this report, the polymerization without profilin was strongly inhibited by small pulling forces even less than 0.4pN[106]. This inconsistency may come from the difference in instrumental setup. Therefore, more experiments with well-controlled conditions are needed to draw final conclusion.

Finally, the current result may also suggest the benefits to test critical concentration, which may be changed more significantly compared to polymerization rate. Since the critical concentration of Mg-ATP-actin is only about 0.1μM, its decrease may contribute more to the acceleration at low G-actin concentration. Future comparison between low and high G-actin concentration may help to unveil the responses of critical concentration and polymerization rate individually.

CHAPTER 7 Conclusion and Discussion

In my PhD studies, in order to quantitatively study the effects of stretching forces on mDia1 mediated actin polymerization, I designed three approaches based on the technologies of single molecule manipulation.

Hydrodynamic flow is the method of highest throughput and simplest setup, which has been shown able to apply pulling forces up to 1.8pN. Using this method, acceleration of mDia1-mediated polymerization was observed in the presence of profilin. As for the polymerization without profilin, no significant effect was found. Although some individual experiments showed weak increase of polymerization rate and decrease of critical concentration by the forces less than 1pN, it is hard to draw any conclusion to support the promoting effects of pulling forces, due to the many limitations of this method. First, the magnitude of force was known based on calculation instead of direct measurement. The flow speed used for calculation was likely to be inaccurate due to system vibration. Second, the forces of different magnitude were mainly obtained by changing the speed of flow, which may cause mechanical disturbance to the system and change the conditions for polymerization. Third, the quantification based on fluorescence imaging is of intrinsic low spatial and temporal resolution. This disadvantage may strongly limit the investigation of slow polymerization events, e.g. at low G-actin concentration and in the absence of profilin.

Optical tweezers, which is in principle a powerful way of manipulation and force detection, has not provided high-quality results in practice. Although the pulling forces can be directly measured using optical trap, the obtained forces did not

completely match the curve of elongation, especially at low force range. It may be resulted from several defects, including the mechanical instability of the instrument and microfluidic system. Meanwhile, the low contrast of wide-field fluorescence imaging and the use of microsphere made it difficult to identify whether the tether was single or not. Overall, it seems that many improvements are still needed to make full use of the optical tweezers, which is currently not reliable enough to manipulate single polymerizing actin filaments.

Magnetic tweezers was the third tested method. By taking the advantages of microfluidics and TIRF imaging, I was able to assemble barbed-end molecular machinery on coverslip surface in a clear way. Efforts were also paid to achieve high efficiency and specificity of filament anchorage, which was important to overcome the weak nature of formin association. Meanwhile, the microfluidic system and magnetic tweezers was also improved to ensure effective force application with low disturbance. Therefore, using this system, a continuous range of forces can be applied to stretch single actin filaments in accurate and constant manner. Both spatial and temporal resolution has been increased much in comparison with the conventional approaches used to study actin polymerization[100]. These advantages make it possible to detect formin mediated actin polymerization in high sampling rates and beyond optical limit, by which even small and fast changes of polymerization speed may be observed.

Later, it was found that small forces less than 0.4pN did not change polymerization rates much in the absence of profilin. This observation is consistent with the principles of statistical mechanics, and suggests a strong need to apply larger forces.

Besides, critical concentration is another important factor that requires to be examined in the future.

Meanwhile, according to the theoretical analysis, depolymerization may be regulated by tension as well. Though an inhibitory effect on depolymerization has been shown in the presence of profilin, it is still important to know the outcome if neither profilin nor hydrodynamic flow is involved[44].

Further, the roles of formin rotation in actin dynamics are still unclear. In 2011, based on fluorescence polarization, it was demonstrated that formin dimer indeed rotates with respect to the actin filament during polymerization[125]. However, it is unknown whether polymerization can still occur if the rotation is not allowed. A novel mechanism of screw mode has been proposed to predict the release of twisting tension even when the rotation is constrained, which probably occurs in vivo[126]. Considering the ability of magnetic tweezers to control bead rotation, it may provide a chance to resolve this paradox at single molecule level.

Finally, as we know, different formin members are diverse in their polymerization activities[73]. Some studies attributed this diversity to the intrinsic difference in FH2 conformation[89]. Now, with the newly developed approach, we are able to compare the activities of different formins more precisely and in the presence of tension. In addition, the functions of many other factors, such as ATP hydrolysis and tropomyosin binding, can be studied in high resolution as well, to uncover the underlying mechanism of actin regulation.

Bibliography

1.   Perry, S. V. When was actin first extracted from muscle? *J. Muscle Res. Cell Motil.* **24,** 597–9 (2003).

2.   Hatano, S. & Oosawa, F. Isolation and characterization of plasmodium actin. *Biochim. Biophys. Acta* **127,** 488–98 (1966).

3.   Pollard, T. D. & Cooper, J. A. Actin, a central player in cell shape and movement. *Science* **326,** 1208–12 (2009).

4.   Narita, A. & Maéda, Y. Molecular determination by electron microscopy of the actin filament end structure. *J. Mol. Biol.* **365,** 480–501 (2007).

5.   Urban, E., Jacob, S., Nemethova, M., Resch, G. P. & Small, J. V. Electron tomography reveals unbranched networks of actin filaments in lamellipodia. *Nat. Cell Biol.* **12,** 429–35 (2010).

6.   Otterbein, L. R., Graceffa, P. & Dominguez, R. The crystal structure of uncomplexed actin in the ADP state. *Science* **293,** 708–11 (2001).

7.   Holmes, K. C., Popp, D., Gebhard, W. & Kabsch, W. Atomic model of the actin filament. *Nature* **347,** 44–9 (1990).

8.   Graceffa, P. & Dominguez, R. Crystal structure of monomeric actin in the ATP state. Structural basis of nucleotide-dependent actin dynamics. *J. Biol. Chem.* **278,** 34172–80 (2003).

9.   Carlier, M. F., Valentin-Ranc, C., Combeau, C., Fievez, S. & Pantoloni, D. Actin polymerization: regulation by divalent metal ion and nucleotide binding, ATP hydrolysis and binding of myosin. *Adv. Exp. Med. Biol.* **358,** 71–81 (1994).

10. Dominguez, R. & Holmes, K. C. Actin structure and function. *Annu. Rev. Biophys.* **40,** 169–86 (2011).

11. Oda, T., Iwasa, M., Aihara, T., Maéda, Y. & Narita, A. The nature of the globular- to fibrous-actin transition. *Nature* **457,** 441–5 (2009).

12. Bindschadler, M., Osborn, E. A., Dewey, C. F. & McGrath, J. L. A mechanistic model of the actin cycle. *Biophys. J.* **86,** 2720–39 (2004).

13. Yang, C. & Svitkina, T. Filopodia initiation: focus on the Arp2/3 complex and formins. *Cell Adh. Migr.* **5,** 402–8

14. Gordon, D. J., Boyer, J. L. & Korn, E. D. Comparative biochemistry of non-muscle actins. *J. Biol. Chem.* **252,** 8300–9 (1977).

15. Pollard, T. D. Regulation of actin filament assembly by Arp2/3 complex and formins. *Annu. Rev. Biophys. Biomol. Struct.* **36,** 451–77 (2007).

16. Campellone, K. G. & Welch, M. D. A nucleator arms race: cellular control of actin assembly. *Nat. Rev. Mol. Cell Biol.* **11,** 237–51 (2010).

17. Kelly, A. E., Kranitz, H., Dötsch, V. & Mullins, R. D. Actin binding to the central domain of WASP/Scar proteins plays a critical role in the activation of the Arp2/3 complex. *J. Biol. Chem.* **281,** 10589–97 (2006).

18. Schönichen, A. & Geyer, M. Fifteen formins for an actin filament: a molecular view on the regulation of human formins. *Biochim. Biophys. Acta* **1803,** 152–63 (2010).

19. Hansen, S. D. & Mullins, R. D. VASP is a processive actin polymerase that requires monomeric actin for barbed end association. *J. Cell Biol.* **191,** 571–84 (2010).

20. Carlier, M.-F. *et al.* Actin Depolymerizing Factor (ADF/Cofilin) Enhances the Rate of Filament Turnover: Implication in Actin-based Motility. *J. Cell Biol.* **136,** 1307–1323 (1997).

21. Ichetovkin, I., Han, J., Pang, K. M., Knecht, D. A. & Condeelis, J. S. Actin filaments are severed by both native and recombinant dictyostelium cofilin but to different extents. *Cell Motil. Cytoskeleton* **45,** 293–306 (2000).

22. Cooper, J. A. & Schafer, D. A. Control of actin assembly and disassembly at filament ends. *Curr. Opin. Cell Biol.* **12,** 97–103 (2000).

23. Weber, A., Pennise, C. R., Babcock, G. G. & Fowler, V. M. Tropomodulin caps the pointed ends of actin filaments. *J. Cell Biol.* **127,** 1627–35 (1994).

24. Broschat, K. O., Weber, A. & Burgess, D. R. Tropomyosin stabilizes the pointed end of actin filaments by slowing depolymerization. *Biochemistry* **28,** 8501–6 (1989).

25. Bernstein, B. W. & Bamburg, J. R. Tropomyosin binding to F-actin protects the F-actin from disassembly by brain actin-depolymerizing factor (ADF). *Cell Motil.* **2,** 1–8 (1982).

26. Pollard, T. D. & Borisy, G. G. Cellular motility driven by assembly and disassembly of actin filaments. *Cell* **112,** 453–65 (2003).

27. Romero, S. *et al.* Formin is a processive motor that requires profilin to accelerate actin assembly and associated ATP hydrolysis. *Cell* **119,** 419–29 (2004).

28. Carlier, M. F., Jean, C., Rieger, K. J., Lenfant, M. & Pantaloni, D. Modulation of the interaction between G-actin and thymosin beta 4 by the ATP/ADP ratio: possible implication in the regulation of actin dynamics. *Proc. Natl. Acad. Sci. U. S. A.* **90,** 5034–8 (1993).

29. Kang, F., Purich, D. L. & Southwick, F. S. Profilin promotes barbed-end actin filament assembly without lowering the critical concentration. *J. Biol. Chem.* **274,** 36963–72 (1999).

30. Clark, A. G., Wartlick, O., Salbreux, G. & Paluch, E. K. Stresses at the cell surface during animal cell morphogenesis. *Curr. Biol.* **24,** R484–94 (2014).

31. Lim, C. T., Bershadsky, A. & Sheetz, M. P. Mechanobiology. *J. R. Soc. Interface* **7 Suppl 3,** S291–3 (2010).

32. Engler, A. J., Sen, S., Sweeney, H. L. & Discher, D. E. Matrix elasticity directs stem cell lineage specification. *Cell* **126,** 677–89 (2006).

33. Lim, T. S. & Ricciardi-Castagnoli, P. Single-cell force spectroscopy: mechanical insights into the functional impacts of interactions between antigen-presenting cells and T cells. *Immunol. Res.* **53,** 108–14 (2012).

34. Mammoto, T. & Ingber, D. E. Mechanical control of tissue and organ development. *Development* **137,** 1407–20 (2010).

35. Ingber, D. E. Mechanobiology and diseases of mechanotransduction. *Ann. Med.* **35,** 564–77 (2003).

36. Galkin, V. E., Orlova, A. & Egelman, E. H. Actin filaments as tension sensors. *Curr. Biol.* **22,** R96–101 (2012).

37. Geiger, B., Spatz, J. P. & Bershadsky, A. D. Environmental sensing through focal adhesions. *Nat. Rev. Mol. Cell Biol.* **10,** 21–33 (2009).

38. Ingber, D. E. Tensegrity: the architectural basis of cellular mechanotransduction. *Annu. Rev. Physiol.* **59,** 575–99 (1997).

39. Isambert, H. *et al.* Flexibility of actin filaments derived from thermal fluctuations. Effect of bound nucleotide, phalloidin, and muscle regulatory proteins. *J. Biol. Chem.* **270,** 11437–44 (1995).

40. Howard, J. *Mechanics of motor proteins and the cytoskeleton.* (Sinauer Associates, Inc., 2001).

41. Tsuda, Y., Yasutake, H., Ishijima, A. & Yanagida, T. Torsional rigidity of single actin filaments and actin-actin bond breaking force under torsion measured directly by in vitro micromanipulation. *Proc. Natl. Acad. Sci. U. S. A.* **93,** 12937–42 (1996).

42. Lee, C. *et al.* Actin depolymerization under force is governed by lysine 113:glutamic acid 195-mediated catch-slip bonds. *Proc. Natl. Acad. Sci. U. S. A.* **110,** 5022–7 (2013).

43. Kovar, D. R. & Pollard, T. D. Insertional assembly of actin filament barbed ends in association with formins produces piconewton forces. *Proc. Natl. Acad. Sci. U. S. A.* **101,** 14725–30 (2004).

44. Jégou, A., Carlier, M.-F. & Romet-Lemonne, G. Formin mDia1 senses and generates mechanical forces on actin filaments. *Nat. Commun.* **4,** 1883 (2013).

45. Tokuo, H. & Ikebe, M. Myosin X transports Mena/VASP to the tip of filopodia. *Biochem. Biophys. Res. Commun.* **319,** 214–20 (2004).

46. Romet-Lemonne, G. & Jégou, A. Mechanotransduction down to individual actin filaments. *Eur. J. Cell Biol.* **92,** 333–8

47. Murrell, M. P. & Gardel, M. L. F-actin buckling coordinates contractility and severing in a biomimetic actomyosin cortex. *Proc. Natl. Acad. Sci. U. S. A.* **109,** 20820–5 (2012).

48. Risca, V. I. *et al.* Actin filament curvature biases branching direction. *Proc. Natl. Acad. Sci. U. S. A.* **109,** 2913–8 (2012).

49. Shimozawa, T. & Ishiwata, S. Mechanical distortion of single actin filaments induced by external force: detection by fluorescence imaging. *Biophys. J.* **96,** 1036–44 (2009).

50. Yao, M. *et al.* Force-dependent conformational switch of α-catenin controls vinculin binding. *Nat. Commun.* **5,** 4525 (2014).

51. Ehrlicher, A. J., Nakamura, F., Hartwig, J. H., Weitz, D. A. & Stossel, T. P.

Mechanical strain in actin networks regulates FilGAP and integrin binding to filamin A. *Nature* **478,** 260–3 (2011).

52. Marcy, Y., Prost, J., Carlier, M.-F. & Sykes, C. Forces generated during actin-based propulsion: a direct measurement by micromanipulation. *Proc. Natl. Acad. Sci. U. S. A.* **101,** 5992–7 (2004).

53. Raucher, D. & Sheetz, M. P. Cell spreading and lamellipodial extension rate is regulated by membrane tension. *J. Cell Biol.* **148,** 127–36 (2000).

54. Zigmond, S. H. *et al.* Formin leaky cap allows elongation in the presence of tight capping proteins. *Curr. Biol.* **13,** 1820–3 (2003).

55. Kleinebrecht, J., Selow, J. & Winkler, W. The mouse mutant limb-deformity (ld). *Anat. Anz.* **152,** 313–24 (1982).

56. Woychik, R. P., Stewart, T. A., Davis, L. G., D'Eustachio, P. & Leder, P. An inherited limb deformity created by insertional mutagenesis in a transgenic mouse. *Nature* **318,** 36–40

57. Woychik, R. P., Maas, R. L., Zeller, R., Vogt, T. F. & Leder, P. 'Formins': proteins deduced from the alternative transcripts of the limb deformity gene. *Nature* **346,** 850–3 (1990).

58. Castrillon, D. H. & Wasserman, S. A. Diaphanous is required for cytokinesis in Drosophila and shares domains of similarity with the products of the limb deformity gene. *Development* **120,** 3367–77 (1994).

59. Evangelista, M. *et al.* Bni1p, a yeast formin linking cdc42p and the actin cytoskeleton during polarized morphogenesis. *Science* **276,** 118–22 (1997).

60. Higgs, H. N. & Peterson, K. J. Phylogenetic analysis of the formin homology 2 domain. *Mol. Biol. Cell* **16,** 1–13 (2005).

61. Wallar, B. J. & Alberts, A. S. The formins: active scaffolds that remodel the cytoskeleton. *Trends Cell Biol.* **13,** 435–46 (2003).

62. Li, F. & Higgs, H. N. Dissecting requirements for auto-inhibition of actin nucleation by the formin, mDia1. *J. Biol. Chem.* **280,** 6986–92 (2005).

63. Watanabe, N. *et al.* p140mDia, a mammalian homolog of Drosophila diaphanous, is a target protein for Rho small GTPase and is a ligand for profilin. *EMBO J.* **16,** 3044–56 (1997).

64. Lammers, M., Rose, R., Scrima, A. & Wittinghofer, A. The regulation of mDia1 by autoinhibition and its release by Rho*GTP. *EMBO J.* **24,** 4176–87 (2005).

65. Xu, Y. *et al.* Crystal structures of a Formin Homology-2 domain reveal a tethered dimer architecture. *Cell* **116,** 711–23 (2004).

66. Otomo, T. *et al.* Structural basis of actin filament nucleation and processive capping by a formin homology 2 domain. *Nature* **433,** 488–94 (2005).

67. Zigmond, S. H. Formin-induced nucleation of actin filaments. *Curr. Opin. Cell Biol.* **16,** 99–105 (2004).

68. Moseley, J. B. *et al.* A conserved mechanism for Bni1- and mDia1-induced actin assembly and dual regulation of Bni1 by Bud6 and profilin. *Mol. Biol.*

Cell **15,** 896–907 (2004).

69.   Harris, E. S., Li, F. & Higgs, H. N. The mouse formin, FRLalpha, slows actin filament barbed end elongation, competes with capping protein, accelerates polymerization from monomers, and severs filaments. *J. Biol. Chem.* **279,** 20076–87 (2004).

70.   Shimada, A. *et al.* The core FH2 domain of diaphanous-related formins is an elongated actin binding protein that inhibits polymerization. *Mol. Cell* **13,** 511–22 (2004).

71.   Yamashita, M. *et al.* Crystal structure of human DAAM1 formin homology 2 domain. *Genes Cells* **12,** 1255–65 (2007).

72.   Lu, J. *et al.* Structure of the FH2 domain of Daam1: implications for formin regulation of actin assembly. *J. Mol. Biol.* **369,** 1258–69 (2007).

73.   Kovar, D. R., Harris, E. S., Mahaffy, R., Higgs, H. N. & Pollard, T. D. Control of the assembly of ATP- and ADP-actin by formins and profilin. *Cell* **124,** 423–35 (2006).

74.   Chang, F., Drubin, D. & Nurse, P. cdc12p, a Protein Required for Cytokinesis in Fission Yeast, Is a Component of the Cell Division Ring and Interacts with Profilin. *J. Cell Biol.* **137,** 169–182 (1997).

75.   Li, F. & Higgs, H. N. The mouse Formin mDia1 is a potent actin nucleation factor regulated by autoinhibition. *Curr. Biol.* **13,** 1335–40 (2003).

76.   Paul, A. S., Paul, A., Pollard, T. D. & Pollard, T. The role of the FH1 domain and profilin in formin-mediated actin-filament elongation and nucleation. *Curr. Biol.* **18,** 9–19 (2008).

77.   Nezami, A. G., Poy, F. & Eck, M. J. Structure of the autoinhibitory switch in formin mDia1. *Structure* **14,** 257–63 (2006).

78.   Schulte, A. *et al.* The human formin FHOD1 contains a bipartite structure of FH3 and GTPase-binding domains required for activation. *Structure* **16,** 1313–23 (2008).

79.   Alberts, A. S. Identification of a carboxyl-terminal diaphanous-related formin homology protein autoregulatory domain. *J. Biol. Chem.* **276,** 2824–30 (2001).

80.   Rose, R. *et al.* Structural and mechanistic insights into the interaction between Rho and mammalian Dia. *Nature* **435,** 513–8 (2005).

81.   Lammers, M., Meyer, S., Kühlmann, D. & Wittinghofer, A. Specificity of interactions between mDia isoforms and Rho proteins. *J. Biol. Chem.* **283,** 35236–46 (2008).

82.   Tobacman, L. S., Brenner, S. L. & Korn, E. D. Effect of Acanthamoeba profilin on the pre-steady state kinetics of actin polymerization and on the concentration of F-actin at steady state. *J. Biol. Chem.* **258,** 8806–12 (1983).

83.   Pollard, T. D. & Cooper, J. A. Quantitative analysis of the effect of Acanthamoeba profilin on actin filament nucleation and elongation. *Biochemistry* **23,** 6631–41 (1984).

84.   Kaiser, D. A., Vinson, V. K., Murphy, D. B. & Pollard, T. D. Profilin is predominantly associated with monomeric actin in Acanthamoeba. *J. Cell Sci.*

112 (Pt 2, 3779–90 (1999).

85. Schafer, D. A., Jennings, P. B. & Cooper, J. A. Dynamics of capping protein and actin assembly in vitro: uncapping barbed ends by polyphosphoinositides. *J. Cell Biol.* **135,** 169–79 (1996).

86. Higashida, C. *et al.* Actin polymerization-driven molecular movement of mDia1 in living cells. *Science* **303,** 2007–10 (2004).

87. Kovar, D. R., Wu, J.-Q. & Pollard, T. D. Profilin-mediated competition between capping protein and formin Cdc12p during cytokinesis in fission yeast. *Mol. Biol. Cell* **16,** 2313–24 (2005).

88. Kovar, D. R., Kuhn, J. R., Tichy, A. L. & Pollard, T. D. The fission yeast cytokinesis formin Cdc12p is a barbed end actin filament capping protein gated by profilin. *J. Cell Biol.* **161,** 875–87 (2003).

89. Paul, A. S. & Pollard, T. D. Energetic requirements for processive elongation of actin filaments by FH1FH2-formins. *J. Biol. Chem.* **284,** 12533–40 (2009).

90. Pellegrin, S. & Mellor, H. The Rho family GTPase Rif induces filopodia through mDia2. *Curr. Biol.* **15,** 129–33 (2005).

91. Yang, C. *et al.* Novel roles of formin mDia2 in lamellipodia and filopodia formation in motile cells. *PLoS Biol.* **5,** e317 (2007).

92. Hotulainen, P. & Lappalainen, P. Stress fibers are generated by two distinct actin assembly mechanisms in motile cells. *J. Cell Biol.* **173,** 383–94 (2006).

93. Watanabe, S. *et al.* mDia2 induces the actin scaffold for the contractile ring and stabilizes its position during cytokinesis in NIH 3T3 cells. *Mol. Biol. Cell* **19,** 2328–38 (2008).

94. Carramusa, L., Ballestrem, C., Zilberman, Y. & Bershadsky, A. D. Mammalian diaphanous-related formin Dia1 controls the organization of E-cadherin-mediated cell-cell junctions. *J. Cell Sci.* **120,** 3870–82 (2007).

95. Sarmiento, C. *et al.* WASP family members and formin proteins coordinate regulation of cell protrusions in carcinoma cells. *J. Cell Biol.* **180,** 1245–60 (2008).

96. Colucci-Guyon, E. *et al.* A role for mammalian diaphanous-related formins in complement receptor (CR3)-mediated phagocytosis in macrophages. *Curr. Biol.* **15,** 2007–12 (2005).

97. Gasman, S., Kalaidzidis, Y. & Zerial, M. RhoD regulates endosome dynamics through Diaphanous-related Formin and Src tyrosine kinase. *Nat. Cell Biol.* **5,** 195–204 (2003).

98. Riveline, D. *et al.* Focal contacts as mechanosensors: externally applied local mechanical force induces growth of focal contacts by an mDia1-dependent and ROCK-independent mechanism. *J. Cell Biol.* **153,** 1175–86 (2001).

99. Kozlov, M. M. & Bershadsky, A. D. Processive capping by formin suggests a force-driven mechanism of actin polymerization. *J. Cell Biol.* **167,** 1011–7 (2004).

100. Neuman, K. C. & Nagy, A. Single-molecule force spectroscopy: optical tweezers, magnetic tweezers and atomic force microscopy. *Nat. Methods* **5,**

491–505 (2008).

101. Perkins, T. T., Quake, S. R., Smith, D. E. & Chu, S. Relaxation of a single DNA molecule observed by optical microscopy. *Science* **264,** 822–6 (1994).

102. Perkins, T. T., Smith, D. E., Larson, R. G. & Chu, S. Stretching of a single tethered polymer in a uniform flow. *Science* **268,** 83–7 (1995).

103. van Oijen, A. M. *et al.* Single-molecule kinetics of lambda exonuclease reveal base dependence and dynamic disorder. *Science* **301,** 1235–8 (2003).

104. Brewer, L. R. & Bianco, P. R. Laminar flow cells for single-molecule studies of DNA-protein interactions. *Nat. Methods* **5,** 517–25 (2008).

105. Jégou, A. *et al.* Individual actin filaments in a microfluidic flow reveal the mechanism of ATP hydrolysis and give insight into the properties of profilin. *PLoS Biol.* **9,** e1001161 (2011).

106. Courtemanche, N., Lee, J. Y., Pollard, T. D. & Greene, E. C. Tension modulates actin filament polymerization mediated by formin and profilin. *Proc. Natl. Acad. Sci. U. S. A.* **110,** 9752–7 (2013).

107. Ashkin, A., Dziedzic, J. M., Bjorkholm, J. E. & Chu, S. Observation of a single-beam gradient force optical trap for dielectric particles. *Opt. Lett.* **11,** 288 (1986).

108. Finer, J. T., Simmons, R. M. & Spudich, J. A. Single myosin molecule mechanics: piconewton forces and nanometre steps. *Nature* **368,** 113–9 (1994).

109. Hayakawa, K., Tatsumi, H. & Sokabe, M. Actin filaments function as a tension sensor by tension-dependent binding of cofilin to the filament. *J. Cell Biol.* **195,** 721–7 (2011).

110. Le, S. *et al.* Mechanical force antagonizes the inhibitory effects of RecX on RecA filament formation in Mycobacterium tuberculosis. *Nucleic Acids Res.* **42,** 11992–9 (2014).

111. Fu, H., Chen, H., Marko, J. F. & Yan, J. Two distinct overstretched DNA states. *Nucleic Acids Res.* **38,** 5594–600 (2010).

112. Gore, J. *et al.* Mechanochemical analysis of DNA gyrase using rotor bead tracking. *Nature* **439,** 100–4 (2006).

113. Nagashima, H. & Asakura, S. Dark-field light microscopic study of the flexibility of F-actin complexes. *J. Mol. Biol.* **136,** 169–82 (1980).

114. Yanagida, T., Nakase, M., Nishiyama, K. & Oosawa, F. Direct observation of motion of single F-actin filaments in the presence of myosin. *Nature* **307,** 58–60

115. Kishino, A. & Yanagida, T. Force measurements by micromanipulation of a single actin filament by glass needles. *Nature* **334,** 74–6 (1988).

116. Footer, M. J., Kerssermakers, J. W. J., Theriot, J. A. & Dogterom, M. Direct measurement of force generation by actin filament polymerization using an optical trap. *Proc. Natl. Acad. Sci. U. S. A.* **104,** 2181–6 (2007).

117. Pardee, J. D. & Spudich, J. A. Purification of muscle actin. *Methods Cell Biol.* **24,** 271–89 (1982).

118. Pollard, T. D. Polymerization of ADP-actin. *J. Cell Biol.* **99,** 769–77 (1984).

119. Strick, T. R., Allemand, J. F., Bensimon, D., Bensimon, A. & Croquette, V. The elasticity of a single supercoiled DNA molecule. *Science* **271,** 1835–7 (1996).

120. Marko, J. F. & Siggia, E. D. Stretching DNA. *Macromolecules* **28,** 8759–8770 (1995).

121. Smith, S. B., Finzi, L. & Bustamante, C. Direct mechanical measurements of the elasticity of single DNA molecules by using magnetic beads. *Science* **258,** 1122–6 (1992).

122. Zhao, C., Liu, C., Hogue, C. W. V & Low, B. C. A cooperative jack model of random coil-to-elongation transition of the FH1 domain by profilin binding explains formin motor behavior in actin polymerization. *FEBS Lett.* **588,** 2288–93 (2014).

123. Chen, H. *et al.* Improved high-force magnetic tweezers for stretching and refolding of proteins and short DNA. *Biophys. J.* **100,** 517–23 (2011).

124. Gelles, J., Schnapp, B. J. & Sheetz, M. P. Tracking kinesin-driven movements with nanometre-scale precision. *Nature* **331,** 450–3 (1988).

125. Mizuno, H. *et al.* Rotational movement of the formin mDia1 along the double helical strand of an actin filament. *Science* **331,** 80–3 (2011).

126. Shemesh, T., Otomo, T., Rosen, M. K., Bershadsky, A. D. & Kozlov, M. M. A novel mechanism of actin filament processive capping by formin: solution of the rotation paradox. *J. Cell Biol.* **170,** 889–93 (2005).